Lawrence Berkeley Laboratory
UNIVERSITY OF CALIFORNIA
Materials & Molecular
Research Division

CROSSED BEAM STUDIES OF FULL AND HALF COLLISIONS

Randal Kenneth Sparks
(Ph.D. thesis)

November 1979

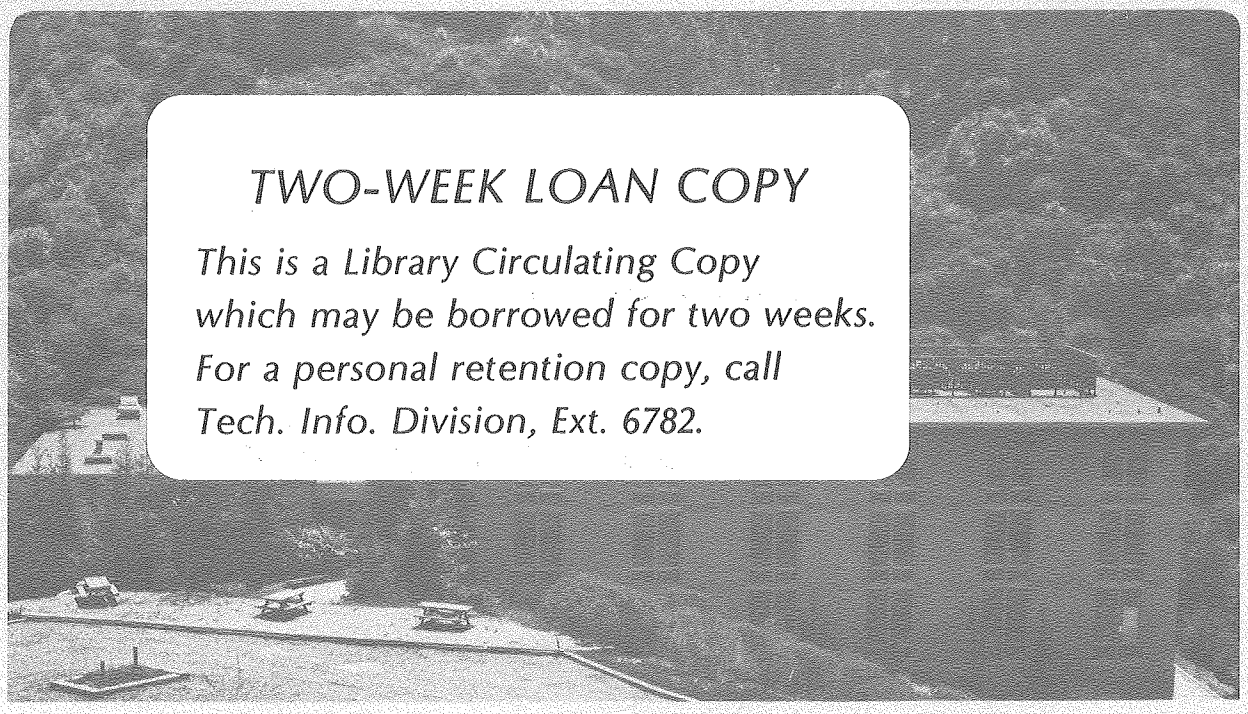

Prepared for the U.S. Department of Energy under Contract W-7405-ENG-48

DISCLAIMER

LBL-10138

CROSSED BEAM STUDIES OF FULL AND HALF COLLISIONS

Randal Kenneth Sparks

Materials and Molecular Research Division
Lawrence Berkeley Laboratory

and

Department of Chemistry
University of California
Berkeley, California 94720

November 1979

ABSTRACT

The results of two experiments performed on a new very high resolution crossed molecular beams apparatus are discussed. The first experiment, photofragmentation of methyl iodide, is deconvoluted to yield vibrational state distributions for the recoiling methyl fragment. These distributions are then analyzed in terms of half-collision models and Franck-Condon factors. The second experiment, a full-collision example, is the reaction of F atoms with H_2 and D_2. Laboratory angular and velocity distributions for both systems are obtained at several energies. Center-of-mass product distributions are calculated and discussed in terms of recently predicted state dependent resonance phenomena for the reaction. The design of the new apparatus is also discussed.

Table of Contents

ACKNOWLEDGEMENTS

My greatest thanks must go to Professor Yuan T. Lee without whose encouragement, advice, and support this work would have been impossible. His eternal optimism, immeasurable enthusiasm, and his willingness to roll up his sleeves and get dirty right along with his students have always had a tremendous impact on all who work with him.

Particular mention must also go to Professor Cheuk Yiu Ng who taught me a great deal of what I know about vacuum technology and mechanical engineering. His friendship always has and always will be greatly appreciated. Dr. Kosuke Shobatake was also of great assistance in teaching me the true appreciation of data analysis. His patience in quietly explaining and demonstrating the real truth to one who so often loudly proclaimed a different truth are kindly remembered. Carl Hayden has also been tremendously helpful in the performance of this work. His ability to get things right and to do it almost always on the first try have made some of the impossible things we have tried doable and the others a lot less impossible. Dr. Lee Carlson also deserves special recognition for having taught me the vagaries of lasers and minicomputers. His get to it and do it attitude always created a high rate of results.

A great many people in our laboratory facilities have been tremendously helpful in the construction of our apparatus and the performance of our work. They know what they do. Their names are Allan Susoeff, Charlie Taylor, Carson Haines, Frank Maxwell, Will Laurence, George Barbero, Bent Larsen, Crystal Llewellyn, Bob Hootman, Fred Vogelsberg,

Ed Arnold, Vince Randolph, Gene Powers, Dick Escobales, Everett Good, Ben Green, Bob Fischer and a host of others who have helped me build it, buy it, and keep it on line. Their work is well recognized and highly appreciated.

There are also a great many past and present members of our research group who have been very helpful and very good friends. They are not forgotten here, only too numerous to list.

Special appreciation must go to Ms. Ann Weightman for patience and tolerance in preparation of this thesis as well as all her other myriad tasks. Great thanks must also be given to Piero Casavecchia, Rick Buss, and Carol Kahler for helping to dig me out of a very deep hole in the final days before this thesis was due.

This work was supported by the Division of Chemical Sciences, Office of Basic Energy Sciences, U.S. Department of Chemistry under contract No. W-7405-Eng-48.

I. PHOTOFRAGMENTATION OF METHYL IODIDE

INTRODUCTION

The study of the mechanisms and dynamics of molecular photodissociation has been an active field for a great many years. An understanding of the processes occurring in molecular electronic dissociative continua is of great importance to many fields. The problems of atmospheric chemistry are illustrative of the typical value of such information. In both high and low altitude situations, it is rarely the primary photodissociation products which have a direct impact on our lives, but rather the end products of a chain of reactions. However, it is clearly impossible to sort out the reaction chains if the primary photolysis step is not understood. Knowledge of the identity and energetics of one's reactants is a necessity for understanding a reaction. Additionally, photolysis processes serve as a fertile testing ground for models of molecular dynamics in general. The energy involved in a photolytic reaction is such that interaction between electronic, vibrational, rotational and translational energies, in any combination, is possible.

A great deal of progress in this field has been made in recent years, both on the experimental and the theoretical front. Experimentally, effort has been applied to ions, both positive and negative, as well as neutrals. Work on negative ions includes photodissociation spectroscopy (of O_3^-),[1] combined photodissociation and photodetachment (hydrates of O_3^-),[2] and photodetachment alone (CH_3O^-, CD_3O^-, CH_3S^-).[3]

Photodetachment, of course, does not dissociate the molecule, and thus one gains information about two different bound potentials rather than a bound and a continuum surface. Very recent positive ion work has included studies on the direct dissociation of Kr_2^+,[4] as well as studies of predissociation of O_2^+.[5] Efforts on photodissociation of neutrals have included studies of the lifetime of van der Waals complexes (I_2He)[6] as well as measurements on the traditional questions of branching ratios and quantum yields of the product electronic states of various dissociation processes (HgI_2,[7] CdI_2,[8] TlBr,[9] IBr[10]). Dissociation of neutrals has also served as a means of preparing otherwise inaccessible species so that their spectroscopy, chemistry, and relaxation dynamics may be studied.[11,12]

On the theoretical front, the frequency of publications is much lower than on the experimental front. Although the theoretical formulations that have been developed are quite general, their applications to specific problems have been almost entirely limited to dissociation of linear molecules. Calculations, however, have been done on the dissociation of T-shaped van der Waals complexes in general[13] as well as special attention devoted the HeI_2 complex.[14] These calculations were done by numerical integration of the close-coupling equations, and thus represent a rather expensive and time-consuming procedure if one wished to perform a trial-and-error fit of a potential surface to the experimental data. Early efforts at producing tractable models were the classical energy forced quantum

osicllator approximation of Holdy, Klotz and Wilson[15] and an extension of it which obeys detailed balance referred to as the ITFITS model.[16] These models are applied to both full and half collisions of collinear triatomic systems. Both of these methods use classical mechanics to calculate an average energy transfer in a collision, which is then used as input into a semi-classical expression for the distribution of vibrational states resulting from the dynamical development on the repulsive surface. No attempt is made to account for Franck-Condon factors in the photon absorption. In fact, in the earlier paper, it is assumed that the initial vibrational state is entirely $v = 0$, which is the functional result of what the authors refer to as the quasidiatomic model. In the ITFITS model, calculations are done for transitions initiating from $v = 1$ as well as $v = 0$ in order to facilitate comparison with exact quantum calculations.[17] One anomalously low value for the ITFITS transition probability was obtained for initial $v = 1$, however, the authors did not seem to recognize that this is a general feature of the semiclassical formula used. Shapiro and Levine have performed quantum, rather than semi-classical, calculations of the scattering dynamics of a half-collision.[18] They also assumed that Franck-Condon factors do not affect the vibrational distribution of the products. Ensuing discussions[19-23] have been directed towards a more complete treatment of both the Franck-Condon factors and the excited state scattering. The formalism of bound-continuum and continuum-continuum interactions was used by

Mukamel and Jortner[19,20,22,23] while Band and Freed[21] developed their presentation directly in terms of Franck-Condon factors and scattering operators. Band and Freed emphasized the proper treatment of the Franck-Condon factors, specifically correct handling of the vibrational coordinates for both the initial and final states of the system. They evaluate the S matrix using the classical path force function inherent in the earlier treatments,[15,16] and conclude that, for certain systems (ICN and HCN), the Franck-Condon factors are the predominant determinant of product vibrational excitation. Thus they claim that it is not always necessary to perform the laborious dynamical claculation. In two subsequent papers Mukamel and Jortner conclude that the final state interactions are important for HCN[22] and for both HCN and ICN.[23] More recent theoretical developments include (all by Band, Morse, and Freed) a comparison of various semi-classical procedures for evaluating Franck-Condon factors,[24] as well as a treatment of the rotational distributions of the diatomic product of photodissociation of a linear triatomic.[25,26]

There certainly seems to be some problem involved with the interaction between theory and experiment. There is clearly a very great deal of experimental data on various systems while the theory has limited itself primarily to the XCN series. Part of this problem is due to the type of experimental data available. Photodissociation of diatomics, whether ions or molecules, can be used to gain information on a previously poorly understood ion or radical by analysis of hot

bands[5] or one-dimensional Franck-Condon factors.[4] Diatomics may also yield information on electronic state interactions.[9,10] Photodetachment studies on negative ions[3,27] are primarily sensitive to Franck-Condon factors.

Since the electronic state interactions of diatomic photodissociation seem to be well represented (at least in one case) by a Landau-Zener treatment,[10] it is clear that the above do not necessarily represent fundamental theoretical challenges. However, increasing the complexity of systems only slightly brings a sudden end to this happy state. Many triatomic molecules and almost all polyatomic molecules are non-linear. However, the present development of theory cannot easily handle non-linear systems. In addition, even for linear cases, there is really not a broad range of experimental data available. For most systems there is essentially no reliable information on the potential surface or surfaces involved. Also, when several surfaces are involved, it is necessary to know the magnitudes and positions of their coupling if one wishes a complete treatment. Clearly, there are not any triatomic systems which we understand well enough such that we may proceed directly to calculate all asymptotic photofragmentation states. And since the theoretical methods themselves do not concur on even very important issues, it is clearly not yet time to use photodissociation theory in order to determine potential energy surfaces.

In an attempt to contribute some additional data relevant to this problem we have investigated the photodissociation of methyl iodide at 266 nm by use of a new very-high-resolution molecular beam apparatus. We have discerned the relative populations of the vibrational states of the CH_3 product for both the $I^2P_{3/2}$ and $^2P_{1/2}$ channels. A case is made that rotational excitation is and should be small and thus that one may treat this polyatomic by the same procedures used for collinear triatomics. Though no full-scale calculations are performed, arguments are developed which indicate that both Franck-Condon factors and scattering interactions are important for this system. Thus it is proposed that CH_3I would serve as an excellent test molecule for photodissociation theories and that both more experimental and theoretical work on this system should be undertaken.

EXPERIMENTAL

The general requirements of a photofragment spectrometer have been discussed both by Dzvonik and Yang[28] and by Busch et al.[29] Both of these previous machines have the laser propagation direction, beam source direction and detector direction mutually perpendicular. Such a design has the disadvantage that fragments recoiling slowly from a fast molecular beam will not enter the detector. Clearly it is advantageous to have the detector able to view angles near the

beam. Also, as will be shown below, it is sometimes advantageous in terms of resolution to be able to move the detector to angles wider than 90° in order to take advantage of velocity subtraction effects. Such an apparatus is found simply in a special case use of a universal crossed molecular beam machine,[30] in which one of the molecular beams is replaced by a laser. The resultant configuration is perpendicularly crossed laser and molecular beams with the detector rotatable in the plane defined by the two beams. We have used for this experiment a newly designed and constructed very high resolution universal crossed molecular beam apparatus. The details of the apparatus are explained in Appendix A. Briefly, the major improvements over existing machines consist of a longer flight path (~34.1 cm for this experiment) for higher velocity analysis resolution, careful choice of and processing of detector materials to result in lower background count rates, replaceable detector apertures to allow choice of laboratory angular resolution up to 2.5°, and a wider total laboratory angular scan range of the detector (170° versus ~120° in previous designs). We have also implemented a newly designed 100% duty cycle 1 μs per channel multichannel scaler which has allowed us to take real advantage of our increased velocity resolution.

The apparatus layout for this particular experiment is shown in Fig. 1. Our molecular beam is produced by supersonic expansion of a mixture of 3.2 mole percent CH_3I in helium carrier gas at a total

stagnation pressure of 4.35 atmospheres. The final 6 cm of the nozzle were heated to a temperature of 182°C by means of a D.C. heated tantalum wire radiation heater. The nozzle itself was constructed from a 6 mm diameter quartz tube drawn down at the tip to produce a nozzle diameter of 0.07 mm. The source was operated with a 0.66 mm diameter skimmer and a nozzle-skimmer distance of 6.25 mm. The nozzle-skimmer region was pumped by a 4500 l/s oil diffusion pump. The beam was collimated at a distance of 3.15 cm from the nozzle tip to a full width of 2.6° and a full height of 6.6°. The distance from the nozzle tip to the interaction region was 5.44 cm. The detector apertures used yield a laboratory resolution of 2.5°. A time-of-flight measurement of the beam, taken with a special beam analysis system which has a flight path of ~93 cm is shown in Fig. 2. The peak beam velocity is 14.9×10^4 cm/sec with a FWHM spread of 5 percent.

The light source for our experiment was a frequency quadrupled Nd:YAG laser (Quanta-Ray model DCR), with an oscillator, amplifier, and harmonic generator crystal set. The laser was operated at a repetition rate of 10 Hz. The factory specified pulse width is approximately 10 ns while our measured output energy at 266 nm was 35 mJ/pulse. The fundamental and second harmonic were separated from the 266 nm fourth harmonic by dispersion with a quartz prism. The fourth harmonic was coupled into the vacuum chamber through a fused silica window and intersected the molecular beam at an angle of 90°. Settings on the Quanta-Ray Harmonic Generator module were chosen to

produce the fourth harmonic linearly polarized in the plane defined by the molecular and laser beams. The laser beam was focused on the collision region by use of a 1/2 m focal length fused silica lens placed 53.8 cm from the interaction region (the lens was outside the vacuum system). Since the actual focal length of the lens at 266 nm should be ~45.8 cm, the initial 6 mm diameter laser beam is focused to a diameter of ~1 mm in the interaction region. Previous attempts at using a longer focal length lens encountered severe problems with increased and time-structured background due to the high intensity (small diameter) of the laser beam at the far vacuum wall of the apparatus. Alignment was achieved by guiding the laser through a precision positioned iris on the laser side of the entrance window and adjusting the laser beam until its position on the far apparatus wall, as observed by fluorescence from a salesman's business card, was determined to be correct. Once the iris and business card (with appropriate graduations inked on) had been positioned with an alignment telescope, it was possible to align the laser beam even while the apparatus was under vacuum, as the fluorescence from the business card could be observed through a plexiglass flange on the main vacuum chamber.

The detector principles are the same as used in previous machines of this type. Scattered product molecules are ionized by electron impact in the innermost pumping region of a triply-differentially pumped ultra-high vacuum rotating chamber. All three regions are

pumped by separate 220 l/s DI ion pumps, while the innermost region is additionally pumped by a liquid helium cryopump. Resulting ions are then mass-selected by a quadrupole mass-spectrometer and detected with a Daly[31] type ion detection system used in pulse-counting configuration. Discriminated pulses are routed to our new CAMAC compatible multichannel scaler (MCS) system. The MCS has a variable channel width of 1-99 μsec in divisions of 1 μsec and can accumulate data for 255 channels after receipt of a trigger pulse. The trigger pulse for this experiment was derived from a photodiode placed so as to detect the green second harmonic light which was scattered from the dispersing prism at each laser pulse. The MCS is interfaced through the CAMAC standard to a 16-bit microcomputer (DEC LSI-11) system containing dual floppy discs, display oscilloscope, graphics plotter, and fast dot-matrix printer. Data is gathered, displayed and written to disc by an assembly language program and then is later accessed by Fortran programs for data analysis.

RESULTS AND ANALYSIS

The data taken at a laboratory angle of 127° relative to the beam direction are shown in Fig. 3. These data were taken with a MCS channel width of 1 μs with detected m/e = 15 corresponding to CH_3^+. Data was accumulated for 300,000 laser shots. The data was taken at

such a large laboratory angle in order to take advantage of the subtraction of the beam velocity from the product velocity. A Newton diagram (velocity vector diagram) showing the laboratory velocities for CH_3 product at both 127° and a typical 30° detector angle are shown in Fig. 4. Since the laboratory velocities for the 127° angle are much lower than for the 30° angle, the small velocity separations due to internal CH_3 excitations will be much better separated in time at 127° than at 30°. Even with the very high resolution capabilities of this new apparatus, the separation of small energy spacings in such a highly energetic process is quite difficult. Previous machines have not been capable of reaching the large laboratory angles needed in order to take advantage of the velocity subtraction scheme. Clearly one also must have a high beam velocity and small velocity spread, thus our use of a high pressure He beam with a small CH_3I concentration.

Two peaks are apparent in the data, a smaller peak with short laboratory arrival times and a larger one with longer laboratory arrival times. The smaller peak shows definite asymmetry, with the rising edge significantly steeper than the falling. The larger peak seems somewhat more symmetric, however, there is clearly a very long "tail" at the end of the larger peak. This tail falls off so slowly that the data has not yet returned entirely to baseline even at the end of 255 channels. A similar long-time-constant tail has been observed in our experiments on the 266 nm photodissociation of

ozone.[32,33] Particularly in the ozone experiment, this long tail remains even at laboratory times that correspond to energies in the center-of-mass system that are dynamically inaccessible. Since, in that experiment, vibrational states are resolved, the tail feature would have to come from rotational excitation of the O_2 fragment. For the higher vibrational states (lower translational energy) of the O_2, the exit channel impact parameter that would have to be achieved in order to produce the necessary degree of rotational excitation is entirely beyond the bounds of reason. Additionally, the tail formed in the ozone experiment does not follow the same angular anisotropy as the resolved vibrational structure.[33] In fact the tail contribution is nearly anisotropic. It is for these reasons that the tail was considered to be an "artifact" of the experimental set-up and it was concluded that a means must be found for modelling it and subtracting it from the data.

Modelling of the tail is actually rather straightforward. Since the tail follows the peaks in time, it is clear that the size of the tail is in some manner related to the amount of m/e = 15 producing gas that enters the detector during the time that the peak enters the detector. As this gas is pumped away, the magnitude of its contribution will decrease in time. In principle the time dependence of the tail could be a rather complicated function since gas could be initially surface-pumped at high speed by the very clean nearby

surfaces in the detector and then more slowly released to be permanently pumped away by the ion and cryopumps. However, since random noise in the background is large enough to make any complicated modelling a total waste of time, it will be assumed here that the tail decays exponentially in time characterized by a single time constant. This form corresponds to that of an ideal pump evacuating an ideal vessel. The remaining issue, then, is the relation of the tail intensity to the peak intensity. We assume that the tail is caused by product molecules actually striking metal surfaces in the ion lens system and thus remaining in the region of the ionizer, allowing them to be ionized and detected. This is a reasonable assumption since these experiments were operated with our largest (2.5°) detector apertures. These apertures are sufficiently large that the product beam width at the ionizer is roughly the same as the inside diameter of the ion lenses. However, the lenses are round and the beam square, so the "corners" of the product beam will hit the ion lenses. This proposed mechanism then implies that the additional contribution to the tail occurring during any given time Δt is proportional to the flux of product molecules arriving in that time Δt. This contribution then decays exponentially with time and forms a new baseline level upon which the signal rides in ensuing Δt's. It is very important to note that the incremental tail contribution is proportional to product flux, however the measured signal is proportional to number density. Since the flux density is the product of the number density and velocity,

then assuming small variations in flight path to be insignificant, one must divide the measured signal in a channel by its arrival time in order to determine the time incremental flux. If one assumes an initial channel in which there has been no previous background contribution, one may calculate that channel's contribution to itself, subtract it, and use the remaining flux to calculate the contribution to the ensuing channels. This process may then be iterated channel by channel to produce a corrected spectrum. Since we have no a priori method of determining either the flux to tail contribution proportionality constant or the exponential time constant, these are treated as variable fitting parameters which are adjusted until the baseline becomes flat and averages to nearly zero. This is done after a background level determined by averaging early channels has been subtracted from the data. The new calculated spectrum is output to a digital plotter and parameters are adjusted until an acceptable result is achieved. Negative numbers are removed from the stripped data for the purposes of plotting. The very short Fortran code used to execute the spectrum stripping task is given as program 3 in Appendix B.

In addition to removal of the exponential tails from the data, we have included in the same program facilities for smoothing of the data in order to reduce the amount of statistical noise. In order to make the procedures rapid and thus interactive, we use digital filter methods. An excellent discussion of these procedures in their

general form is given by Hamming.[34] The specific filters that we use are given by Savitzky and Golay.[35] Though they are not optimum filters, they have the advantage that they correspond exactly to least squares fitting of a sliding polynomial to the data. This analytical property allows one to very easily obtain derivative spectra if it is desired. Again, we determine the number of channels to use in our filter by plotting out the results and visually determining the largest amount of smoothing that can be applied without attenuating spectral features. Figure 5 shows the effects of the above procedures applied to the data of Fig. 3. The upper trace shows the data after a 5 pt. polynomial smooth and channels 3-86 averaged for background subtraction. The lower trace is the result of exponential tail removal from the upper trace. Input parameters for program 3 of Appendix B are shown.

For a proper analysis of the data it is necessary to determine what the flux distribution is in the molecular center-of-mass system. In general, it is necessary to do this by a forward calculating simulation procedure, since apparatus resolution factors have a significant effect on the observed distribution. When convolution effects are at all significant and the actual data has any believable amount of statistical noise in it, all of the non-simulation deconvolution procedures that we have tried found themselves doomed to a numerical holocaust. Thus the need for trial-and-error forward fitting procedures. However, when resolution factors are sufficiently

small, even if they do obscure some features of the data, the use of direct inversion of the data can be very helpful as a first step in the analysis. This is done by simply solving the transformation equations for the center-of-mass to lab transformation with use of delta function resolution parameters set at either the average or the most probable value for each parameter. The transformation equations have been very well discussed before[36,37] and will be only briefly stated here. Equation 1 expresses the conversion of the center-of-mass flux per unit time per unit solid angle into the laboratory distribution of the same units at a given lab angle.

$$I_{LAB}(v, \theta_{LAB}) = \frac{v^2}{u^2} I_{C.M.}(u, \theta_{C.M.}) \tag{1}$$

The laboratory velocity is v and the center-of-mass velocity is u. Since an electron impact ionizer is sensitive to number density not flux, the lab signal is given by

$$N_{LAB}(v, \theta_{LAB}) \propto \frac{v}{u^2} I_{C.M.}(u, \theta_{C.M.}) \tag{2}$$

However, we measure this distribution as a function of time, not velocity, and since $t = l/v$ where l is the flight path length, we achieve:

$$N_{LAB}(t, \theta_{LAB}) \propto \frac{v^3}{lu^2} I_{C.M.}(u, \theta_{C.M.}) \tag{3}$$

Additionally, it is more convenient to discuss the center-of-mass distribution in terms of energy rather than velocity, and since $E_{C.M.} \propto u^2$ we find:

$$N_{LAB}(t, \theta_{LAB}) \propto \frac{v^3}{lu} I_{C.M.}(E_{C.M.}, \theta_{C.M.}) \quad (4)$$

For direct inversion purposes, l is assumed constant and may be ignored, thus solving for the desired quantity:

$$I_{C.M.}(E_{C.M.}, \theta_{C.M.}) \propto t^3 u N_{LAB}(t, \theta_{LAB}) \quad (5)$$

where t is the laboratory flight time. The center-of-mass velocity is used instead of $\sqrt{E}$ since it is directly calculated by vector subtraction. Care must, of course, be taken in the use of this formula to insure that all calibration effects (ion flight times and electronic delays, etc.) are accounted for in t, otherwise large errors will result.

The results of applying equation 5 to the smoothed and stripped data of Fig. 5 are shown in Fig. 6. The listing of the program CMNRG4 used in this inversion is given in Appendix B. The program outputs the results both to a line printer and to a Hewlett-Packard 7200A Graphic Plotter. Peaks from both the $I\ ^2P_{3/2}$ (higher translational energy) channel and the $I\ ^2P_{1/2}$ channel are seen. The $^2P_{3/2}$ channel has an energy spread of approximately 15 kcal/mole while

the $^2P_{1/2}$ channel has a spread of roughly 10 kcal/mole. Since we will proceed below with a full forward convolution analysis, we need to use these inversion results only to determine a "threshold" for the peaks and a rough initial vibrational state distribution. Since the difference in the center-of-mass angles for the center of the two peaks is only ~4° angular dependence effects are small and skewing of the distributions can be ignored. Sparing the reader the actual trial and error iterations, we found the most acceptable threshold for the I $^2P_{1/2}$ channel to be 32.5 ± 0.5 kcal/mole. With the known spectral splitting in I of 7603 cm^{-1} (21.74 kcal/mole),[38] and a photon energy of 266 nm (107.49 kcal/mole), we calculate a value for the bond dissociation energy of the C-I bond in CH_3I to be 52.9 ± 0.5 kcal/mole. This is significantly lower than the value of 55.0 ± 1 kcal/mole calculated by Riley and Wilson[39] from data complied by Kerr.[40] Riley and Wilson were not able to produce an independent measurement of the bond strength as they used an effusive beam source and did not have sufficient apparatus resolution. The recommended value from the National Bureau of Standards is 54 ± 3 kcal/mole.[41]

The question of which vibrational states are excited and to what degree must also be answered. Fortunately, we are able to determine that only the umbrella motion is excited. The normal modes of CH_3I are given by Herzberg.[42] There are six types of vibrations of which three are of a_1 symmetry and three are of e symmetry. Since both the ground and excited electronic states involved are of A_1

symmetry,[43] the vibrations of e symmetry will not be excited. This leaves only the a_1 modes, two of which asymptotically correlate to the CH_3 umbrella bend and one to the symmetric C-H stretch. Since the stretching force constant for a C-H bond in a radical does not severely differ from that in an sp^3 hybridized system,[42] we may expect the symmetric stretch to have an energy of the order of 3000 cm^{-1} (~8.6 kcal/mole). Certainly we would have resolved in the laboratory such a large spacing between states if these were the only states excited or even the major contribution. Thus we can conclude that our distribution consists primarily of umbrella bends. If there were significant amounts of the symmetric stretch, it should be superimposed on the umbrella bend distribution and one might expect evidence of an extra peak or at least a shoulder. Since there are no obvious breaks in the shape of our curves, we will assume that the amount of symmetric stretch is negligible.

The forward convolution simulation analysis is now much simplified with only one vibrational mode to consider. The basic methodology of forward simulation has been discussed by Carlson[33] wherein he includes a listing and description of his program. The procedure that we use here takes into account the same instrument factors, as it must, and thus will produce the same output for a given input. However, the algorithms used to perform the task are very different. Carlson's program required computational time of the order of a minute on a

CDC 7600 to calculate the time-of-flight distribution due to a delta function energy distribution. Our program (SIMS7, written by Dr. K. Shobatake) requires less than one half hour on a PDP 11/03 with EIS/FIS to calculate the entire time-of-flight distribution resulting from over 300 energy distribution points. Considering that we are comparing execution times of a 16 bit microcomputer against an awesome mainframe number cruncher, this represents a factor of several thousand increase in program efficiency. Unfortunately, Dr. Shobatake's program is not in a sufficient state of documentation to allow its inclusion in an appendix, thus only the relevant parameterizations and results will be discussed here.

The center-of-mass energy distribution is represented by a sum of RRK type functions, each function normally corresponding to a single vibrational state with the functional distribution intended to represent the distribution of rotational states for each vibrational state. The functional form for the translational energy released is:

$$P(E) + \sum_{i=1}^{n} \begin{cases} C_i(E-A_i)^{\alpha}(B_i-E)^{\beta} & A_i \leq E \leq B_i \\ 0 & E < A_i \text{ or } E > B_i \end{cases} \qquad (6)$$

Since we normally held α, β, and B_i-A_i constant for all vibrational states, the relative intensities were represented by the C_i. In general one must integrate this function (the result is a combination

of Gamma functions) and normalize it. The parameter B_i serves as the effective "threshold" of the vibrational state while B_i-A_i represents the maximum amount of rotational excitation allowed. The slopes of the function at A_i and B_i as well as the position of the peak between A_i and B_i are determined by $\breve{\alpha}$ and β. Our nominal best fit translational energy distribution and the result of its forward convolution into laboratory time space are shown in Fig. 7. The results of a calculation with the same parameters except for a doubling of the assumed rotational width is shown in Fig. 8. The parameters used for both of these fits are shown in Table I. We have used the bond energy of the C-I bond discussed above and a CH_3 vibrational spacing of 612 cm^{-1} (1.75 kcal/mole)[44-46] to determine the B_i values for the narrow rotational state fit. For the doubled rotational width, the position of the distribution maximum for each vibrational state was held constant while B_i-A_i was doubled. Constancy of the peak position resulted in an increase in the B_i paramters of 0.3 kcal/mole.

A careful inspection of Figs. 7 and 8, concentrating on the slower ($I^2P_{1/2}$) peak for which the resolution is higher, shows that the increase in the rotational width of the states does have a broadening effect on the calculated distribution. Also the position of the peak seems to have moved to slightly longer times. This is admittedly somewhat difficult to see in the figures, however, it is quite evident in a full scale plotter output. If

Table I. Translational Energy Distribution Parameters

Channel	State	Best Fit C_i	Best Fit B_i kcal/mole	Best Fit (B_i-A_i) kcal/mole	Double Rotational Width C_i	Double Rotational Width B_i kcal/mole	Double Rotational Width (B_i-A_i) kcal/mole
$I^2P_{1/2}$	v=4	1.8	25.79	1.0	1.8	26.09	2.0
	3	8.0	27.54	1.0	8.0	27.84	2.0
	2	20.0	29.29	1.0	20.0	29.59	2.0
	1	6.0	31.05	1.0	6.0	31.35	2.0
	0	1.5	32.80	1.0	1.5	33.10	2.0
$I^2P_{3/2}$	10	0.32	37.04	1.0	0.32	37.34	2.0
	9	0.64	38.79	1.0	0.64	39.09	2.0
	8	0.94	40.54	1.0	0.94	40.84	2.0
	7	1.30	42.29	1.0	1.30	42.59	2.0
	6	1.80	44.04	1.0	1.80	44.34	2.0
	5	3.17	45.79	1.0	3.17	46.09	2.0
	4	4.07	47.54	1.0	4.07	47.84	2.0
	3	3.86	49.29	1.0	3.86	49.59	2.0
	2	1.87	51.04	1.0	1.87	51.34	2.0
	1	0.56	52.79	1.0	0.56	53.09	2.0
	0	0.04	54.54	1.0	0.04	54.84	2.0

$\beta = 0.9$, $\alpha = 2.1$ for all states.

the rotational width were again doubled, the calculated peak shape would differ from the measured by much more than statistical error. From this information, we conclude that the widths of the rotational distribution of the vibrational states (at least from the $^2P_{1/2}$ channel) is on the order of or less than the spacing between the vibrational states.

Also the positioning of the threshold, determining the C-I bond strength, may be investigated. Certainly, in order to maintain the same calculated TOF peak position, the "center-of-mass" of the input energy distribution must remain essentially constant. Again concentrating on the $^2P_{1/2}$ channel, if we shift the positions of the vibrational states by half of their spacing, we would require two peaks in the center of nearly the same height. This produces a very flat-topped peak relative to the measured one. Additionally, the necessity of fitting intensities in the wings of the peak becomes a problem. In fact, there is really rather little fexibility in the positions of the peaks of the vibrational distributions and their relative intensities. The main factor causing uncertainty in our assigned threshold values are the shapes and widths of the rotational distributions. If there is no rotational excitation at all, our threshold released energies would have to be reduced by 0.3 kcal/mole thus increasing the assigned C-I bond strength by the same amount. If rotational excitation is significant (which seems unlikely), the opposite effect would occur, however its magnitude would depend on the shape of the actual rotational distribution. One further point,

we have assumed that all of the vibrational states are separated by the same energy as the v=0→1 transition, however, calculations have shown the potential to have a very strong negative anharmonicity.[44] Since it is the positioning of the v=2 state which is most accurately determined, this would increase the v=0→2 spacing, thus increase released energy, and decrease the assumed C-I bond strength. However, this effect should be much lower than other uncertainties.

It is at least instructive to now compare the results of the single Newton diagram inversion with the results of the forward convolution calculation. Since we now recognize that, for the $I^2P_{1/2}$ channel, the peak of the TOF distribution is produced almost solely from the v=2 state, we can determine the relative vibrational state distribution from the inverted data by simply looking at the intensity right at the peak and at points displaced from the peak by an amount equal to the vibrational state energy separation. The results of applying this procedure to the trace of Fig. 6 are shown in Table II. If we compare these results to those in Table I, we find that they are remarkably similar. This similarity is, of course, due to the fact that the convolution broadening is on the order of the separation between states and not significantly larger than that. The convolution calculation was instrumental in determining an accurate threshold value which could only be roughly guessed from the inversion calculation, as well as in indicating that the rotational width is probably less than or near the vibrational spacing. These conclusions are quite good for the $I\ ^2P_{1/2}$ channel, since it has significantly lower lab velocity than the $^2P_{3/2}$

Table II. Relative Intensities from Direct Inversion

Channel	State	Intensity	Channel	State	Intensity
$I^2P_{1/2}$	v=4	2.3	$I^2P_{3/2}$	10	0.32
	3	13.1		9	0.64
	2	20.0		8	1.04
	1	7.0		7	1.44
	0	1.4		6	2.12
				5	3.52
				4	4.12
				3	3.40
				2	1.76
				1	0.56
				0	0.04

channel. The resolution factors for the $^2P_{3/2}$ channel are, of course, worse than for the $^2P_{1/2}$ channel, thus we cannot claim to have hardly any information on the rotational distribution for that channel, however, the vibrational distribution should be good if one allows that the true distribution does not have any oscillatory structure.

DISCUSSION

The first ultra-violet absorption band of CH_3I has been extensively investigated both experimentally[43,47-49] and theoretically.[50,51] The transition corresponds to the excitation of an electron from a non-bonding npπ orbital localized on the I atom to an anti-bonding σ* molecular orbital between the C and I atoms. The band consists of the superposition of transitions to three states, the ^1Q, $^3Q_0$ and $^3Q_1$ in Mulliken's notation.[50] The ^1Q and $^3Q_1$ correlate to ground state I atoms and ground electronic state CH_3 radicals. The $^3Q_0$ state correlates to an excited $I(^2P_{1/2})$ atom and ground state CH_3. The magnetic circular dichroism resolution of the bands by Gedanken and Rowe[48] shows that approximately 95% of the absorption at 266 nm is due to the $^3Q_0$ band. When the symmetry of the states are considered under strong spin orbit interaction, a state of A_1 symmetry correlating to $I(^2P_{1/2})$ is seen.[51] This state corresponds to the $^3Q_0$ state. The state is non-degenerate and thus does not exhibit a Jahn-Teller distortion[50] while the transition moment is parallel to the C-I bond. The other two Q contributions are perpendicular transitions and can exhibit Jahn-Teller distortions.

The polarization dependence of the photodissociation of CH_3I has been studied by Riley and Wilson[39] and by Dzvonik, Yang and Bersohn.[52] Both have found the transition to be parallel. Riley and Wilson were able to distinguish between the $I(^2P_{1/2})$ and $I(^2P_{3/2})$ channels and observed that approximately 20% of product is formed in the ground $^2P_{3/2}$ state. The production of the ground state by a parallel transition indicates the existence of a curve crossing in the dissociation. Donohue and Wiesenfeld[43] have studied the relative production of ground state I atom from photodissociation after broad-band irradiation and found that roughly 8% of I atoms are produced in the ground state.

The knowledge that the excited state symmetry is A_1 has already been used above to determine that only the umbrella bend vibration is excited in the CH_3 radical. However, the fact that the $^3Q_0$ state cannot Jahn-Teller distort is also relevant to the product energy disposal. If, in the excited molecular state, the equilibrium position for the C-I bond is on the molecular symmetry axis, an impulse acting along that bond will have little ability to excite rotations in the departing methyl group. The center-of-mass of the methyl group would lie directly in line with the force vector, and no angular momentum could be imparted. However, if the excited state had a bent or otherwise distorted geometry, two factors could cause significant rotational excitation. First, the methyl group center-of-mass might not lie on the same line as the C-I bond axis and even a force acting directly on

that line could cause rotational excitation. Second, the C-I force might not be exactly in line with the bond, but rather could have a "sideways" component which would force rotation of the methyl group. This second factor would be significant for the case of a normal ground state being excited to a bent excited state. The fact that the excited state which we are probing cannot distort means that the methyl group will see very little if any torque upon dissociation and thus should not be highly rotationally excited. This is consistent with the results of the forward convolution analysis.

The energetics of CH_3I dissociation have also been investigated in matrix studies by Bass and Pimentel[53] and with photofragment spectroscopy by Riley and Wilson.[39] Bass and Pimentel predicted an umbrella bend excitation of CH_3 of the order of 10 kcal/mole, however they measured an effective temperature in the range of 1500 to 3000°K. They attributed this low temperature to a moderation of the methyl radicals' energy before they reacted with matrix partners. Riley and Wilson reported an internal excitation of the CH_3 radical of 3.9 kcal/mole for the $I(^2P_{1/2})$ channel and 8.6 kcal/mole for the $I(^2P_{3/2})$ channel. They were not able to obtain information on the distribution of vibrational states, however they performed an array of model calculations to attempt to determine the major features of the energy disposal mechanism. They determined that statistical models vastly overestimated the internal excitation, while a model in which the C-I interaction was treated as strictly impulsive was much better but still

yielded too great a value. Due to lack of resolution in their data, they did not attempt calculations for realistic (less than impulsive strength) potentials.

Consistent with our higher resolution data, it is only appropriate that we give a more thorough discussion of the mechanism of internal excitation. We present below model calculations for both a classical and a semi-classical forced oscillator as well as a discussion of Franck-Condon factors. The forced oscillator treatments will be based on relationships derived for a collinear triatomic system, however, this should be a good approximation for methyl iodide due to the lack of importance of product rotation and the lack of assymetric distortions of the excited state.

FORCED OSCILLATOR

A. Classical

The analytical expression for the amount of energy transferred to a classical oscillator initially at rest but undergoing a time dependent force F(t) is well known.[54] The result for the energy ΔE absorbed is:

$$\Delta E = \frac{1}{2m} \left| \int_{-\infty}^{\infty} F(t) e^{-i\omega t} dt \right|^2 \qquad (7)$$

where m is the reduced mass of the oscillator and ω is its charasteristic angular frequency. A derivation of ΔE for a particular system must, then, concentrate on determining the force F(t). We will sketch below a derivation of the relative energy transferred, ΔE/E, where E is the total energy available to the oscillator. We will concentrate on the results for a half collision although the results for a full collision will be shown for comparison. The method used is that of Mahan.[55,56] The point of the exercise is to get the mass factors correct, since they differ between full and half collisions. Also the mass factors used for full collisions were incorrect for many years.[56] Care must be taken to insure that the function behaves properly in the pure impulsive limit. Additionally, it will be shown that the crude approximation:

$$\Delta E_{\text{half collision}} = \frac{1}{4} \Delta E_{\text{full collision}} \qquad (8)$$

is in general quite incorrect and dangerous. Even though it seems

intuitively reasonable, since $\Delta E = (\Delta p)^2/2m$ and $\Delta p = F\Delta t$, and recognizing that $\Delta t_{\text{half collision}} = \frac{1}{2}\Delta t_{\text{full collision}}$, the above relation only holds for forces of very short duration such that $e^{i\omega t} \sim 1$ whenever $F(t) \neq 0$.

We wish to solve the problem for a tractable but fairly realistic model. We will consider the interaction of an atom A with a diatomic molecule BC. All three particles will be constrained to a line. The interaction between B and C will be a harmonic oscillator potential $V_o(y) = \frac{1}{2} f(y-y_o)^2$ where y_o is the equilibrium separation. The influence of the atom A will be through an exponential potential acting only between atom A and B; that is $V'(x,y) = A'e^{-(x-\gamma y)/L}$. The coordinate system is shown in Fig. 9. After the standard decoupling approximation[55] and the appropriate transformation of variables,[55] the equations we need to solve are:

$$m_1 \ddot{X} = \frac{D}{L} e^{-X/L} \tag{9}$$

$$m_2 \ddot{Y} + f(y-y_o) + \frac{\gamma A''}{L} e^{-X/L} = 0 \tag{10}$$

where

$$A'' = A'e^{\gamma y_o/L}, \quad \gamma = \frac{C}{B+C} \tag{11}$$

D is the potential energy at $y = y_o$ and the turning point in x. x is zero at the turning point. A, B, and C represent the masses of particles A, B, and C. m_1 must be considered as the reduced mass AB/(A+B) rather

than the once used A(B+C)/(A+B+C), since the interaction is considered to take place between A and B impulsively, thus not involving C.[56] m_2 is the reduced mass of the diatomic oscillator BC/(B+C). Equation 9 may be solved for x, which may then be used to determine the force between A and B:

$$F(t) = -\gamma \frac{D}{L} e^{-X/L} = -\gamma \frac{D}{L} \operatorname{sech}^2\left(\frac{v_o t}{2L}\right) \tag{12}$$

where v_o may be considered as either the initial or final (if no energy exchange occurs) velocity of the projectile A relative to B. Our expression for the total energy transferred is now

$$\Delta E = \frac{1}{2m_2}\left(\frac{\gamma D}{L}\right)^2 \left(\frac{2L}{v_o}\right)^2 \left| \int_{-\infty}^{\infty} \operatorname{sech}^2(\tau) e^{i\lambda\tau} d\tau \right|^2 \tag{13}$$

where $\lambda = 2\omega L/v_o$.

Of course, the limits of integration should be from 0 to ∞ for the case of half collisions. As Mahan points out, the proper evaluation of D is[55]

$$D = \frac{1}{2} \frac{AB}{A+B} v_o^2 \tag{14}$$

not

$$D = \frac{1}{2} \frac{A(B+C)}{A+B+C} v_o^2 \tag{15}$$

This is true (14) for both full and half collisions. To determine the relative energy transferred $\Delta E/E$, we must know the total energy E available to the system. This is the point of major divergence between full and half collisions. Equivalently asked, we have the problem of the proper calculation of the parameter v_o. For full collisions the answer is the standard expected term. The energy E is just the total available collision energy and v_o is the initial relative velocity between A and B. However, since B is attached to C at initial asymptotic conditions, v_o is just the initial relative velocity of A with BC, thus:

$$E_{\text{full collision}} = \frac{1}{2} \mu_{A,BC} v_o^2 = \frac{1}{2} \frac{A(B+C)}{A+B+C} v_o^2 \qquad (16)$$

For half collisions, the total energy available is equal to the potential energy at the starting conditions (turning points for a full collision), but that is properly related to v_o by equation (14), thus

$$E_{\text{half collision}} = D = \frac{1}{2} \frac{AB}{A+B} v_o^2 \qquad (17)$$

The difference between these two terms is not so much due to a difference in the physics of the two processes, but rather in the semantic terms we use to discuss it. Since we are using an impulse approximation (particle C does not participate in the dynamics during the time of the collision), the actual energy available to the system is given by

equation (14). The energy that we normally talk about for photodissociation is exactly this potential energy available to the system and thus the simplicity of equation (17). However, the amount of energy that we conventionally discuss for full collisions is calculated in terms of the center of mass frame of the entire system A + BC. The reduced mass for the total system is larger than that for the system A + B within which we assume the actual dynamics is occurring, thus we calculate a higher available energy than is consistent with our original assumptions. Of course, if the system were not purely impulsive, some of this "excess" calculated energy could participate in the dynamics. This ambiguity in choice of center-of-mass systems does not occur for a photodissociation problem, since at the initial conditions in which we define our energy terms, the three particles have no relative motion thus the two center-of-mass frames are equivalent. The confusion for half collisions enters into the interpretation of the v_o term. For half collisions, v_o must be carefully treated as the asymptotic velocity between A and B if C were not present. This distinction is unnecessary for full collisions since one reaches the same answer with or without C. There simply is one and only one initial collision velocity.

One may now perform a little simple algebra and calculate expressions for $\Delta E/E$. The results are (from equation (13)):

$$\left(\frac{\Delta E}{E}\right)_{\text{full collision}} = \frac{ABCM}{(A+B)^2(B+C)^2} \left| \int_{-\infty}^{\infty} \text{sech}^2(\tau) e^{i\lambda\tau} d\tau \right|^2 \qquad (18)$$

and

$$\left(\frac{\Delta E}{E}\right)_{\text{half collision}} = \frac{AC}{(A+B)(B+C)} \left| \int_0^\infty \text{sech}^2(\tau) e^{i\lambda\tau} d\tau \right|^2$$

where $M = A+B+C$ and $\lambda = 2\omega L/v_o$.

In the first of equations 18, we have a symmetric range of integration and thus only the cosine term of the exponential will contribute. This integral is known analytically.[57] Making this simplification we now have:

$$\left(\frac{\Delta E}{E}\right)_{\text{full collision}} = \frac{4ABCM}{(A+B)^2(B+C)^2} \lambda'^2 \text{csch}^2(\lambda') \qquad (19)$$

where $\lambda' = \pi\omega L/v_o$

and

$$\left(\frac{\Delta E}{E}\right)_{\text{half collision}} = \frac{AC}{(A+B)(B+C)} \left[\lambda'^2 \text{csch}^2(\lambda') + \left| \int_0^\infty \text{sech}^2(\tau) \sin\lambda\tau d\tau \right|^2 \right] \qquad (20)$$

To insure the correctness of these expressions, one should investigate the limit of purely impulsive behavior. This would occur either with a sharp potential (L small), a weak oscillator (ω small) or high collision energy (v_o large). Thus the classical impulse limit is reached

for λ' and λ tending to zero. The term $\lambda'^2 \mathrm{csch}^2(\lambda')$ tends to 1 while the integral containing $\sin\lambda\tau$ vanishes. It can readily be verified that the remaining factors do correspond exactly to a classical hard impulse for each case. One may also show that this limiting value is the same as the expression containing a ratio of reduced masses used by Riley and Wilson.[39]

The dangers of considering a half collision as being merely a simple special case of a full collision should now be obvious. Indeed we do see a factor of 4 appearing in the full collision case that is not in the half collision expression, however even the mass factors expressing the hard impulse limit are different. Also, for any collision softer than purely impulsive, the sine integral in the half collision expression will contribute additional excitation. The fact that the force is turned on suddently at t=0 actually can make a significant contribution to the vibrational excitation. A quantitative measure of this contribution is certainly in order and is quite instructive.

Figure 10 shows the contribution of both transform terms in equation (20) compared with the contribution of only the cosine term. Since it was necessary to evaluate the contribution of the sine term numerically anyway, the total contribution and each component were evaluated using Simpson's rule with a simple interactive Fortran program. The integration grid density was interactively increased for each value of λ until satisfactory convergence was obtained. It should be clear from the figure that, as the system parameters move

further away from the hard impulse limit, the effect of the sine term becomes more and more significant. For $\lambda \geq 3$, almost the entire contribution to the excitation comes from the sine term. In fact, in the high λ regime, a full collision would produce essentially no energy transfer whereas a half collision may still produce nearly 10% of its limiting value. Certainly half collisions may behave very differently from full collisions and should be treated with care.

A crude first order application of this model to CH_3I photodissociation is quite straightforward, if we assume that the most probable observed excitation corresponds to the classical predicted excitation. Our most probable observed excitation for the $I(^2P_{1/2})$ channel is to v=2, which corresponds to 10.7% excitation of the available 32.8 kcal/mole. The hard impulse limit excitation is 18.3%, thus we see 58% of the limiting value. Reading directly off of Fig. 10, we find this value of 0.58 corresponds to a value of λ of 1.35. A vibrational spacing of 613 cm^{-1} implies that $\omega = 1.155 \times 10^{14}$ sec^{-1} and an available energy of 32.8 kcal/mole gives a value for v_0 of 5.003×10^5 cm/sec. These parameters, then produce a value for L, the exponential range parameter of the potential, of 0.29 Å. This number alone certainly does not determine the potential for this state. We would need also some knowledge of the turning point for the C-I bond distance. One could assume that distance is near the equilibrium ground state C-I bond length, and could thus have a complete potential form. However, it is certainly presumptory to assume that the potential is actually represented well by an exponential form or that this very

simplistic procedure should be adequate to determine potential parameters.

In any case, it is instructive to attempt to determine whether our simple classical model yields a potential of roughly reasonable values. Since any estimation of the potential at these energies should hopefully produce a reasonable value of the slope of the potential even if the functional forms differ, we will compare the slope of the above determined form with two other determinations. Even though we have not determined the turning point for our model we can evaluate the slope of the potential at the turning point. The slope at the turning point is -D/L which equals -113.1 kcal/Å mole. We can compare this directly to the value of -108.6 kcal/Å mole given by Porret and Goodeve.[47] This amazingly close agreement is almost certainly accidental, but it does suggest that the classical impulse model is at least not grossly in error. Another potential form that can be used as a test of reasonableness is the anti-Morse function proposed by Sato.[58] It has, however, been proposed that the anti-Morse function is, in fact, a factor of two too strong.[59] This, of course, changes the slope by a factor of two. The standard anti-Morse function has the form:

$$V_{\text{anti-bond}}(r) = \frac{D_e}{2}\left[e^{-2\beta(r-r_0)} + 2e^{-\beta(r-r_e)}\right] \qquad (21)$$

where D_e, β, and r_e are to be determined from the bonding potential.

D_e is the value of the potential minimum relative to zero asympotically. r_e is the equilibrium internuclear distance for the bound state, and β determines the force constant of the bound state potential. Using approximate relations[60] between these parameters and known spectroscopic constants[61]

$$D_e\beta^2 \cong \frac{1}{2} k_e \tag{22}$$

and

$$D_e \cong D_0 + \frac{1}{2} hc\omega_e \tag{23}$$

we can determine the potential function. To determine the oscillator force constant k_e one needs a frequency and a reduced mass. For CH_3I, the $\nu_3(a_1)$ mode[61] corresponds very closely to a simple C-I stretch with little hydrogen motion, thus we can approximate it as harmonic with the given frequency and a reduced mass of 15·127/142. The resulting values we find are:

$$\beta \cong 1.74 \text{ Å}^{-1}$$

and

$$D_e \cong 53.66 \text{ kcal/mole}$$

If we use the full anti-Morse function, we find that it has a value of 32.8 kcal/mole at $r-r_e$ = 0.41 Å, and at that point has a slope of -68 kcal/Å mole. Using the half-magnitude anti-Morse function one finds a potential match at $r-r_e$ = 0.0697 Å where the slope would now be -77.8 kcal/mole Å. The slopes at $r=r_e$ would be -186 and -93 kcal/mole Å respectively. As one may demonstrate with a very simple calculation, the classical amplitude for the C-I stretch is only 0.069 Å, and this value when used with the reflection principle, well approximates the width of the CH_3I absorption peak. Thus it is clear that the full anti-Morse function is a very bad approximation for CH_3I since an energy matching at 0.41 Å = $r=r_e$ would produce almost no oscillator strength in contrast to the actual strong absorption of CH_3I. The half anti-Morse function, however, seems to be a fairly good approximation in that it matches the available energy in the absorption at an $r-r_e$ value near what one would estimate and it also produces a slope that is near the other two determinations. It is certainly neither obvious nor necessary that this should be so since we have used ground electronic manifold bonding parameters to predict the anti-bonding potential of a different electronic manifold. Also since there seems to be a curve crossing that produces ground state iodine atom, there are clearly potentials in this system with widely differing slopes.

The simple classical model used above certainly seems to be surprisingly successful if comparison to the results of Porret and

Goodeve[47] is any measure. However, in spite of its apparent success, it lacks the ability to calculate the distribution of vibrational states. It can only calculate a single amount of energy transferred. We can, however, use a simple semi-classical extension of the classical forced oscillator to allow us to calculate a distribution of states. The semi-classical transition probabilities (squares of S matrix elements) are given by:[16]

$$P_{nm} = |S_{nm}|^2 = m!n!\varepsilon^{m+n}e^{-\varepsilon}\left|\sum_{\ell=0}^{\min(m,n)}\frac{(-\varepsilon)^{-\ell}}{\ell!(m-\ell)!(n-\ell)!}\right|^2 \qquad (24)$$

where ε is the classical energy transferred to the oscillator in units of oscillator quanta and n and m are the final and initial oscillator quantum numbers. Since the expression is just the square of a single S matrix element, it only represents the transition probability to state n from a <u>pure</u> initial state m. The expression also has the distressing analytic property of having a great many zeroes and at some physically unrealistic places. In particular $P_{lm}(\varepsilon)$ is identically zero for all integer $\varepsilon = m$. In fact, if one fixes n and tries to solve for $\varepsilon(m)$ such that $P = 0$, you rapidly find that you get polynomials in ε of order n. For all odd n you must have at least one real root, and for many even n you are likely to get a few real roots. Due to this disgusting and non physical analytic behavior, the general form above was not used.

However, if we only wish to calculate a distribution based on the same assumptions made above for the purely classical case, life is a little happier. In the classical calculations, it was assumed that the oscillator was initially at rest. If we make the same assumption for the semi-classical case, the general distribution reduces to a well-behaved Poisson distribution:

$$P_{n\leftarrow 0} = \frac{\varepsilon^n e^{-\varepsilon}}{n!} = \frac{e^{n\ell n\varepsilon} e^{-\varepsilon}}{\Gamma(n+1)} \tag{25}$$

We may use this function to obtain an estimate of ε from our data and then from ε we may use the above classical procedure again to estimate the steepness of the potential. One may readily show that, at the maximum of the Poisson distribution, the following relation holds:

$$\frac{\Gamma'(n+1)}{\Gamma(n+1)} = \ell n\varepsilon \tag{26}$$

Since, from our data, we know that $n = 2$ at the maximum of the measured distribution, we may determine ε. Conversely, we may use the value of $\varepsilon = 2$ assumed above for the classical calculation and determine the value of n where the maximum would then occur. In either case, we need knowledge of the values of the function Γ'/Γ. This function itself is well characterized and is referred to as the Ψ function. Tables for values of $\Psi(x)$ for $1 \leq x \leq 2$ may be found in Abramowitz and Stegun.[62]

To extend the table into the value range we need, we have used the recursion relation:[62]

$$\Psi(z+1) = \Psi(z) + \frac{1}{z} \tag{27}$$

With the extended table, one finds that a value of $\varepsilon = 2$ corresponds to $n \cong 1.48$ and that a value of $n = 2$ corresponds to $\varepsilon = 2.516$. Certainly a value of $n = 1.48$ is too low, as this would imply that the amount of $v = 1$ and $v = 2$ CH_3 product were exactly equal. This is certainly not the case; the $v = 2$ intensity strongly predominates. Thus it seems reasonable that we adjust upward our estimate of ε from 2 to something near 2.5. This is, of course, reasonable behavior for the Poisson distribution, as ε represents the average amount of energy transferred. However, due to the long tail of the Poisson distribution, the average value exceeds the most probable value. Using this new estimate of ε we may determine, from Fig. 10, a new value for $\lambda(L)$ and thus a new slope of the potential. The new value for λ is 0.98 which gives $L = 0.21$ Å and thus a slope of -155 kcal/Å mole. This value is actually approaching that of the full anti-Morse function calculated above at $r = r_e$ and much exceeds the Porret and Goodeve value.

Although we can match the peak of a Poisson distribution to that of our measured distribution, the question of the appropriateness of the distribution as a whole is still open. Figure 11 shows our

measured distribution plotted for comparison along with the Poisson distributions for both $\varepsilon = 2$ and $\varepsilon = 2.5$. We see that the distribution for $\varepsilon = 2$ gives values for $v = 0$ and $v = 1$ that are completely unreasonable, while those for $v = 3$ and 4 are more reasonable, but the calculated distribution still has a tendency to be too broad. The calculated distribution for $\varepsilon = 2.5$ clearly has the right peak position as it must, but it very clearly is too broad, indicating a much higher intensity for $v = 5$ and 6 than is possible. Though our data cannot really determine that the amount of $v = 5$ and 6 is zero, it is certainly less than 26% of the $v = 2$ intensity. Certainly a simple Poisson distribution does not adequately represent our data. It is, of course, possible that the semi-classical model itself is at fault, however, the work of Heidrich, Wilson, and Rapp[16] showed remarkably close agreement for the semi-classical and fully quantum calculations for a oscillator starting in $v = 0$. This agreement broke down for an initially excited oscillator due to the bad analytic nature of the semi-classical procedure discussed above. It seems, rather, more likely that the model itself is reasonably accurate but that the assumption of an initially at rest oscillator is in error. The Poisson distribution even for $\varepsilon = 2$ was too broad, indicating that too much excitation and mixing from the potential surface is being assumed. If a value of ε sufficiently small to reproduce the measured width is used, then the total amount of excitation produced is too small. It seems that the oscillator begins its scattering on the potential surface already in excited vibrational states.

The amount of vibrational excitation in a molecule immediately following the absorption of a photon is determined by the Franck-Condon factors for that absorption. We will discuss here, qualitatively, the importance of the Franck-Condon factors for CH_3I photodissociation. Although the above analysis is suggestive of the need to consider Franck-Condon factors, other information about CH_3I makes their consideration mandatory. The methyl group undergoes a very strong change both in the geometry of its equilibrium configuration and in the force constants of the potential during the transition from CH_3I to free CH_3. The ν_2 vibration in CH_3I corresponds most closely to the free methyl umbrella bend, and has a vibrational energy of 1251 cm^{-1}.[42] The free methyl group is planar and has a vibrational energy of 613 cm^{-1}.[44,46] Assuming that the effective reduced mass factors for the two systems are nearly the same, this difference in vibrational spacing by a factor of 2 corresponds to roughly a factor of 4 change in the force constant. Using the geometrical parameters estimated in reference 42, p.439, one may calculate that the C-H bond in CH_3I is roughly 16.6° out of the plane that passes through the carbon atom perpendicular to the C-I bond. This angle is the angular change that the methyl group must undergo in becoming a free methyl radical. Both of these factors constitute a rather severe change in the forces seen by the methyl group as it undergoes the change in its orbital hybridization from sp^3 to sp^2.

One should be careful not to carry the comparison between ground state CH_3I and free CH_3 radical too far. Certainly a reasonable amount of information is available on both species and many comparisons can be made. It is even tempting to try to calculate the Franck-Condon factors between the two species. Bass and Pimentel used such a type of argument to estimate the expected vibrational excitation of CH_3 assuming its potential were near that of BBr_3.[53] However, the truly important issue is the differences between the ground state potential and the excited state potential with the C-I bond length still the same as in the ground state. The free methyl radical potential is what the system sees asymptotically after dissociation is complete. The two potentials can and should be quite different. In general, it is even possible for a system to dissociate into products with geometry radically different from the ground state but with no vibrational excitation at all. This could happen if the excited state potential for a vertical transition looked exactly like the ground state and all the change in the equilibrium geometries occurred as the particles separated. If the particles separated slowly enough (adiabatically) no crossing even of vibrationally labeled surfaces would occur and the asymptotic products would be unexcited. This condition could be met for a system with either a very slowly varying excited state potential (very large L in above models) or with very little asymptotic transitional energy (very small v_0 in above models). Of course few, if any, real systems will behave in this fashion, but one must be wary when making arguments based on asymptotic potentials.

Now, being aware of the above dangers, we shall proceed with a qualitative comparison of the asymptotic states and then do a little guesswork as to what might be happening in the vertically excited state. The Franck-Condon factors between the asymptotic states may be crudely estimated by pictorially locating the positions of the nodes and turning points of the free methyl vibrational wavefunctions and determining for which states significant overlap occurs without the effect of cancellation of two opposite signed "lobes". The vibrational state energies for the free radical were calculated and graphed by Ellison, Engelking, and Lineberger[27] from the potential determined by Marynick and Dixon.[44] In Fig. 12 is shown the potential surface for the umbrella motion along with the vibrational levels and visually located estimates of the wavefunction nodes. Also shown are two vertical lines indicating the probable maximum extent of the ground state vibrational wavefunction for CH_3I. This extent is centered around the θ_e of 16.6° with a width of 12°. The width is estimated by assuming that the force constant for the CH_3I potential is 4 times that of the free CH_3 potential and then computing the ratio of displacements to the classical turning points for particles with the zero point energies of each system. The turning point to turning point distance for free CH_3 is taken as 16°. One may now, by inspection, determine the probable relative values of the Franck-Condon factors. The overlap to v = 0 of free CH_3^* should be quite small, all overlap being in classically forbidden regions, while

v = 1 should have some reasonable overlap. v = 2 and v = 3 probably have the highest overlap and it is not qualitatively clear which is higher. For v = 4 and higher states, nodes have moved into the region of extent of the ground state function, and it can be expected that these states will have very small overlaps due to cancellation effects. A simple classical turning point energy balance argument would place the free CH_3 at an energy between its v = 1 and v = 2 states.

These estimated asymptotic state Franck-Condon factors are really quite similar to our measured vibrational state distributions. However, there seems to be little question from the preceding discussion that collisional effects should be significant. Since, in a classical picture, both the dynamic deformation and the force between the C and I atoms are acting to separate the C and I atoms, it seems very unlikely that CH_3 vibrational energy would be efficiently transferred to translation. It is more reasonable that the oscillator forcing should excite it even further above its Franck-Condon excitation and that this additional excitation should be on the order of one to two quanta, consisted with the above estimate of the potential strength. The overall effect of using asymptotic Franck-Condon factors would almost certainly be to produce a calculated distribution with more excitation than the measured distribution.

Since we do not have any even semi-quantitative information on the vertically excited state potential, its discussion here is forced

to be highly heuristic. The excited state configuration of concern is derived from the ground state by promotion of a non-bonding π electron located on the I atom into an anti-bonding σ^* molecular orbital between the C and I atoms. The excited state bond then contains two bonding electrons and one anti-bonding electron. The anti-bonding electron is obviously of very high energy and has a very rapid energy change with respect to C-I bond distance, since it is sufficient to overcome the effect of both bonding electrons and cause molecular dissociation. The lowest energy state for this configuration will be one which has a low energy for this anti-bonding orbital. Since "hybridizations" which decrease the energy of a bonding orbital will increase the energy of the corresponding anti-bonding orbital, a reduction in the energy of an anti-bonding orbital can be achieved by reducing the hybridizations which decrease the bonding orbital energy. In the ground state CH_3I a good deal of the bond energy is contributed by the sp^3 hybridization of the C atom. With the anti-bonding orbital dominating the energetics of the excited state, it seems likely that the degree of sp^3 hybridization would be much reduced in order to lower the anti-bonding orbital energy. The carbon atom orbitals should tend much more towards sp^2 hybridization in the excited state than in the ground state. Thus we could expect the excited state to be closer to a planar CH_3 structure than the ground state. This tendency toward planarity, of course, cannot be complete since the orbitals around the hydrogen atoms will always tend to avoid those near the I atoms. Thus the

excited state structure should not be totally planar. The force constant for the bending motion probably also lies somewhere between that of the ground state and the free radical. It certainly should be stronger than the free radical since motion towards planarity causes interference with I atom orbitals and motion towards tetrahedral shape should elevate the anti-bonding orbital energy. The hydrogen atoms are caught between a rock and a hard spot relative to the rather unhindered motion in the free radical. A comparison with the ground state force constant is less clear. The reduction in the amount of sp^3 hybridization might argue for a lower force constant, however if the effect of the anti-bonding electron and interference with the I atom orbitals are really quite strong, the excited state force constant could be on the order of or even higher than that of the ground state.

Overall then, we most reasonably expect the excited state potential to lie somewhere between that of the ground state and the free radical. Since, as demonstrated above, even a change in a force constant of a factor of 4 only changes the extent of a wavefunction by $\sim 1/\sqrt{2}$, the excited state wavefunctions should have nearly the same angular widths as the free radical. However, the positions of the wavefunctions will be displaced more towards that of the ground state functions. The resulting effect on the Franck-Condon factors would be to increase the overlap of the lower states and produce sign-change cancellations at a lower vibrational level

than for the free radical. Thus it seems clear that calculating Franck-Condon factors from the asymptotic states would overestimate the initial excitation. The degree of this overestimation is dependent upon the degree to which the excited state tends to look more like the ground state than the free radical.

The overestimation of excitation by the asymptotic Franck-Condon factors is consistent with the above estimation of total product energy. Use of the asymptotic Franck-Condon factors overestimated total excitation. If proper excited state factors were used, the excitation should be reduced and it is quite believable that the combination of both the correct Franck-Condon factors and the impulsive excitation effects would produce results in good agreement with our experiment. It seems certain that scattering effects are important, but they alone should not be sufficient. Franck-Condon factors must be included but should be handled with great care.

Our modelling efforts and discussion have centered almost entirely on the energetics of the excited state $I(^2P_{1/2})$ product channel. This is due to the greater simplicity of that channel since it is the result of development on a single potential energy surface. However, the ground state channel is, in principle, amenable to the same kind of analysis. If it is indeed the result of a curve crossing which occurs some distance down the repulsive potential, the same Franck-Condon analysis should apply for it as for the excited state. That the ground state channel is probably due to a curve crossing rather than state mixing is evident in the lack of any unusual features in the absorption spectrum.

Given that the initial distributions producing the ground and excited states are the same, the rest of the analysis would follow a similar course. Unfortunately, due to the "kink" in the potential surface caused by the curve crossing our simple analytical classical model would have to be replaced by numerical calculations. The qualitative features that would result from such a calculation are, however, quite evident from the single potential case. Sharp slopes and discontinuities in the potential are major cuases of vibrational excitation. Thus the steepness of the walls of both segments of the potential are of importance as is the half collision nature of the event. The major new factor would be the effect of the kink in the potential at the crossing. This feature would contribute significantly to the Fourier spectrum of the potential and thus should have a significant effect on the vibrational excitation. The net result would be that the ground electronic state channel should have significantly more vibrational excitation than the excited state channel, which is in agreement with what we observe. No actual calculations have been attempted due to lack of information concerning the relevant potential parameters.

SUMMARY AND CONCLUSIONS

We have performed a new high resolution measurement of the translational energy distributions of CH_3 fragments resulting from the

photofragmentation of CH_3I at 266 nm. The data have been analyzed both by direct inversion and by forward convolution to yield the distribution of the vibrational levels for the CH_3 umbrella bend for both the ground and excited state I atom channels. The average amount of energy occurring in vibrations from the $I(^2P_{1/2})$ channel has been found to be consistent with a simple classical forced oscillator model. However, when an attempt is made to fit the distribution of states by means of a semi-classical extension of the model, the agreement with experiment is poor. This poor agreement is attributed to possible initial excitation of the methyl radical during the absorption process. A heuristic effort is made at estimating the possible magnitude and distribution of this initial excitation, and it is concluded that the initial excitation should be of importance. However, it is also certain that the scattering effects are significant since a potential surface with a slope sufficient to reproduce the observed absorption spectrum will definitely produce changes in the oscillator vibrational states as the products separate. The energy distribution of the products in the ground state channel must be dominantly determined by the scattering effects since the Franck-Condon factors should be the same as for the excited state channel but the potential surface would have a high slope over a greater extent than the excited state surface.

Thus it seems clear that CH_3I photofragmentation dynamics is determined by Franck-Condon factors and scattering effects. This is

in contrast to the CN containing systems in which it is not clear whether scattering effects are significant. Certainly methyl iodide would present a more rigorous test of present photofragmentation theories than the CN systems. Also, since the dynamics are dominated by effects on the line of the C-I bond, it should not be necessary to extend present theories to bent molecules in order to begin a treatment of this system. It is hoped that this work will prompt a renewal of the theoretical effort in photofragment dynamics as well as serve as an impetus for further experimental investigations.

REFERENCES

1. P. C. Cosby, J. T. Moseley, J. R. Peterson, and S. H. Ling. J. Chem. Phys. 69(6), 2771 (1978).

2. P. C. Cosby, G. P. Smith, and J. T. Moseley, J. Chem. Phys. 69(6), 2779 (1978).

3. P. C. Engelking, G. B. Ellison, and W. C. Lineberger, J. Chem. Phys. 69(5), 1826 (1978).

4. R. Abouaf, B. A. Huber, P. C. Cosby, R. P. Saxon, and J. T. Moseley, J. Chem. Phys. 68(5), 2406 (1978).

5. M. Tadjeddine, R. Abouaf, P. C. Cosby, B. A. Huber, and J. T. Moseley, J. Chem. Phys. 69(2), 710 (1978).

6. K. E. Johnson, L. Wharton, and D. H. Levy, J. Chem. Phys. 69(6), 2719 (1978).

7. H. Hofmann and S. R. Leone, J. Chem. Phys. 69(8), 3819 (1978).

8. M. Kawasaki, S. T. Lee, and R. Bersohn, J. Chem. Phys. 71, 1235 (1979).

9. J. C. White and G. A. Zdasiuk, J. Chem. Phys. 69(5), 2256 (1978).

10. M. S. DeVries, N. J. A. Van Veen and A. E. DeVries, Chem. Phys. Lett. 56(1), 15 (1978).

11. T. I. Quickenden, J. A. Irvin and D. F. Sangster, J. Chem. Phys. 69(10), 4395 (1978).

12. J. P. Reilly, J. H. Clark, C. B. Moore, and G. C. Pimentel, J. Chem. Phys. 69(10), 4381 (1978).

13. J. A. Beswick and J. Jortner, J. Chem. Phys. 69(2), 512 (1978).

14. J. A. Beswick, G. Delgado-Barrio, and J. Jortner, J. Chem. Phys. 70(8), 3895 (1979).

15. K. E. Holdy, L. C. Klotz, and K. R. Wilson, J. Chem. Phys. 52(9), 4588 (1970).

16. F. E. Heidrich, K. R. Wilson, and D. Rapp, J. Chem. Phys. 54(9), 3885 (1971).

17. D. Secrest and B. R. Johnson, J. Chem. Phys. 45, 4556 (1966).

18. M. Shapiro and R. D. Levine, Chem. Phys. Lett. 5(8), 499 (1970).

19. S. Mukamel and J. Jortner, J. Chem. Phys. 60(12), 4760 (1974).

20. S. Mukamel and J. Jortner, J. Chem. Phys. 61(1), 227 (1974).

21. Y. B. Band and K. F. Freed, J. Chem. Phys. 63(8), 3382 (1975).

22. S. Mukamel and J. Jortner, J. Chem. Phys. 65(9), 3735 (1976).

23. O. Atabek, J. A. Beswick, R. Lefebvre, S. Mukamel and J. Jortner, J. Chem. Phys. 65(10), 4035 (1976).

24. Y. B. Band, M. D. Morse, and K. F. Freed, J. Chem. Phys. 68(6), 2702 (1978).

25. M. D. Morse, K. F. Freed, and Y. B. Band, J. Chem. Phys. 70(8), 3604 (1979).

26. M. D. Morse, K. F. Freed, and Y. B. Band, J. Chem. Phys. 70(8), 3620 (1979).

27. G. B. Ellison, P. C. Engelking, and W. C. Lineberger, J. Am. Chem. Soc. 100(8), 2556 (1978).

28. M. J. Dzvonik and S. Yang, Rev. Sci. Instrum. 45(6), 750 (1974).

29. G. E. Busch, J. R. Cornelius, R. T. Mahoney, R. I. Morese, D. W. Schlosser and K. R. Wislon, Rev. Sci. Instrum. 7, 1066 (1970).

30. Y. T. Lee, J. D. McDonald, P. R. LeBreton, and D. R. Herschbach, Rev. Sci. Instrum. 40, 1402 (1969).

31. N. R. Daly, Rev. Sci. Instrum. 31, 264 (1960).

32. R. K. Sparks, L. R. Carlson, K. Shobatake, M. L. Kowalczyk, and Y. T. Lee, J. Chem. Phys. in press.

33. Lee Richard Carlson, Ph.D. dissertation, University of California, Berkeley, 1979.

34. R. W. Hamming, Ditital Filters, Prentice Hall Inc., New Jersey, 1977.

35. A. Savitzky and M. Golay, Anal. Chem. 36, 1627 (1964).

36. T. T. Warnock and R. B. Bernstein, J. Chem. Phys. 49, 1878 (1968).

37. G. L. Catchen, J. Husain, and R. N. Zare, J. Chem. Phys. 69(4), 1737 (1978).

38. H. G. Kuhn, Atomic Spectra, Academic Press, 1969.

39. S. J. Riley and K. R. Wilson, Far. Disc. Chem. Soc. 53, 132 (1972).

40. J. A. Kerr, Chem. Rev. 66, 465 (1966).

41. B. deB. Darwent, NSRDS-NBS 31, 1970.

42. G. Herzberg, Infrared and Raman Spectra II, van Nostrand Reinhold Company, New York, 1945.

43. T. Donohue and J. R. Wiesenfeld, J. Chem. Phys. 63(7), 3130 (1975).

44. D. S. Marynick and D. A. Dixon, Proc. Natl. Acad. Sci. 74(2), 410 (1977).

45. G. B. Ellison, P. C. Engelking and W. C. Lineberger, J. Am. Chem. Soc. 100(8), 2556 (1978).

46. L. Y. Tan, A. M. Winer, G. Pimentel, J. Chem. Phys. 57, 4028 (1972). D. E. Milligan and M. E. Jacox, J. Chem. Phys. 47, 5146 (1967). A. Snelson, J. Phys. Chem. 74, 537 (1970).

47. D. Porret and C. F. Goodeve, Proc. Roy. Soc. A 165, 31 (1938).

48. A. Gedanken and M. D. Rowe, Chem. Phys. Lett. 34(1), 39 (1975).

49. K. Kimura and S. Nagakura, Spect. Acta. 17, 166 (1961) and M. Ito, P. C. Huang and E. M. Kosower, Trans. Far. Soc. 57, 1662 (1961).

50. R. S. Mulliken, Phys. Rev. 47(3), 413 (1935) and R. S. Mulliken, J. Chem. Phys. 8(5), 382 (1940).

51. A. B. Nikolskii, Opt. Spectrosc. 29, 560 (1970).

52. M. Dzvonik, S. Yang, and R. Bersohn, J. Chem. Phys. 61(11) 4408 (1974).

53. C. D. Bass and G. C. Pimentel, J. Am. Chem. Soc. 83, 3754 (1961).

54. L. D. Landau and E. M. Lifshitz, Mechanics, Pergamon Press, New York, 1969.

55. B. H. Mahan, lecture notes, unpublished.

56. B. H. Mahan, J. Chem. Phys. 52(10), 5221 (1970).

57. I. S. Gradshteyn and I. M. Ryzhik, Table of Integrals, Series and Products, Academic Press, Massachusetts, 1965, page 505.

58. S. Sato, J. Chem. Phys. 23, 592 (1955).

59. H. S. Johnston, Gas Phase Reaction Rate Theory, The Ronald Press Company, New York, 1966, page 60.

60. M. Karplus and R. N. Porter, Atoms and Molecules, W. A. Benjamin, Inc., New York, 1970.

61. G. Herzberg, Infrared and Raman Spectra, Van Nostrand Reinhold Company, New York, 1945, page 310.

62. M. Abramowitz and I. A. Stegun, Handbook of Mathematical Functions, Dover Publications Inc., New York, 1970.

FIGURE CAPTIONS

Fig. 1. Schematic top view of photofragmentation apparatus.

Fig. 2. Time-of-flight measurement of CH_3I beam seeded in helium.

Fig. 3. Laboratory time-of-flight for CH_3 product of CH_3I photofragmentation. The asymptotic states of the I atom are indicated for the two peaks.

Fig. 4. Newton diagrams for CH_3I photofragmentation with detection of CH_3. Velocity circles for v = 0 and 1 of both the $I\,^2P_{1/2}$ and $^2P_{3/2}$ channels are shown. Laboratory velocity vectors for both 30° and 127° detector angles are shown. Note that lab velocity for $^2P_{1/2}$ channel at 127° is almost half of that at 30°.

Fig. 5. Time-of-flight data for CH_3 product after smoothing (upper curve) and after subtraction of exponential flux tails (lower curve). Input parameters used with program 3 of Appendix B to produce the lower curve are shown.

Fig. 6. Results of conversion of lower trace of Fig. 5 into center-of-mass flux as a function of center-of-mass energy.

Fig. 7. Best fit results of the forward convolution analysis. The upper frame shows the assumed center-of-mass flux distribution. The lower frame shows the results of its convolution into laboratory time space. The upper trace of the lower frame is the smoothed and stripped data of Fig. 5. It is vertically offset to aid comparison.

Fig. 8. Forward convolution results for the same parameters as Fig. 7 except that the rotational width of the input peaks has been doubled.

Fig. 9. Coordinate system for collinear collisions of atom A with diatomic oscillator BC.

Fig. 10. Contributions of Fourier transform terms to collinear collisional excitation. The lower trace shows the effects of only the cosine transform while the upper curve gives the results for inclusion of both transform terms.

Fig. 11. Comparison of measured vibrational state distribution with calculations from a Poisson distribution. Poisson for $\varepsilon = 2$ has the same average excitation as the measured distribution while that for $\varepsilon = 2.5$ has the same peak excitation.

Fig. 12. Estimated positioning of nodes for vibrational wavefunctions of CH_3 and their relationship to the ground state function for CH_3I. The vertical lines indicate the estimated classical turning points for the CH_3I umbrella motion.

Schematic top view
photofragment spectroscopy

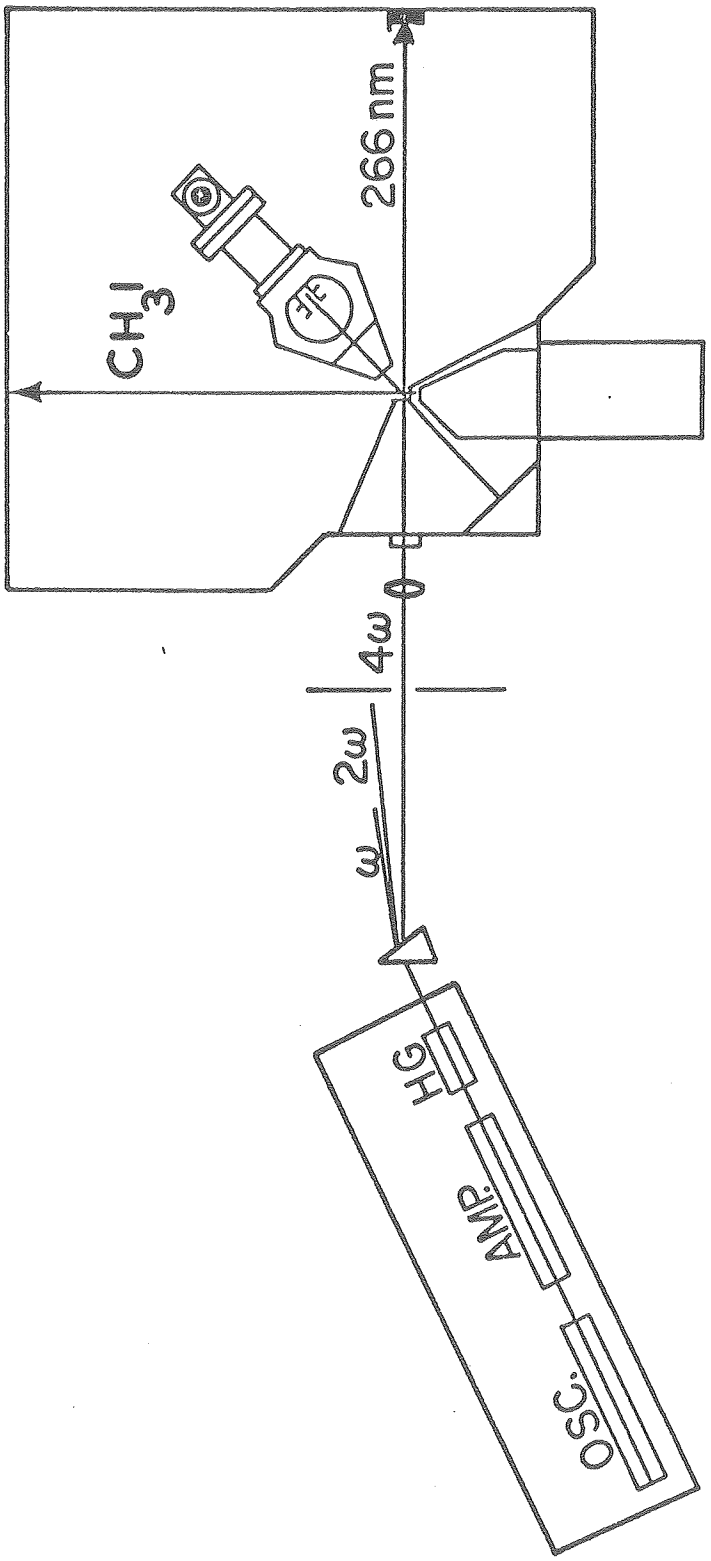

Fig. 1

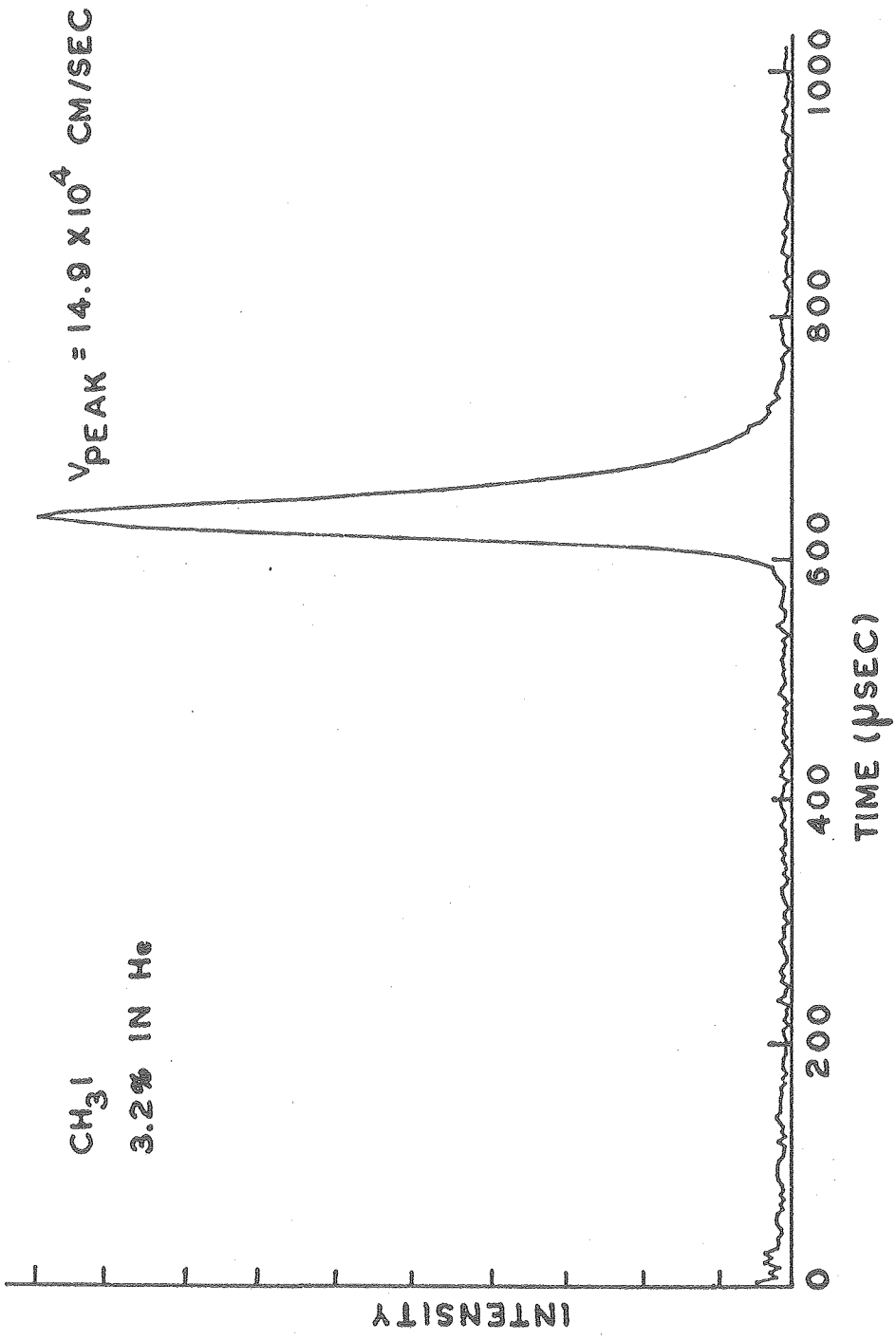
$V_{PEAK} = 14.9 \times 10^4$ CM/SEC
CH_3I
3.2% IN H_e
INTENSITY
0
200
400
600
800
1000
TIME (μSEC)

Fig. 2

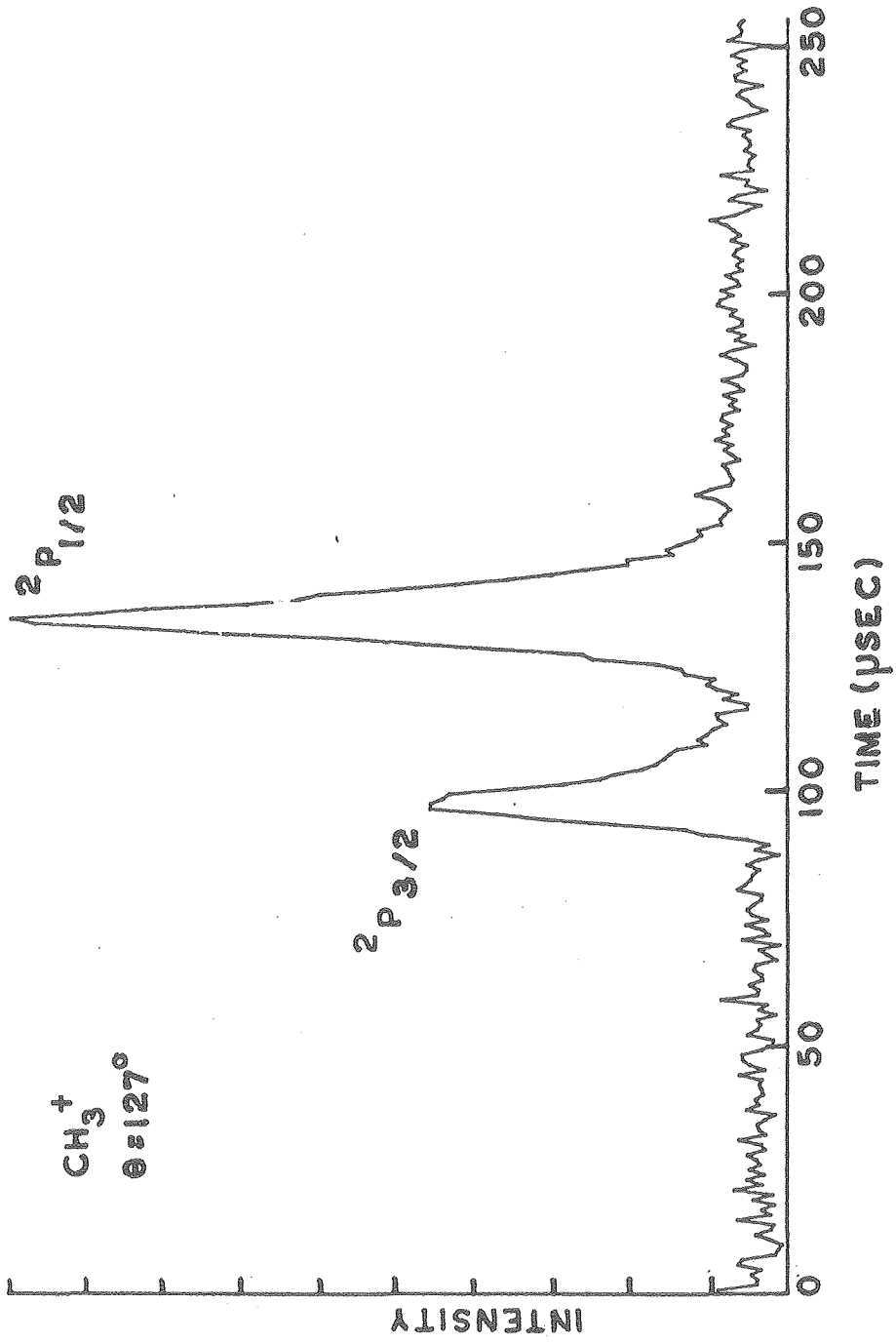

Fig. 3

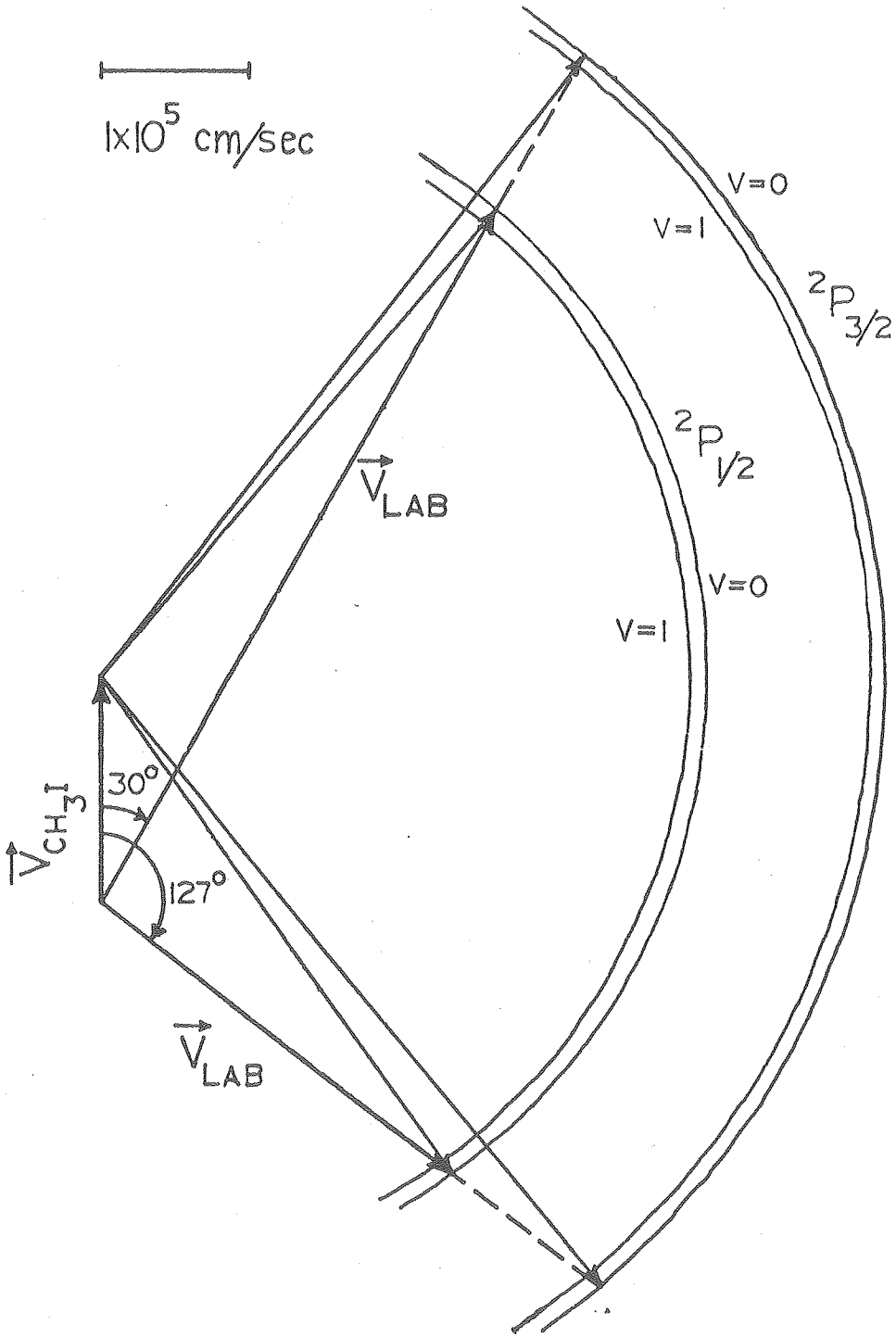

Fig. 4

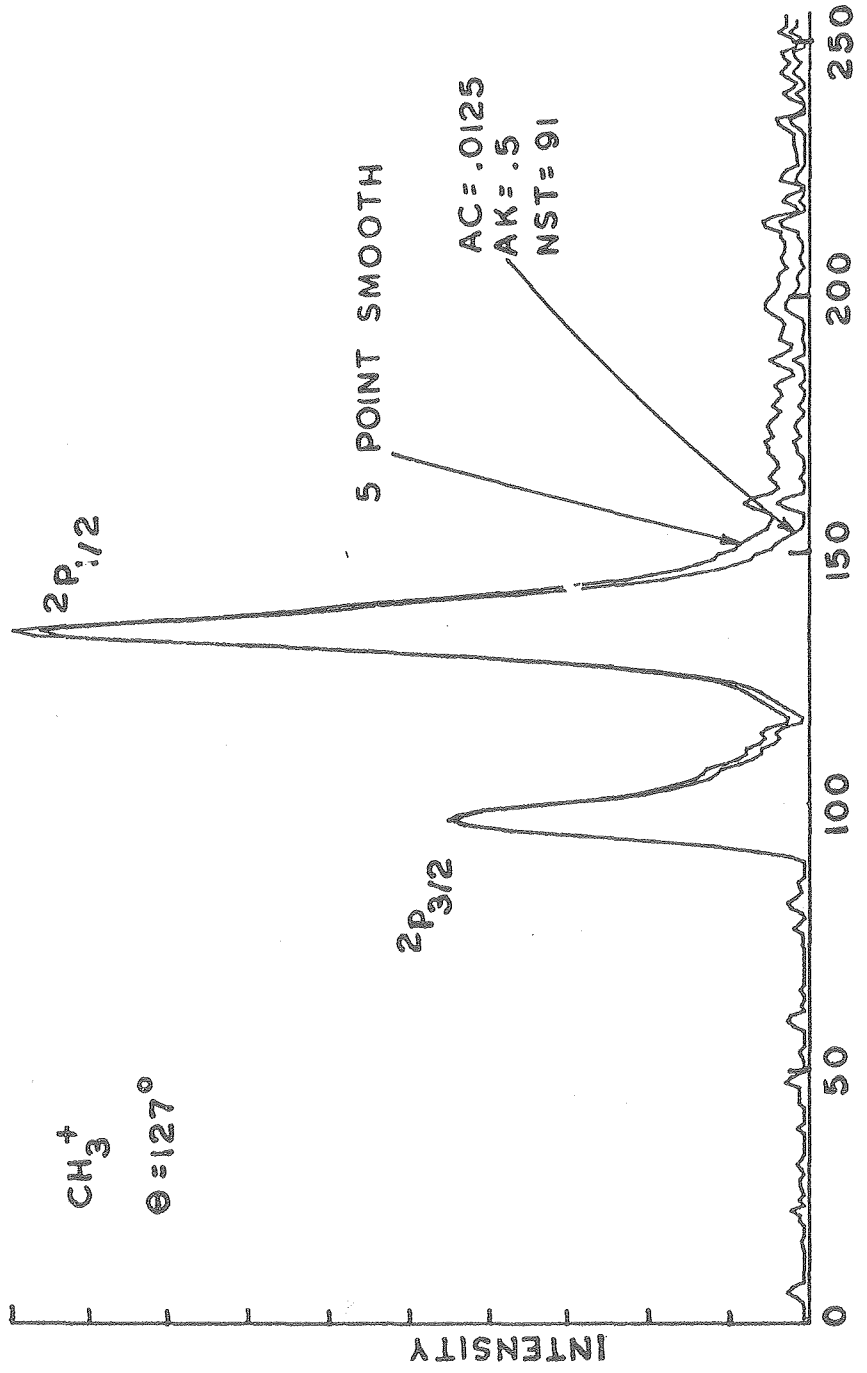
CH_3^+
θ=127°
$2P_{3/2}$
$2P_{1/2}$
5 POINT SMOOTH
AC=.0125
AK=.5
NST=91
INTENSITY
0
50
100
150
200
250
TIME (μSEC)

Fig. 5

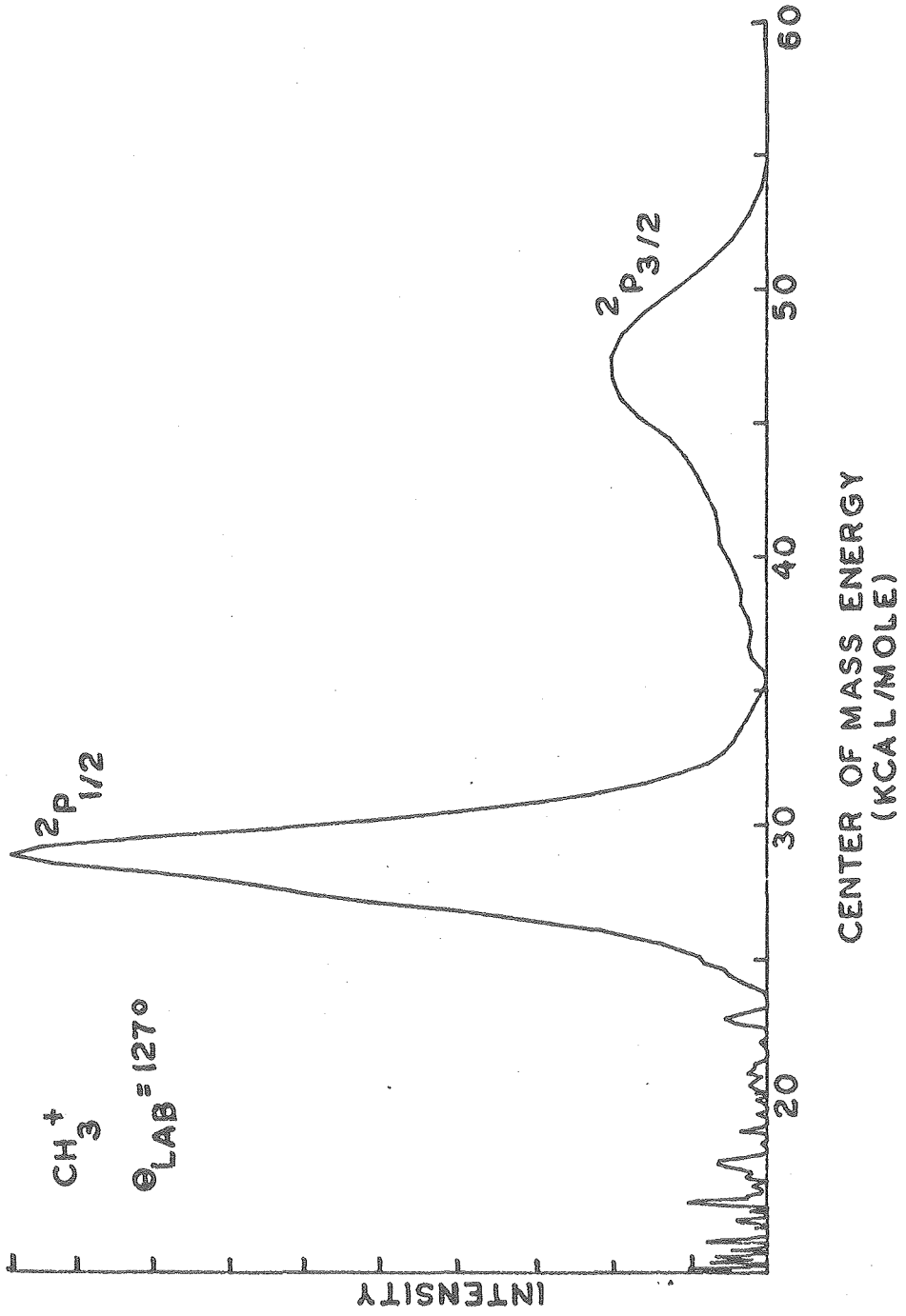
CH_3^+
$\theta_{LAB} = 127°$
$^2P_{1/2}$
$^2P_{3/2}$
INTENSITY
20
30
40
50
60
CENTER OF MASS ENERGY
(KCAL/MOLE)

Fig. 6

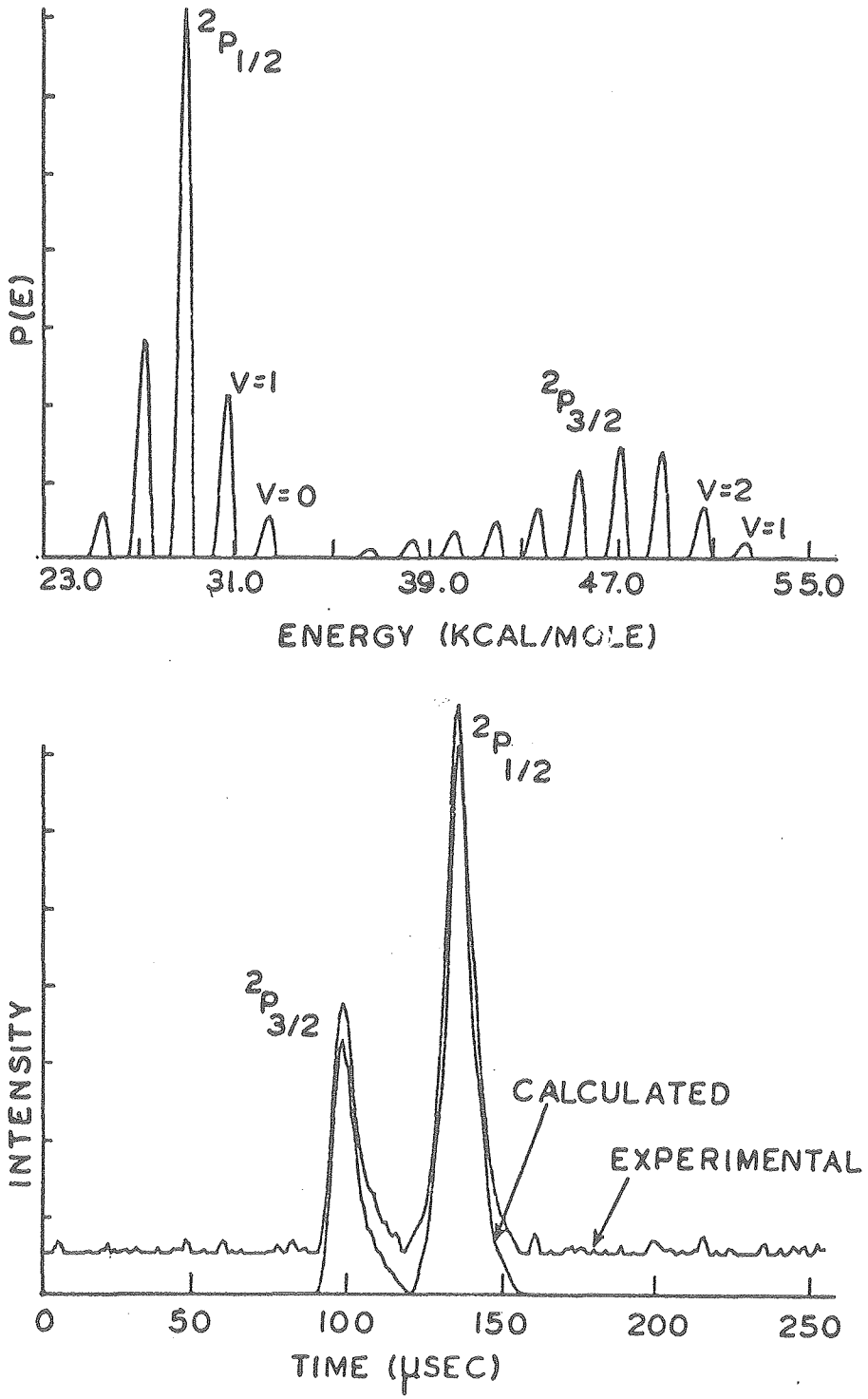
$^2P_{1/2}$
V=1
$^2P_{3/2}$
V=0
V=2
V=1
P(E)
23.0
31.0
39.0
47.0
55.0
ENERGY (KCAL/MOLE)
$^2P_{1/2}$
$^2P_{3/2}$
CALCULATED
EXPERIMENTAL
INTENSITY
0
50
100
150
200
250
TIME (μSEC)

Fig. 7

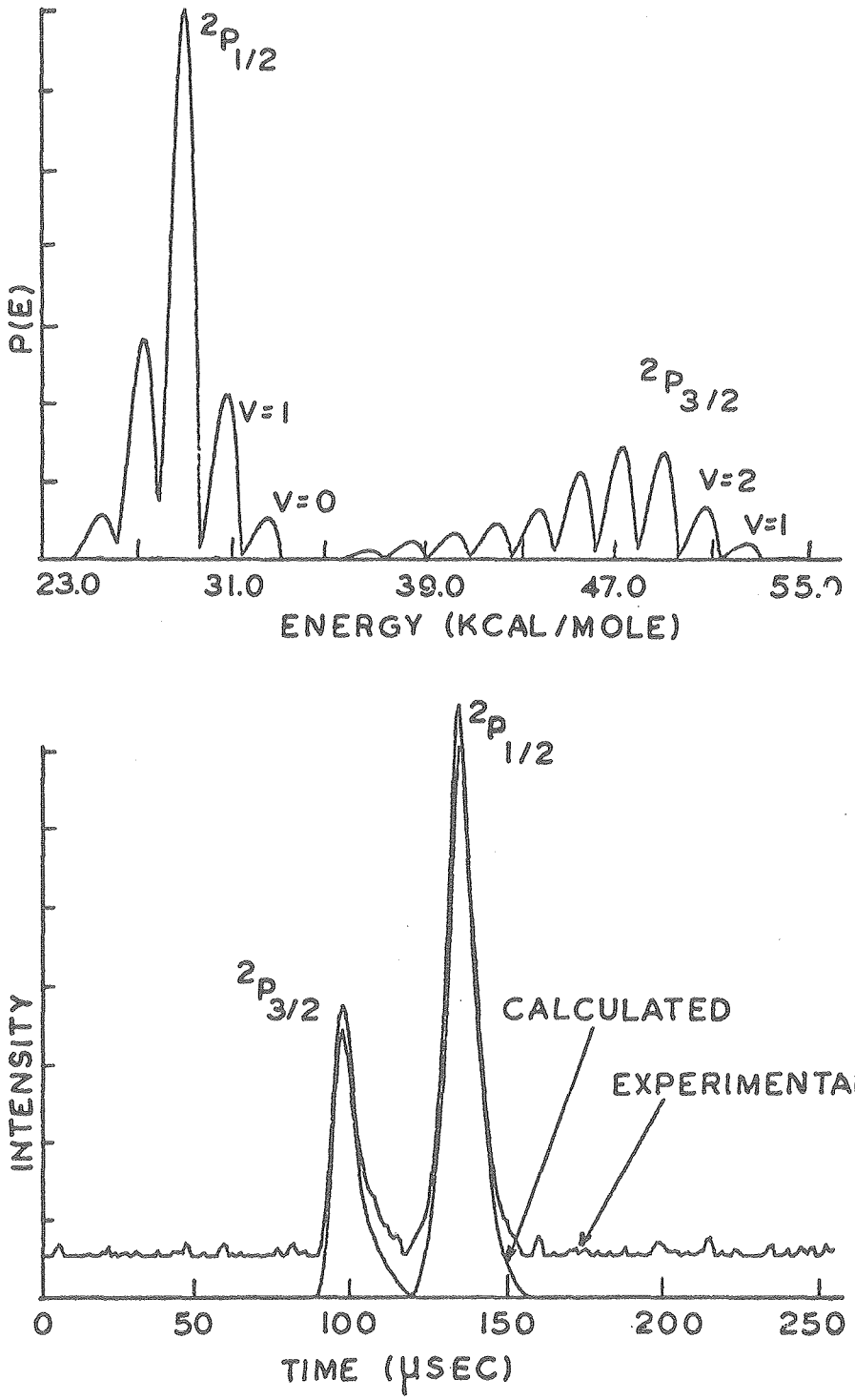
$^2P_{1/2}$
P(E)
V=1
V=0
$^2P_{3/2}$
V=2
V=1
23.0
31.0
39.0
47.0
55.0
ENERGY (KCAL/MOLE)
$^2P_{1/2}$
$^2P_{3/2}$
CALCULATED
EXPERIMENTAL
INTENSITY
0
50
100
150
200
250
TIME (μSEC)

Fig. 8

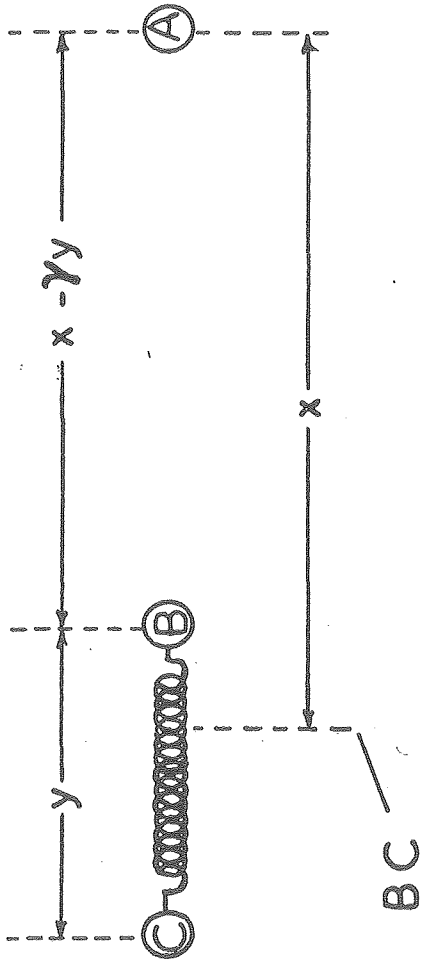

Fig. 9

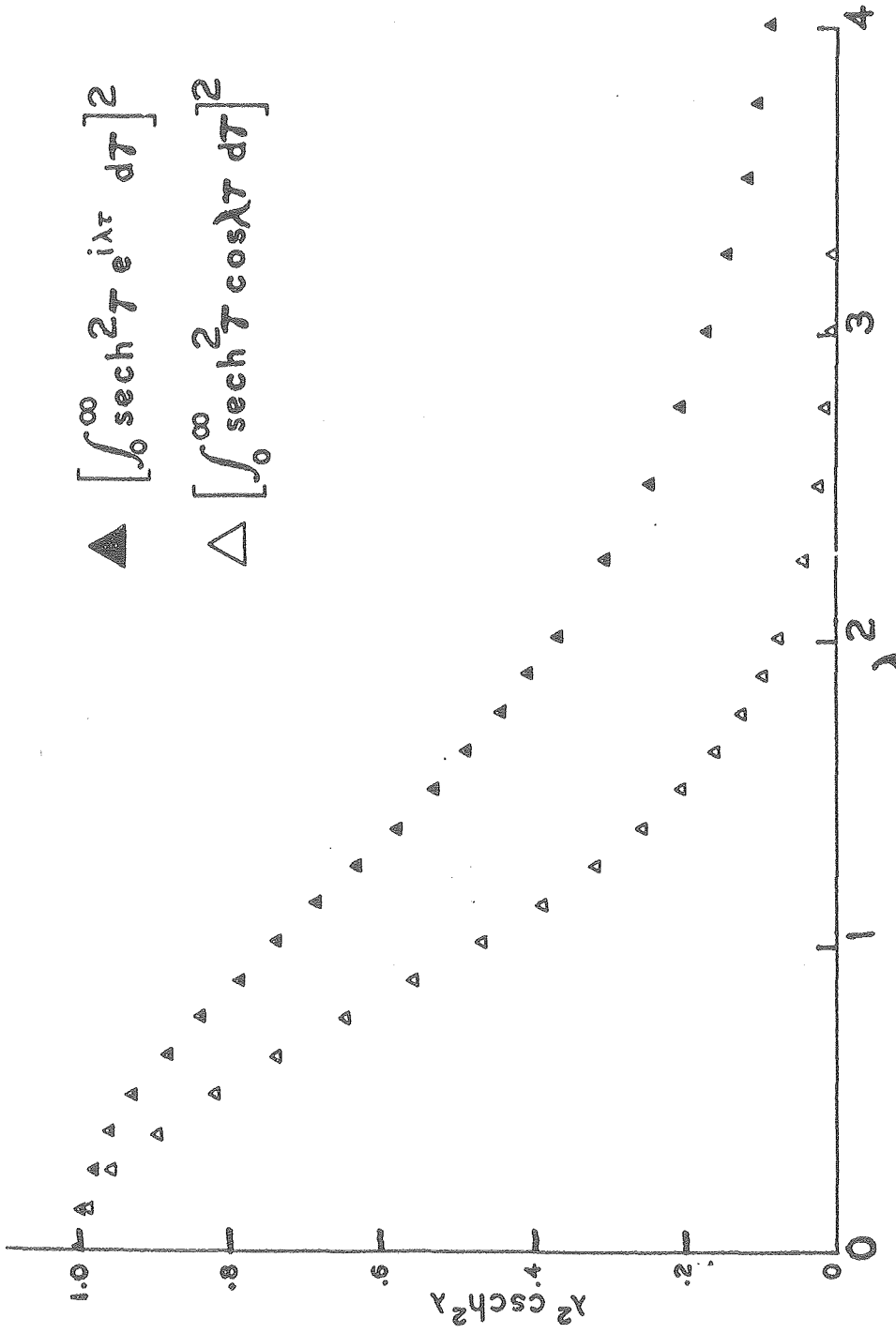
▲ $\left[\int_0^\infty \operatorname{sech}^2\tau\, e^{i\lambda\tau}\, d\tau\right]^2$
△ $\left[\int_0^\infty \operatorname{sech}^2\tau \cos\lambda\tau\, d\tau\right]^2$
$\lambda^2 \operatorname{csch}^2\lambda$
1.0
.8
.6
.4
.2
0
1
2
3
4
λ

Fig. 10

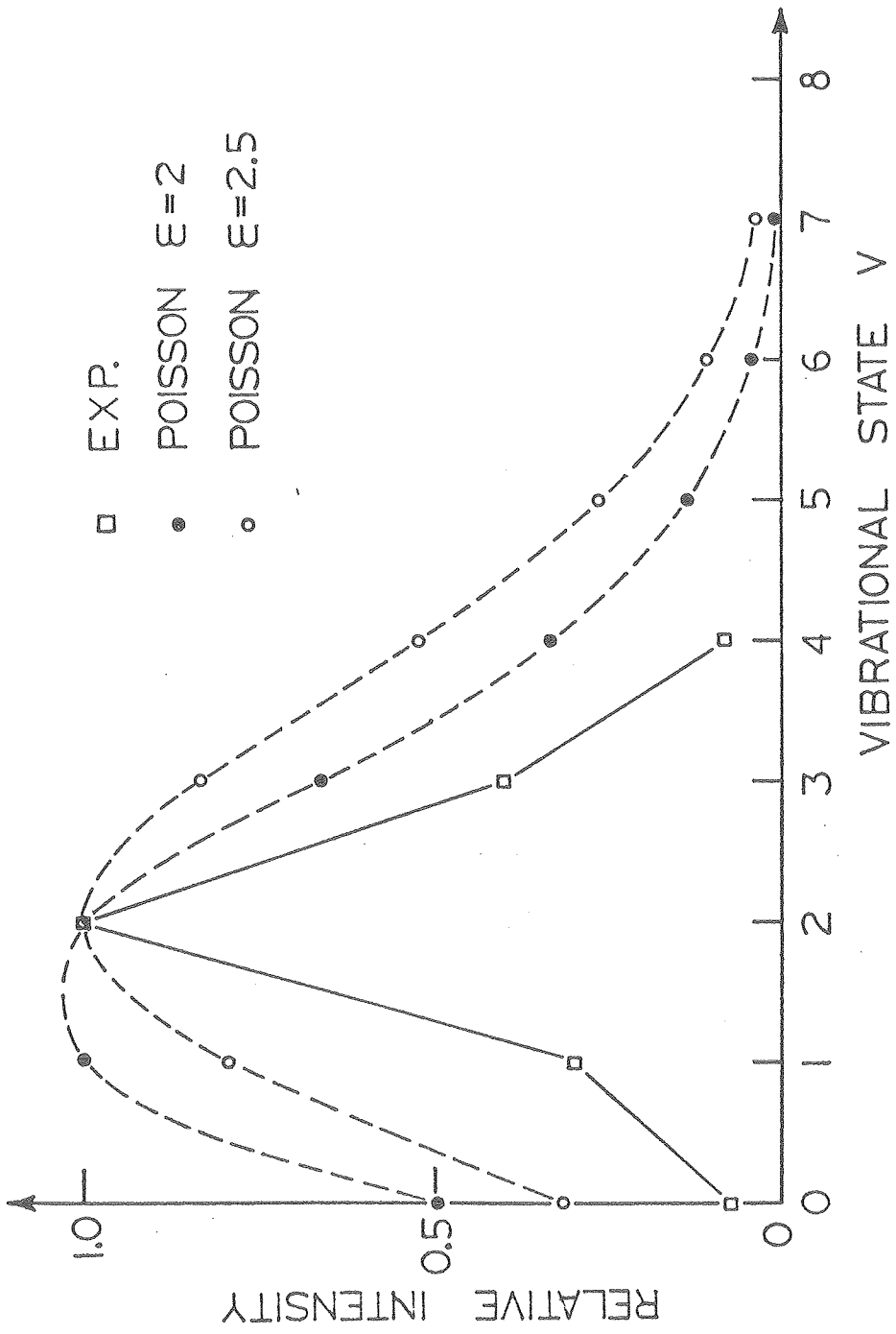
EXP.
POISSON E=2
POISSON E=2.5
RELATIVE INTENSITY
1.0
0.5
0
0
1
2
3
4
5
6
7
8
VIBRATIONAL STATE V

Fig. 11

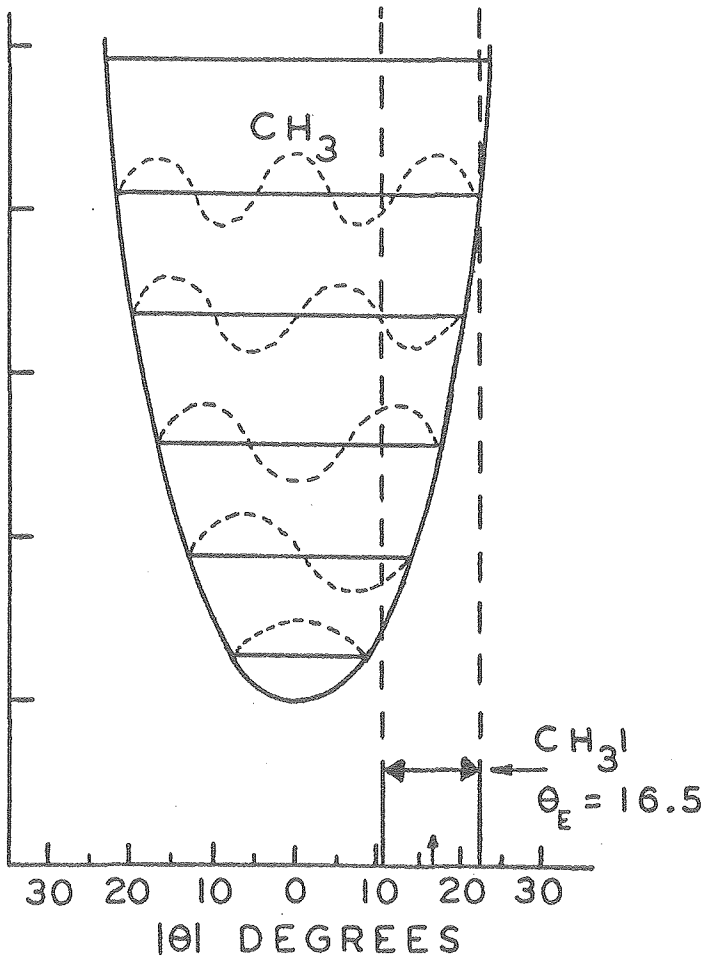

Fig. 12

II. MOLECULAR BEAM STUDIES OF REACTION DYNAMICS OF F + H_2, D_2

INTRODUCTION

Recent advances in quantum chemistry have made it possible to understand some important features of the reaction dynamics of such simple systems as H + H_2 → H_2 + H entirely based on quantum mechanical calculations.[1] The extension of this remarkable achievement to other simple hydrogen containing triatomic systems, especially the calculation of accurate ab initio potential energy surfaces, is progressing rapidly, although full three dimensional quantal calculations still await the development of more efficient methods. For the understanding of reaction dynamics of hydrogen containing systems, quantal scattering calculations are very important, since the significant quantum effects of tunneling and resonance phenomena which appear in these systems preclude the usage of classical trajectory calculations as a means of obtaining reliable information on the reaction dynamics. In the development of efficient approximation methods for carrying out three dimensional quantal calculations, comparison with accurate experimental results is necessary when the results of exact theoretical calculations are not available.

One of the hydrogen-containing three atom systems which has already attracted extensive experimental and theoretical attention in the past and will undoubtedly become the prototype reaction in the detailed understanding of reaction dynamics is the reaction of fluorine atoms with hydrogen molecules. The calculation of a limited ab initio

potential energy surface of chemical accuracy has been carried out.[2] The basic features of this calculation were adopted in the determination of more complete semiempirical potential energy surfaces which have been utilized in extensive classical trajectory calculations.[3,4] In exact one dimensional scattering calculations,[5,6] interesting quantum resonance phenomena were predicted at certain specific collision energies while a very recent three dimensional calculation using an angular momentum decoupling approximation[7] has provided some important information regarding resonance phenomena in three dimensional reactive scattering. The advances in recent years of various experimental approaches such as chemical lasers,[8] chemiluminescence methods[9] and crossed molecular beams experiments,[10] have not only revealed detailed information on product state distributions, but also have provided angular distributions of products in various quantum states at well defined collision energies. These results and expected improvements in the near future will certainly provide an unprecedented opportunity for making very meaningful comparisons between theoretical calculations and experimental observations.

In particular, the experimental observation of resonance phenomena via their effect on the state and angular distributions of the products under well-defined initial conditions could provide a very stringent test of the accuracy of theoretical calculations. Since the resonance phenomena in chemical reactions are very sensitive to the potential energy hypersurface at the critical configuration of the reaction

intermediate, the observation of resonance phenomena at specific collision energies in the laboratory provides an opportunity to evaluate the reliability of the potential energy surface in the close contact region.

In one dimensional quantum mechanical calculations, a sharp resonance has been predicted for the production of HF(v=2) at a collision energy of ~1 kcal/mole.[5,6] This sharp enhancement of the production of HF(v=2) at a specific collision energy was not observed in recent three dimensional calculations,[7] although a similar resonance phenomenon in the production of HF(v=2) predicted in the one dimensional calculation is still evident as collision energies are varied at a fixed orbital angular momentum of reactants. Because of both the shift of the resonance to higher collision energies when the orbital angular momentum is increased and the averaging of the distribution over orbital angular momenta in three dimensional reactive scattering, no pronounced variation of the state distribution as a function of collision energies is predicted in spite of the presence of resonance phenomena. This means that the measurement of state distributions as a function of collision energies will not be the appropriate method for the search for resonance phenomena. On the other hand, in the energy range where the resonance is occurring, there is a substantial variation in the reaction probability as a function of orbital angular momentum, or, equivalently, of impact parameter, for collisions at a given initial relative velocity. Since the angular distribution of product molecules to a large extent reflects the dependence of reaction probability on

impact parameter, especially for a system with the lowest entrance barrier for the collinear approach, the search for unusual features in the angular distributions of various quantum states of HF measured in a high resolution crossed molecular beams experiment is probably the best approach for finding reactive resonance phenomena in the laboratory.

In this paper, recent state resolved high resolution crossed molecular beams studies on $F + H_2 \rightarrow HF + H$ and $F + D_2 \rightarrow DF + D$ carried out at several collision energies will be discussed. The results reveal such detailed information as the dependence of the angular distribution of product molecules on both collision energy and product vibrational quantum state. These measurements illustrate the current state of the art of crossed molecular beams studies of reactive scattering and reflect predicted quantum mechanical resonances as well as other interesting features in the experimental observations of reactive scattering.

EXPERIMENTAL

The experiment is performed by crossing two supersonic molecular beams, one of atomic fluorine seeded in N_2, and one of H_2 or D_2, in a newly designed high resolution universal crossed molecular beams machine. The two beams cross at 90° in a well-defined interaction region. The detector, a triply-differentially pumped electron-impact

ionization mass spectrometer, is rotated about the interaction region in order to obtain the product angular distributions. The product velocity distributions are determined by measuring time-of-flight for molecules passing through a rapidly spinning slotted disc to the ionizer.

The design of the new apparatus closely follows that of the original universal crossed molecular beam machine described by Lee et al.,[11] but several modifications extend its capabilities beyond those of the original design. The detector is suspended from a 35" diameter rotating chamber which allows one to obtain a 30 cm flight path in contrast to the 17 cm flight path in the original 25" design. This nearly doubles the resolution of the time-of-flight spectra and consequently allows the product state distribution to be more accurately determined than was previously possible. In addition, the main chamber has been enlarged in order to increase the laboratory angular scan range from 115° to 170°.

Other modifications include a set of removable precision-machined apertures for the detector slits to allow the detector angular resolution to be varied simply by inserting a different set of apertures. Extreme care was taken in the choice and processing of all materials used in the three ultra-high vacuum detector regions, which has resulted in a background count rate at most masses that is nearly a factor of ten lower than in any of our previous machines. Also, a newly designed 1 μs per channel multi-channel scaler compatible with

the CAMAC standard has been utilized for the time-of-flight analysis in conjunction with a new on-line computer system.

The fluorine atom beam was produced by thermal dissociation of a 3% mixture of F_2 in N_2 at 700 torr in a nickel oven heated by thermocoax[12] heating elements to a temperature of 706°C. The heated gases expand through a 0.15 mm nozzle at the tip of the oven. A 0.66 mm diameter skimmer was used with a nozzle-skimmer distance of 6 mm. The beam was collimated in a second chamber to an angular spread of 2.2°. The nozzle to interaction center distance was 5.5 cm. Nitrogen was used as a seed gas to avoid the increased background at mass 20 (HF) that would have resulted from the use of Ar or Ne. Using He as a seed gas resulted in such high F atom velocities that the orientation of the resulting Newton diagram was unfavorable for observing many important center-of-mass angles. The F atom beam obtained had a peak velocity of 13.7×10^4 cm/sec and a FWHM velocity spread of approximately 25%.

Hydrogen and deuterium beams were produced by a very high pressure expansion of the gases through a 0.030 mm diameter nozzle. The nozzle-skimmer region was pumped by a Varian 10" NHS diffusion pump backed by a Leybold Heraeus WS-500 Roots blower package. The nozzle skimmer distance used was approximately 10 mm and was externally adjusted to allow maximization of beam intensity. The skimmer itself was constructed of electro-formed nickel[13] and has the advantages of very sharp edges and very small included angles. The beam was collimated

to a width of 2.2° and the nozzle was located at a distance of 6.5 cm from the scattering center. The collision energy of the experiment was varied by changing the stagnation temperature of the D_2 or H_2 beam. The beam source was heated with a short section of thermocoax wire powered by a regulated D.C. power supply. At the higher temperatures, the stagnation pressures behind the nozzle were increased in order to maintain number density, and thus intensity and high quality of expansion. The operating conditions of the H_2/D_2 beam source for the four different sets of data to be presented here are shown in Table I along with the most probable collision energy for each condition.

Product velocity analysis for the F + D_2 experiments was performed by single shot time-of-flight. The single shot time-of-flight wheel consisted of a 0.13 mm thick stainless steel disk of 17.5 cm diameter. Eight slots, each 1.5 mm wide, were machined on its perimeter. A reducing slit, also 1.5 mm wide, was mounted to the front of the detector. The wheel was rotated at a speed of 200 Hz. Data was collected for 600 μs following each wheel opening using a multichannel scaler channel width of 5 μs (120 channels). Typical counting times were two hours at each angle.

Velocity distributions for the F + H_2 experiment were obtained by cross-correlation time-of-flight. Our particular implementation of this method has been described before.[14] Cross-correlation was necessary for F + H_2 due to the much higher background at mass 20 (HF) than at mass 21 (DF). However, it is not an appropriate technique

Table I. H_2/D_2 Operating Conditions

	Collision Energy kcal/mole	Temperature °C	Stagnation Pressure (Atm)	Peak Velocity cm/sec
H_2	2.00	32°C	27	27.2×10^4
	3.17	219°C	40	35.7×10^4
D_2	2.34	32°C	27	20.9×10^4
	4.5	421°C	54	39.9×10^4

for a system such as F + D_2, since, in that case, the signal to background ratio is sufficiently high such that cross-correlation would actually reduce the quality of the data.[15] Additionally, we are presently limited by wheel design and wheel speed to a channel width of 10 μs with cross-correlation. Data for F + H_2 was taken with this lower limit channel time of 10 μs corresponding to a wheel speed of 392 Hz with 255 channels on the wheel. Typical counting times were approximately 70 minutes at each angle.

Angular distributions were obtained by modulation of the H_2/D_2 beam with a 150 Hz tuning fork chopper. Data was collected for equal times during the open and closed portion of the tuning fork cycle in a dual channel NIM scalar. The difference of the counts in the two channels constitutes the angular scan signal. Typical counting times for the angular scans were 2 minutes at each angle. Typical signal near the maximum in the angular distribution for F + H_2 would be about 6000 counts with a background of 19,000 counts. For F + D_2 we usually achieved 1700 counts of signal with about 120 counts of background. These numbers represent about one sixth of the actual count rate due to our intentionally low duty cycle of the tuning fork chopper. Detector aperture slits were set to achieve a laboratory angular resolution of 1° for both angular scans and the TOF data.

RESULTS AND ANALYSIS

The measured laboratory angular distributions for F + H_2 at 2.00 and 3.17 kcal/mole collision energy are shown in Figs. 1 and 2 along with the calculated best fits. The nominal Newton diagrams for each system are also shown. The corresponding data and Newton diagrams for F + D_2 at collision energies of 2.34 and 4.51 kcal/mole are shown in Figs. 3 and 4.

Time-of-flight data for all of these systems has been obtained. TOF spectra were generally taken for every other angle at which angular data was taken, however, over regions in which interesting effects were anticipated, spectra were taken for every angle at which angular scan data was taken. Angles with less than one fourth of the total intensity at the peak of the angular distribution were not considered profitable for TOF analysis. This procedure resulted in 11 to 18 TOF spectra for each system. Figure 5 shows the experimental TOF data for F + H_2 at 2.00 kcal/mole collision energy. The plots also show our calculated best fit to the data, including the separate contributions of the various vibrational states.

Data for both of the F + H_2 systems and for the lower energy F + D_2 have been analyzed to obtain the center-of-mass (C.M.) product distribution. We have used a forward convolution trial and error fitting technique in which the C.M. angular and energy distribution is input as a trial function. The corresponding laboratory angular and velocity distributions are then calculated from it and compared to the experimental data. The original trial function is adjusted and the

process repeated until a satisfactory fit is obtained simultaneously to both the TOF spectra and the angular scan. The appropriate equations and basic methodology of forward convolution have been well discussed elsewhere.[16] We, however, found it necessary to write an entirely new computer program for the actual calculation. Our very large quantity of data forced us to use direct graphical output of our calculated distributions. We considered completely different angular and energy distributions for each vibrational state, as well as having the energy distribution of each state being angular dependent.

The C.M. angle-recoil energy distribution that we have used is a generalized RRK form with separate parameterization for each vibrational state. The functional form used is:

$$I_{C.M.}(E,\theta) = \sum_{v=0}^{n} C_v(\theta) N_v(\theta) \cdot \begin{cases} (E-E_{min}(\theta,v))^{\alpha(\theta,v)} (E_{max}(\theta,v)-E)^{\beta(v)} \\ 0 \text{ if } E < E_{min}(\theta,v) \text{ or } E > E_{max}(\theta,v) \end{cases} \quad (1)$$

where $C_v(\theta)$ is a relative angular intensity factor, which is input in point form every 10° and interpolated linearly by the program for points between 10° intervals. $N_v(\theta)$ is a normalization factor calculated by the program to normalize the rest of the function to an area of 1 at each angle. $\alpha(\theta,v)$ is input in point form and interpolated in the same manner as $C_v(\theta)$. E_{min} and E_{max} were defined as circles in (E,θ) space with a given radius in E and a given displacement along the 0°-180° axis. Usually the radius and displacement for E_{min} were chosen as 0, while the displacement for E_{max} was usually chosen as zero with the

radius being set at the sum of the collision energy and the exothermicity minus the vibrational energy of the paricular state. The parameter β was fixed for each vibrational state. The total distribution, then, represents the entire product flux recoil energy distribution while the contribution from each vibrational state, in principle represents the flux as a function of rotational excitation of that vibrational state.

Thus the final result of our data fitting analysis is a center-of-mass flux distribution as a function of angle and product recoil energy. In order to represent this distribution in the usual form superimposed on a Newton diagram it must be converted from an energy space to a velocity space distribution. The transformation is straightforward and the results are shown in Figs. 6-8.

Figures 6 and 7 show the velocity space contour maps of our best fit distribution for $F + H_2$ at 2.00 and 3.17 kcal/mole respectively. Figure 8 shows the corresponding information for $F + D_2$ at 2.34 kcal/mole. When transformed to laboratory angular and velocity space, these contour maps correspond to the total calculated distributions shown in the angular scan plots of Figs. 1-3 and the velocity distribution plots of Fig. 5.

DISCUSSION

The dynamics of the F + H_2 and F + D_2 reactions produce several features which lend themselves well to study by the crossed molecular beams method. The large product vibrational spacings in conjunction with narrow rotational energy distributions in many cases allow the vibrational states of the HF and DF products to be identified from distinct peaks which appear in the measurements of laboratory velocity. The potential energy barrier to reaction is lowest in the configuration where the fluorine atom approaches collinear to the axis of the hydrogen molecule. At low collision energies this is expected to cause the products to scatter predominantly along the relative velocity vector of the reactants, and consequently peaks corresponding to individual vibrational states are observed in the laboratory angular distributions. Thus, both the laboratory velocity measurements and angular distributions provide detailed information on product state distributions and the two measurements effectively complement one another.

At low collision energies the angular distributions of HF and DF in the center of mass coordinate system shown in Fig. 6 and Fig. 8 are found to peak backward with respect to the direction of the incident fluorine atom. This is consistent with the nature of the potential energy surfaces derived from ab initio and semi-empirical calculations for F + H_2. The potential energy barrier for this reaction depends on the bending angle of H-H-F. The barrier is lowest for the collinear configuration, with a value of about 1 kcal/mole. Consequently, only

those collisions involving a nearly collinear configuration of the two hydrogen atoms and the fluorine atom contribute to the formation of products, and these products are predominantly backward scattered.

The center-of-mass angular and velocity distribution for HF product from the $F + H_2 \rightarrow HF + F$ reaction at a collision energy of 3.17 kcal/mole is shown as a contour map in Fig. 7. At this collision energy the center-of-mass angular distribution differs markedly from that at the lower energy. The distributions for different vibrational states seem to be entirely decoupled. The products in v=1 and v=3 remain backward peaked as at the lower collision energy, but the angular distribution for product in v=2 is very unusual. The intensity remains high as the center-of-mass scattering angle decreases, and even shows a sideways peaked relative maximum. This is illustrated more clearly when the center-of-mass velocity distributions are plotted as a function of angle as in Fig. 9. The laboratory angular distribution also shows a significant change between the two energies. The structure due to strongly backward peaked HF(v=2) product at 2.00 kcal/mole is absent when the collision energy is raised to 3.17 kcal/mole. The dramatic change in the center-of-mass angular distribution of the product formed in v=2 at 3.17 kcal/mole compared to that at 2.00 kcal/mole is consistent with the reactive resonance phenomenon predicted by the three dimensional calculations of Redmon and Wyatt. In that study it was shown that the effect of resonances in the $F + H_2$ reaction appears as a change in the dependence of the reaction

probability on reactant orbital angular momentum. The reaction probability for forming HF(v=3) is maximum at zero orbital angular momentum, independent of collision energy, while the probability for forming HF(v=2) peaks at non-zero orbital angular momentum for a collision energy around 3 kcal/mole, and the orbital angular momentum corresponding to the peak reaction probability changes as a function of collision energy. Since the orbital angular momentum is determined by the impact parameter for the collision, the reaction probability for forming HF(v=2) peaks at a non-zero impact parameter for a collision energy around 3 kcal/mole. Products formed from a larger impact parameter collision should scatter at smaller center-of-mass angles, so our experimentally observed results at 3.17 kcal/mole are in qualitative agreement with what one would expect from the reactive resonance in $F + H_2 \rightarrow HF(v=2) + H$ predicted in the calculation of Redmon and Wyatt.

In the laboratory angular distribution of DF product from the reaction $F + D_2 \rightarrow DF + D$ at 4.51 kcal/mole (Fig. 4), there is another surprising feature: a sharp peak appears at the laboratory angle corresponding to forward scattering of DF(v=4). Such a sharp forward product peak has not been observed previously in a reaction which does not form a long lived complex. But just as the extent of the polarization of product orbital angular momentum determines the sharpness of forward-backward peaks in angular distributions of products from a long lived complex, the strong forward peaking of DF(v=4) indicates a strong correlation between the final orbital angular momentum of the product and the initial orbital angular momentum. The reliability of the angular momentum decoupling calculations carried out on $F + H_2 \rightarrow HF +$

H by Redmon and Wyatt depend on the extent of this correlation. For the $F + H_2$ and $F + D_2$ reations, this approximation might appear to be valid. Once again, this strong correlation of final and initial angular momentum might be the consequence of the nature of the potential energy surface for these reactions, which has a bending angle dependent barrier which is minimum at the collinear configuration.

CONCLUSION

The experimental results presented in this paper are examples of what can be measured at present in the laboratory by the crossed beams method. The experimental resolution could be further improved in the future, but the incentive for future effort toward carrying out a better experiment certainly depends on the advancement of a theoretical calculations, making possible a more quantitative comparison between theory and experimental results.

REFERENCES

1. A. Kupperman and G.C. Schatz, J. Chem. Phys. 62, 2502 (1975).
2. C.F. Bender, P.K. Pearson, S.V. O'Neil, and H.F. Schaefer III, J. Chem. Phys. 56, 4626 (1972).
3. J.T. Muckerman, J. Chem. Phys. 54, 1155 (1971).
4. R.L. Wilkins, J. Chem. Phys. 58, 3038 (1973).
5. G.C. Schatz, J.M. Bowman, and A. Kupperman, J. Chem. Phys. 58, 4023 (1973).
6. S.L. Latham, J.F. McNutt, R.E. Wyatt, and M.J. Redmon, J. Chem. Phys. 69, 3746 (1978).
7. M.J. Redmon, and R.E. Wyatt, Chem. Phys. Lett. 63, 209 (1979).
8. J.H. Parker, and G.C. Pimentel, J. Chem. Phys. 51, 91 (1969); R.D. Coombe, and G.C. Pimentel, J. Chem. Phys. 59, 251 (1973).
9. J.C. Polanyi, and K.B. Woodall, J. Chem. Phys. 57, 1574 (1972).
10. T.P. Schafer, P.E. Siska, J.M. Parson, F.P. Tully, Y.C. Wong, and Y.T. Lee, J. Chem. Phys. 53, 3385 (1970).
11. Y.T. Lee, J.D. McDonald, P.R. LeBreton, and D.R. Herschbach, Rev. Sci. Instr. 40, 1402 (1969).
12. Semco Instruments Incorporated, 11505 Vanowen Street, North Hollywood, California 91605 USA.
13. Beam Dynamics Corporation, 623 East 57th Street, Minneapolis, Minnesota 55417 USA.
14. James Martin Farrar, Ph.D. dissertation, The University of Chicago, Chicago, Illinois, 1974.
15. Hans-Dieter Meyer, Diplomarbeit, Max-Planck-Institut für Strömungsforschung, Göttingen, West Germany, 1974.

16. Richard James Buss, Ph.D. dissertation, the University of California, Berkeley, California, 1979.

FIGURE CAPTIONS

Fig. 1. Experimental LAB angular distribution of the HF product from the F + H_2 reaction at 2.00 kcal/mole.

Fig. 2. Experimental LAB angular distribution of the HF product from the F + H_2 reaction at 3.17 kcal/mole.

Fig. 3. Experimental LAB angular distribution of the DF product from the F + D_2 reaction at 2.34 kcal/mole.

Fig. 4. Experimental LAB angular distribution of the DF product from the F + D_2 reaction at 4.51 kcal/mole.

Fig. 5. Time-of-flight analysis of the HF product from F + H_2 reaction at 2.00 kcal/mole. Plots show experimental LAB TOF spectra at indicated angles along with the best fits calculated from center-of-mass angular and velocity distributions for various vibrational states of HF. (●) Experimental. (——) Calculated best fit summed over contributions from v=1,2, and 3. (· ——) v=1. (—— ——) v=2. (·····) v=3.

Fig. 6. Center-of-mass velocity-space contour plot of HF product distribution from F + H_2 reaction at 2.00 kcal/mole.

Fig. 7. Center-of-mass velocity space contour plot of HF product distribution from F + H_2 reaction at 3.17 kcal/mole.

Fig. 8. Center-of-mass velocity-space contour plot of DF product distribution from F + D_2 reaction at 2.34 kcal/mole.

Fig. 9. Center-of-mass distributions at indicated angles of HF product from F + H_2 reaction at (a) 2.00 kcal/mole and (b) 3.17 kcal/mole.

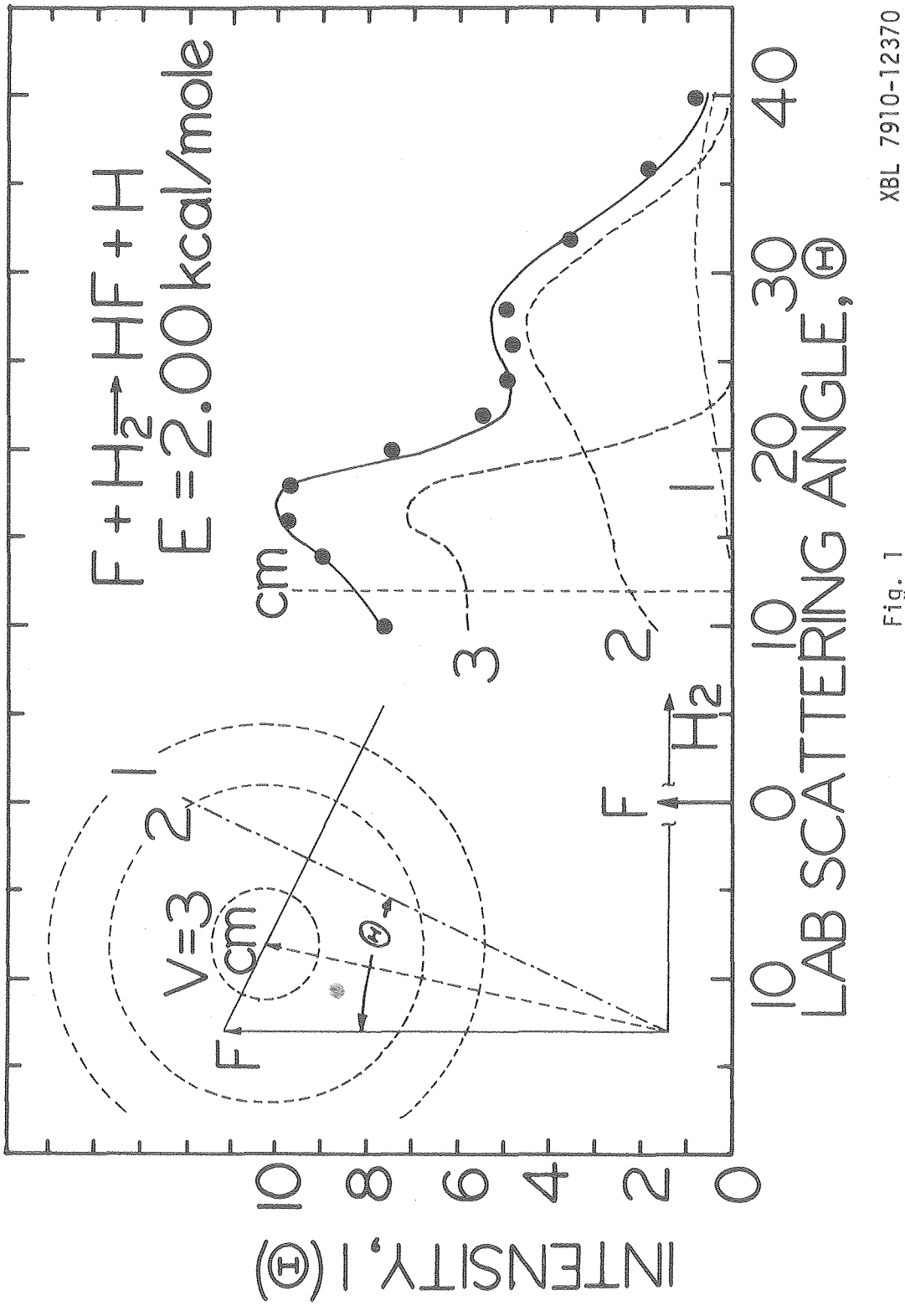

XBL 7910-12370

Fig. 1

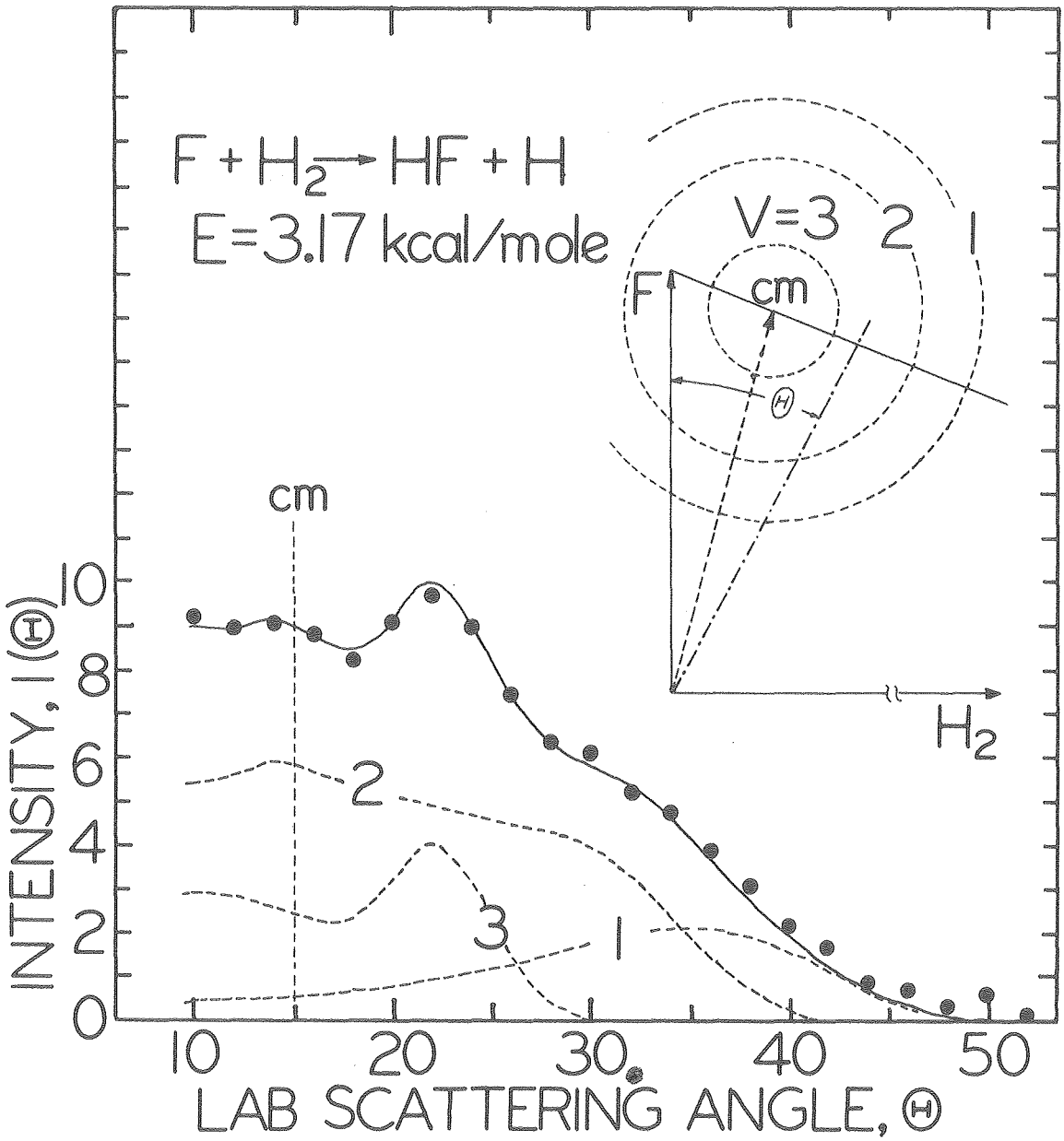

XBL 7910-12372

Fig. 2

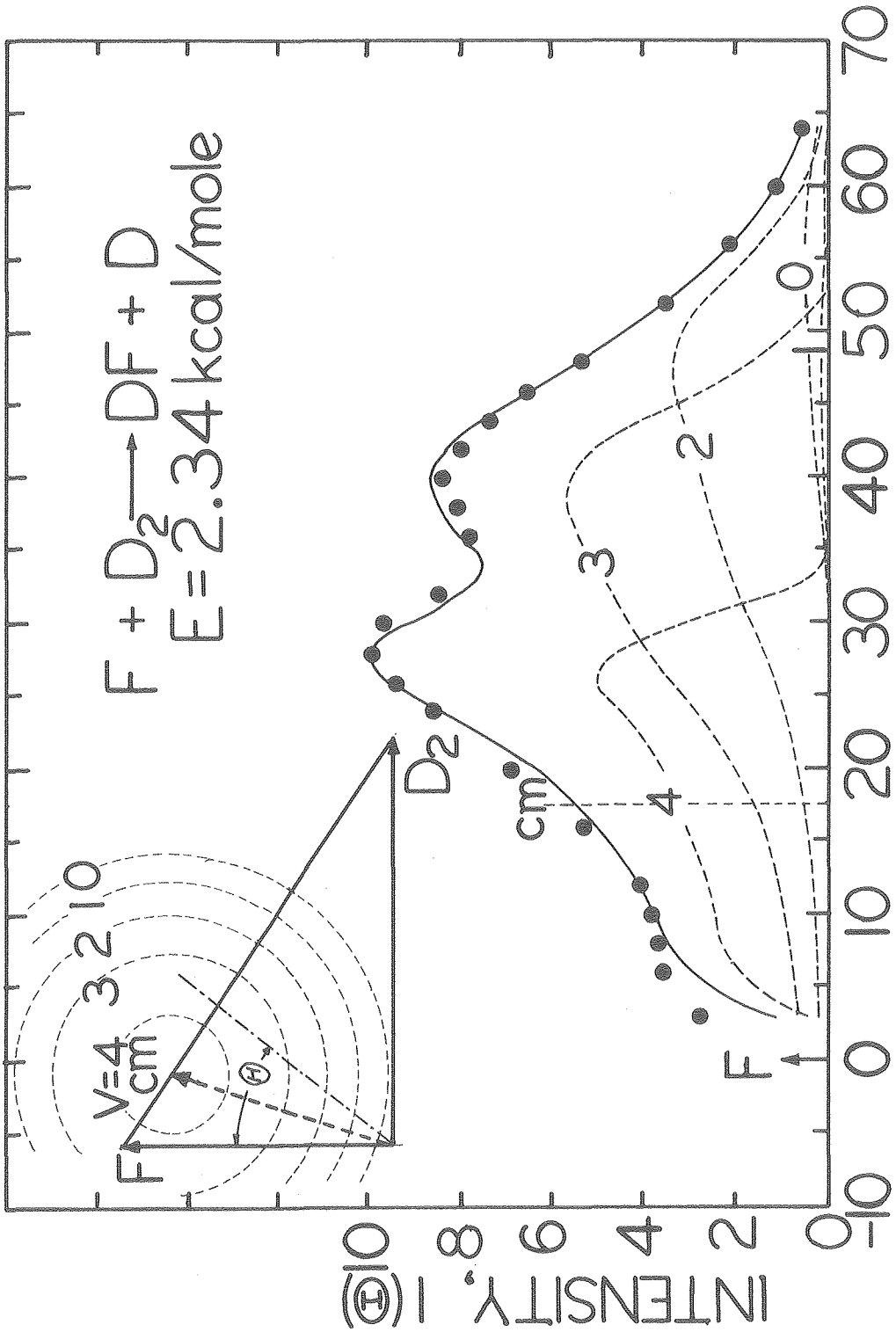

XBL 7910-12371

Fig. 3

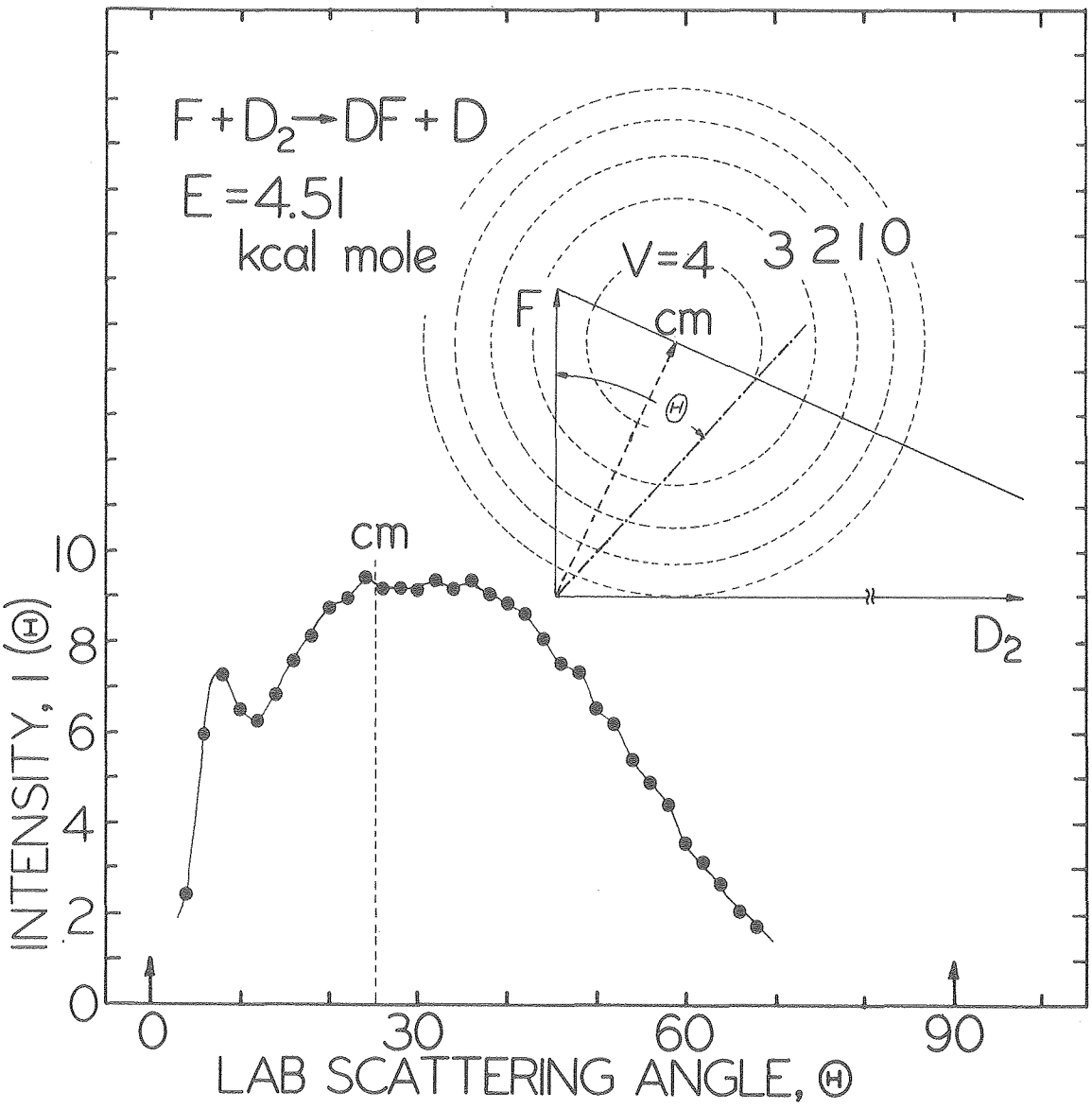

XBL 7910-12373

Fig. 4

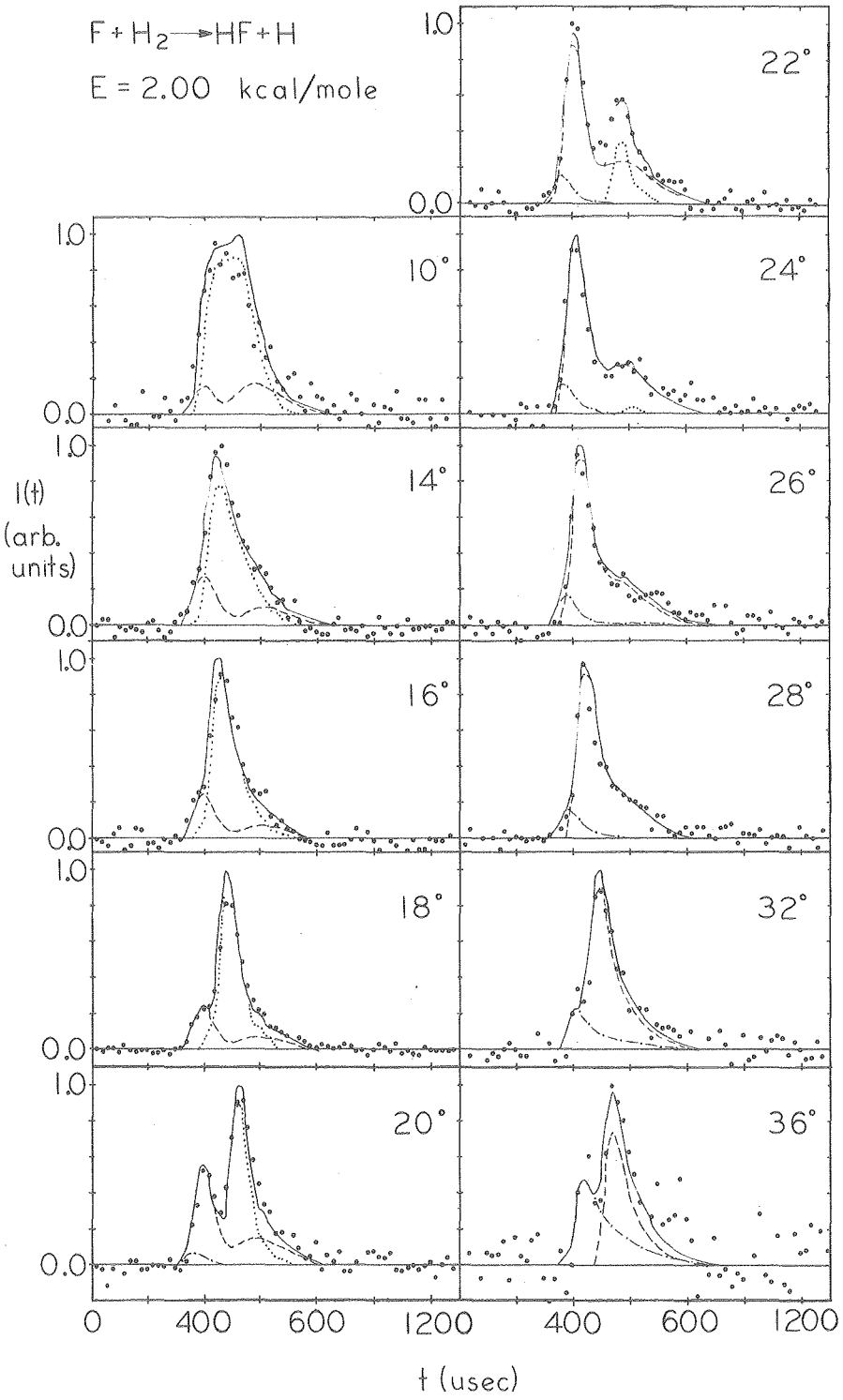

Fig. 5

XBL 7910-12377

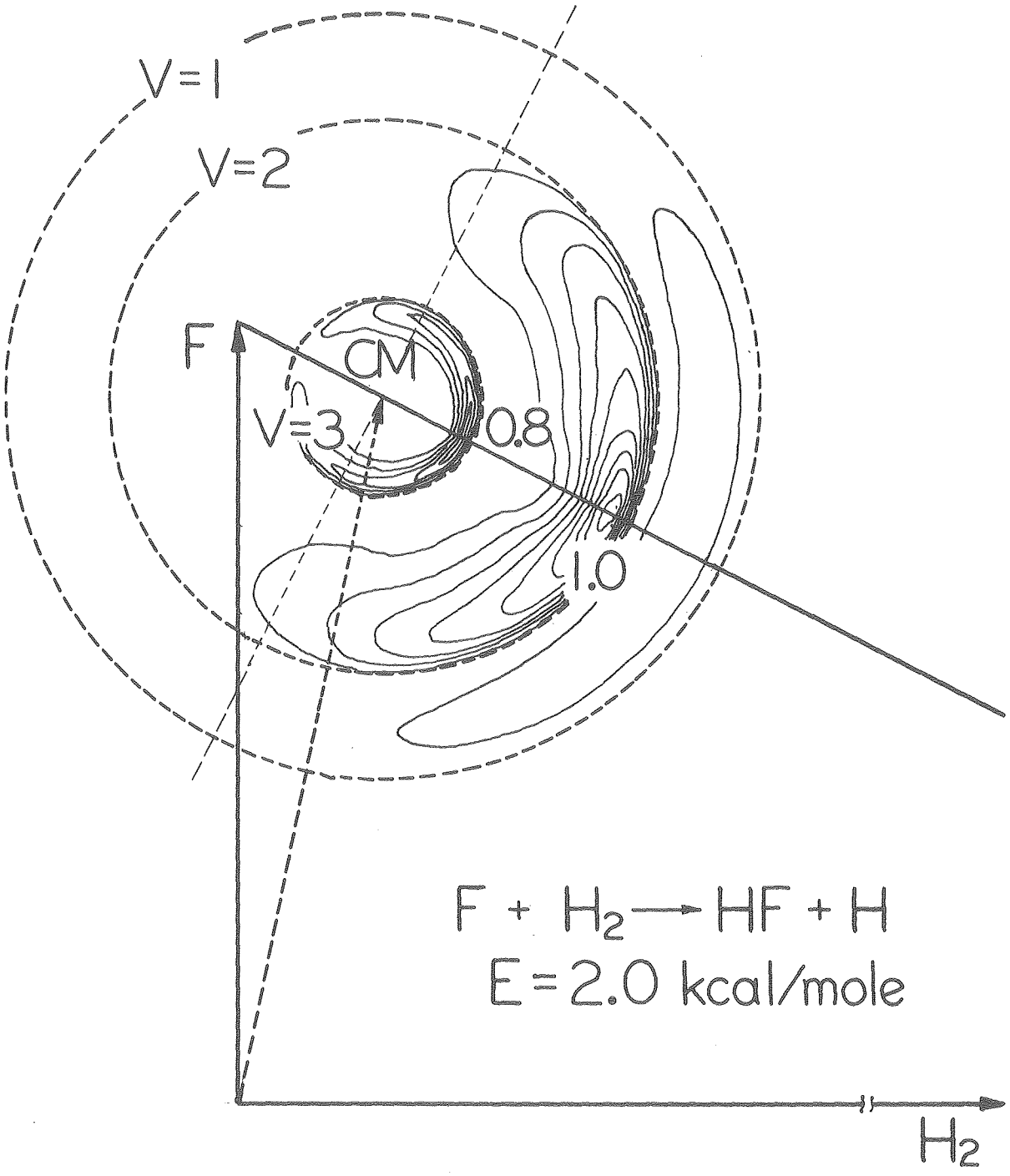

Fig. 6

XBL 7910-12374

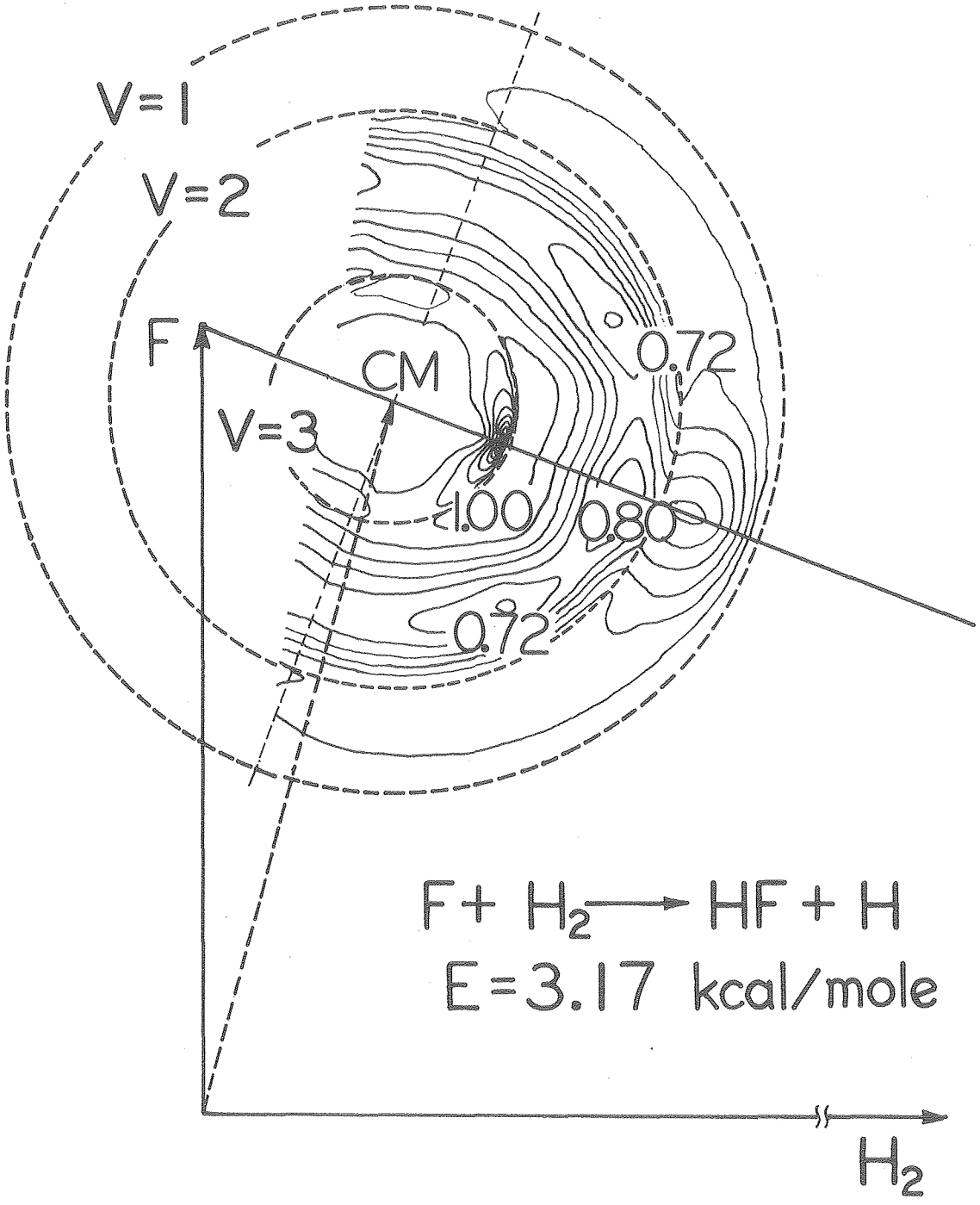

Fig. 7 XBL 7910-12376

$$F + D_2 \longrightarrow DF + D$$

$$E = 2.34 \text{ kcal/mole}$$

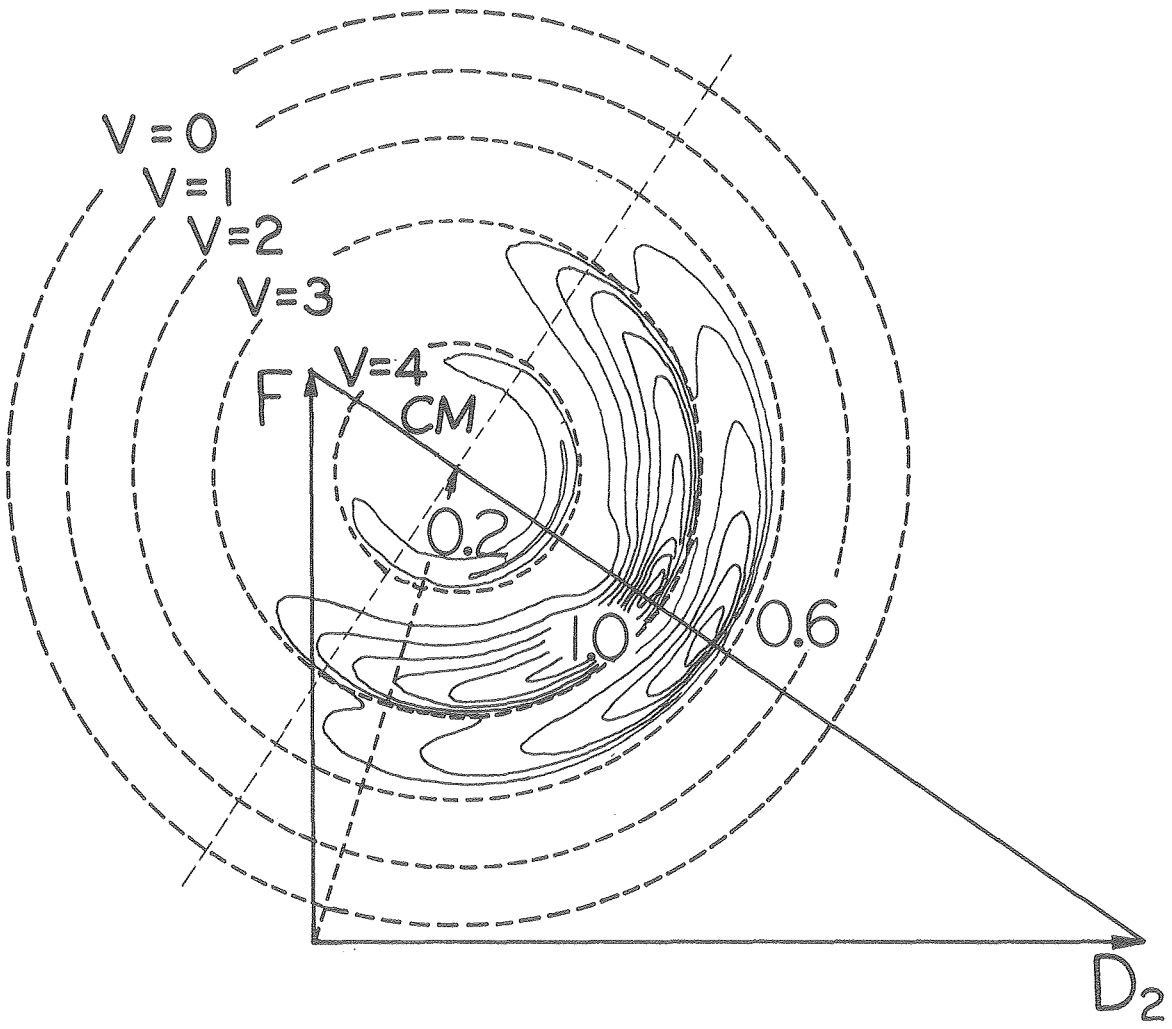

Fig. 8

XBL 7910-12375

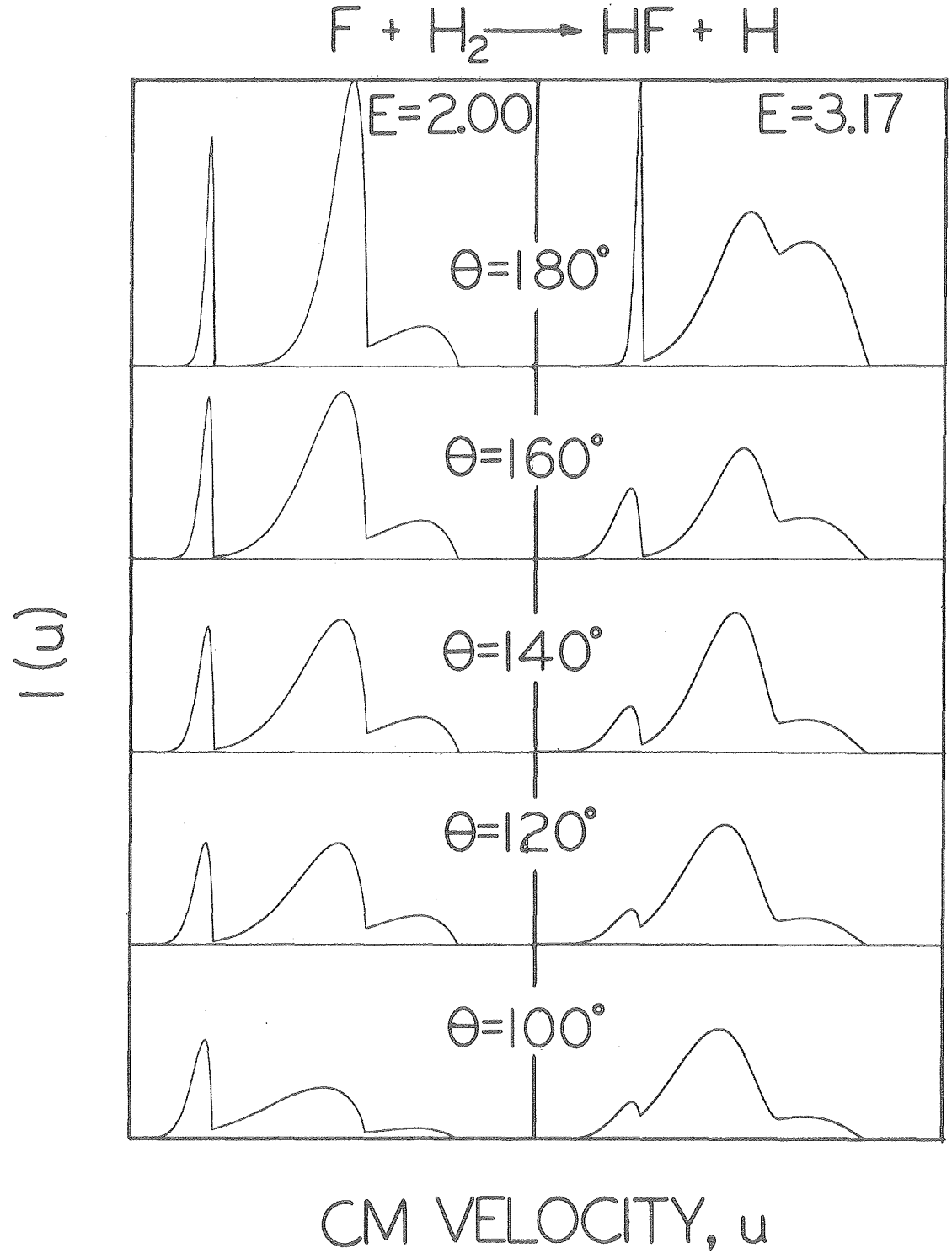

XBL 7910-12369

Fig. 9

Appendix A. Description of New 35" Crossed Molecular Beams Machine.

INTRODUCTION

The basic experimental requirements for study of chemical processes by means of crossed molecular beams are well known and will be only briefly outlined here. The information that one desires is the product energy and angle distribution in the center-of-mass system. Quantum state resolution is ideal but very rarely achievable. The products should result from reactants whose translational and internal energies are known. In order to define the initial conditions, we must have well collimated molecular beams of known velocity and well defined intersection angle. The experiment must also be carried out under single collision conditions for obvious reasons. In order to determine the center-of-mass product distributions, one must measure laboratory data as a function of angle and product velocity as well as determining which product species are created. Thus our apparatus must have some type of beam source system, a detector which can differentiate between product species, a method of rotating the detector and beam sources relative to each other, and a technique for measuring product velocities.

Of course, certain design considerations must always be met for an experiment to be reasonably executable. Molecular beam experiments are almost always plagued with problems of signal/noise ratios and limited resolution. It is necessary to achieve maximum beam intensity while at the same time minimizing the angular and velocity spreads of

the beam. The detector must be one of high sensitivity and low background level while also possessing adequate angular resolution and angular scan range. The velocity analysis technique must also possess adequate resolution and range to be able to view and distinguish relevant processes.

A particularly successful and widely copied implementation of these principles has been the design developed by Lee et al.[1] The apparatus features supersonic expansion molecular beam sources which are placed very close to the collision center for high beam intensity. Each beam source is surrounded by its own differential pumping region as an aid in collimating the beam and in reducing gas flow into the main chamber. The detector consists of an electron impact ionizer followed by a quadrupole mass spectrometer and particle counting system. The ionizer is located in the innermost region of a triply differentially pumped ultra high vacuum chamber which is rotatable with respect to and in the plane defined by the molecular beams. Velocity analysis of product molecules is achieved by modulating the incoming product beam with a rotating chopping wheel at the entrance slit of the detector chamber. Flight times for the molecules to travel from the chopping wheel to the ionizer are then measured using a computer controlled data acquisition system employing a high speed multichannel scaler. These time-of-flight (TOF) spectra are then readily converted into laboratory velocity spectra.

We shall describe below the main features of a newly constructed beam machine, similar to the above design, but with many enhanced capabilities.

BASIC DESIGN CONSIDERATIONS

The original incentive for designing a new apparatus which differed significantly from the earlier machines was a desire to increase the velocity resolution for time-of-flight analysis. Since the velocity resolution is most fundamentally limited by the ratio of the length of the effective detection zone and the mean flight path, a reduction in this ratio was necessary. This could be achieved either by reducing the effective length of the ionizer or by increasing the flight path. Reducing the length of the ionization region has the advantage of not requiring a mechanical redesign of the apparatus. However, due to space charge and ion trapping effects that become significant at high electron current density, it would be quite difficult to make a smaller ionizer that possessed the same detection efficiency as the larger one. A reduction of detection efficiency was certainly not desirable.

In order to maintain the same detection efficiency, then, it is necessary to achieve greater velocity resolution by means of increasing the flight path. This option, though requiring a redesign of the vacuum chambers, has several additional advantages beyond maintenance of detection efficiency. These advantages are, of course, related to the longer absolute flight times incurred for the longer flight path apparatus.

Longer absolute flight times reduce the design requirements, or, for a given design, enhance the performance of two other aspects of the time-of-flight system. First, the design of the multichannel

scaler (MCS) system can be less difficult due to the reduction in the speed at which the various clocking and arithmetic operations within the scaler have to occur. Correspondingly, with an equivalent MCS, the longer flight path machine can measure molecules of higher velocity before the resolution becomes limited by the channel times of the MCS. Secondly, the rotation speed for the time-of-flight chopping wheel can be much slower for a given molecular velocity, or again, for a given rotation speed, one can analyze much faster molecules. This is quite important since wheel speeds are not fundamentally limited by motor technology but rather by the strength to weight ratio of the material making up the TOF wheel. It is already possible to get motors that will spin fast enough to cause wheels of reasonable diameter to disintegrate from the centrifugal acceleration.

Due to the combination of advantages inherent in a long flight path design versus a short ionizer design, the long flight path approach was chosen. Moreover, during the design of the new apparatus, it was determined that certain enhancements to the basic characteristics could be included at nominal cost which would significantly improve the performance of the machine. These include a greatly increased laboratory angular scan range, variable laboratory angular resolution, and much reduced background count rate. In addition, a new-high speed multi-channel scaler, which was concurrently under design in our laboratory, was first implemented on the new machine. The major aspects of the main chamber and detector system of the new apparatus

will be described below as will the layout and capabilities of the new MCS and computer system. Relevant programs for the computer system will be discussed in Appendix B.

MAIN CHAMBER AND DETECTOR GEOMETRY

The major difference between the new apparatus and the previous ones is that the detector chamber is mounted in a 35" bearing diameter rotating support ring rather than the previous value of 25". Since, in machines of this type, the ionizer is mounted in a liquid nitrogen cooled insert which forms the detector's third differential pumping region, and this insert is vertically oriented at the outside edge of the rotating chamber, the radius of the rotating ring system is a fundamental constraint on the flight path. Thus increasing the ring diameter was the obvious first requirement for increasing the flight path. Smaller additional increases are then obtained by painstaking minimization of all mechanical clearances that separate the outside edge of the cooled insert from the inside edge of the bearing. The final flight path achieved was approximately 30 cm for TOF wheel modulated systems or about 34 cm for pulsed laser initiated events in which the entire distance from the rotation center can be utilized.

An increase in the bearing diameter obviously necessitated an increase in many other dimensions of the apparatus. However, one part of the system which we wished to leave essentially the same as in the earlier machines was the beam source pumping system and geometry.

This presented a problem in terms of the support and seal design for the rotating ring system, since the beam source reference surfaces must then lie inside the diameter of the bearing. The original square box design of the main chamber would not suffice. The solution, as illustrated in Fig. 1, was to construct the entire top plate of the apparatus from a 4 inch thick plate of stainless steel, utilizing the upper 2-1/2 inches of thickness for the vacuum seal for the rotating ring and thus allowing an ample 1-1/2 inches at the bottom to complete the vacuum system wall and provide mechanical support. This admittedly generated a somewhat extensive machining task, but it resulted in a design with very high confidence of successful completion as well as a lower total cost than could be achieved by welding separate plates of complicated geometries.

One additional complication was introduced by the desire to retain the previous beam source dimensions, and that was the question of the laboratory angular scan range. If the main chamber walls on the sides where the beam sources are introduced were to be kept coplanar with the beam source reference surfaces, the total angular scan range of the detector would be limited to only slightly better than 90°. Since we wished to maintain at least the same angular scan range as the previous machines, it was necessary to put a "bulge" in the two sides of the main chamber. Since the cost of including the bulges would be relatively independent of the size of the bulges, it was clear that they could be chosen so as to maximize the total angular scan range. This maximization had to be performed against the constraints of maintaining most

of the original beam source geometry and of not drastically reducing the pumping speed available in the beam source differential chambers.

The criteria of maintaining basic beam source geometry and differential chamber pumping speed were somewhat arbitrary, but became severely limiting factors at nearly the same detector angle. The actual angle chosen was such that the inner wall of the source differential pumping region is exactly tangent to the circular hole beneath which the source differential diffusion pumps are mounted. Clearly any further increase in detector scan range would begin covering the diffusion pump throat and thus rapidly reducing pumping speed. Also at this point, space in the beam sources and differential chambers had become sufficiently confined that further reduction would have necessitated complete redesign of all of our earlier beam sources if they were to be used with the new machine. This was thought to be a good place to quit. The resulting full angular scan range was 170° versus approximately 115° for the earlier machines.

A top view of the layout of the machine is shown in Fig. 2. The beam sources, beam source differential chambers, and the three regions of the detector are shown. The chambers through which the first and second differential pumping regions of the detector are pumped are not shown in order to more clearly show the relationship of the beam sources and the rotating ring system. The defining slits in the beam source differential chambers are both located a distance of 5/8" from the collision center in contrast to the previously used asymmetric configuration. This feature allowed for many more degrees of angular

scan range with a calculated loss in signal of less than 2% relative to the asymmetric configuration. Also, the front surface of the detector is located 2-1/2" from the collision center, versus the previous value of 1-3/4", again chosen as an aid in achieving the full angular scan range.

PUMPING SYSTEM AND VACUUM PROPERTIES

In addition to changes in the mechanical design of the machine its vacuum system has also been significantly improved. These improvements have had their greatest effect in terms of detector background levels but also have resulted in improvements elsewhere. The most straightforward and obvious difference is the increased pumping speed in the main chamber. The new main chamber is pumped by two ten inch and one six inch Varian VHS oil diffusion pumps in contrast to the single 10 inch pump on the previous machines. This change was made possible by the increased size of the main chamber. Increasing main chamber pumping speed does not have a significant effect on the ultimate pressure in the chamber since it seems to be limited to some degree by the vapor pressure of the diffusion pump oil. However, the partial pressures of gases which flow into the main chamber as part of the reactant beams will be reduced in inverse proportion to the pumping speed. Since these beam gases effuse into the detector and form a major contribution to background levels for many types of experiments, the increased pumping speed can be of value.

Increasing the physical dimensions of the detector chamber also presented an opportunity to increase pumping speeds, but, for the detector, this opportunity is also a mandate. Since the effectiveness of the differential pumping in the detector is determined by the ratio of the pumping speed in each differential pumping region and the conductance of the beam aperture connecting that region to the one at higher pressure, any increase in aperture area will reduce the effectiveness of the differential pumping. However, increasing the length of the detector requires that the beam apertures also be increased in size if one wishes to maintain a constant angular resolution. Thus it is necessary to increase the pumping speed in the detector if only to maintain previous perfomance parameters.

Very simple first order scaling laws can show that one can readily create havoc by nonchalantly increasing the size of an apparatus. Under ideal conditions in which the partial pressure of a detected gas is determined solely by pumping speed considerations, the pressure in the ionization region is roughly given by:

$$P_{III} = P_m \frac{C_I C_{II} C_{III}}{S_I S_{II} S_{III}} \qquad (1)$$

where P_{III} is the partial pressure in the third or ionization region, P_m is the main chamber partial pressure, and the C's and S's represent the aperture conductances and pumping speeds respectively of the three differential pumping chambers. The conductances C are proportional to the areas of the apertures, which, for constant angular resolution, will

each be proportional to the square of the length of the detector. However, due to various pragmatic considerations, the overall pumping speeds that one is realistically able to achieve in each region scale roughly linearly with the detector length. Thus the background pressure, in this crude treatment, will actually increase for a larger detector by the cube of the detector length. This is certainly not a desirable relationship and we are fortunate in that, when real beam aperture sizes are used, the increase is not nearly so dramatic. Also, one must be careful, in doing an accurate modelling calculation, to include the effect of the direct effusive beams entering the ionizer from both the main chamber and the first two detector differential chambers. The effect of these beams favors the larger detector and further mitigates the advantage of the short detector. The end result, however, is still that the larger detector must have signficantly increased pumping speed in all regions in order to maintain the same dynamic background pressures as the smaller one.

The pumping speed in the new detector has been increased by pumping all three regions of the detector with 220 l/s Perkin-Elmer Ultek DI ion pumps. This represents a doubling of the total speed presently on our oldest machine and an increase of 35% over that on our new 25" bearing machine. However, due to non uniformity in the sizes of the ion pumps on the other two machines, the product of the pumping speeds (the important factor by equation 1) is respectively 11.8 and 2.7 times that of the previous two machines. This factor is sufficient to counteract the effect of increased aperture sizes.

The great importance of the areas of the detector beam apertures should be quite clear from equation 1. For experiments in which the background really does come primarily from the main chamber and can be effectively pumped by the ion pumps, it is clear that smaller aperture areas will much reduce the background counte rate. Moreover, the signal that one observes would be reduced by only the first power of the aperture area. This presents the enticing possibility of making the signal to background ratio as high as one might desire simply by reducing the area of the detector apertures. This only reaches its limit when the inherent detector background begins to make a significant contribution. Of course, one actually wishes to maximize the signal to noise ratio not the signal to background ratio, thus absolute count rates must be estimated if one wishes to calculate an optimum aperture area. However, it is evident that for certain systems, small detector slits could be highly advantageous. As a bonus, one would also get higher angular resolution.

There do, though, exist many problems involved with very small detector slits. First, one wishes to study many various systems with greatly varying cross sections and detector backgrounds. Very small apertures would limit study to only the most favorable systems. Second, many systems of chemical interest do not suffer from main chamber generated detector background. Reactive systems in which the product is heavier than either of the reactants do not have this problem, since reactant fragmentation in the ionizer cannot generate ions of the product mass. For these systems, equation 1 is not valid and the

above conclusions do not hold. Background would be primarily determined by inherent detector count rate and reducing aperture areas would only serve to throw away signal. For these situations, large apertures are desired. Thus it is clear that no single choice of detector aperture sizes will best satisfy all experimental needs. A method of varying aperture sizes is needed.

Since the entire detector is an ultra high vacuum system, implementation of variable slits is not trivial. On the one hand, one does not wish to have to vent the detector in order to change the slits, due to the time of pumpdown and bakeout, as well as increased contamination. On the other hand, the mechanical linkages and ultra-high vacuum feedthroughs that would be necessary for remote adjustment would be complicated and expensive and would themselves contribute to background and reduce internal pumping speeds. Additionally, such linkages would also seriously reduce the hard won increased angular scan range. Replaceable slits were chosen over externally adjustable ones since they seemed to have a shorter list of disadvantages.

The actual design of the replaceable slit system is really quite straightforward. An example of the geometry is shown in Fig. 3. The aperture itself is square and is referenced to a precision square hole in the wall of each differential pumping region. The flange to accommodate the retaining screws is round and is kept from significant surface contact with the wall by a small raised ledge. This feature was intended to reduce possible entrapment of surface contaminants between the pieces. The design does, though, produce an included

volume, which is pumped out through the chamfers at the corners of the aperture piece. These chamfers must be included to prevent gas entrapment.

The time required to change the apertures must be kept to a minimum so as to reduce the time that the detector is exposed to atmosphere. Thus aperture replacement must be convenient and rapid. For this reason, the square precision hole for the innermost aperture is made sufficiently large that the entire aperture assembly for the second aperture can pass through it. In this way, removal of the second region aperture is trivial once the third aperture has been removed. Removal of the third region aperture is possible after the quadrupole housing has been unbolted from the rotating chamber and the ionizer has been removed from the insert through the quadrupole housing reference hole. Removal of the first aperture is achieved simply by raising the detector isolation slide valve to its highest position, which exposes the aperture and O-ring seal. The entire process of opening the detector, changing the apertures, and resealing the detector can be performed in less than four hours. The ensuing pumpdown and bakeout then takes at least three days.

The final difference in the vacuum system of the new apparatus is the great care in choice and processing of the materials used in the detector. This has resulted in much lower inherent detector partial pressures and thus much lower inherent background count rates. Background count rates are roughly a factor of ten lower at almost all masses than in our two older machines.

The materials in the detector chamber were all chosen to be ultra-high vacuum compatible whenever possible. This was also the case for the previous machines, but it was not carried to quite the same degree. All of the major steel components in the new detector are constructed of extra low carbon type 304 stainless steel. The low carbon steel was often quite difficult to get, thus occasionally parts were made from stock of other than originally desired thicknesses, but it was possible to get almost all of the desired pieces. Conflat flanges were, of course, commercially purchased and consisted of standard carbon content 304 S.S. The ion pumps and the cryopump also contained regular 304 S.S. Other materials were OFHC copper, high density alumina ceramics, and tantalum wire, all consistent with standard UHV techniques.

The materials processing consisted of extensive use of high temperature vacuum oven degassing of all parts which would withstand the temperatures. All steel only parts were degassed for 1-3 hours, depending on thickness, at 1023°C. The heating and cooling cycles were as rapid as the oven could withstand in order to avoid carbon grain deposition which occurs betweens 500° and 1000°C. The insert assembly for the third differential pumping region was well degassed at the time that the copper block housing the ionizer was brazed to the insert's liquid nitrogen jacket. A vacuum brazing operation was also performed on the entire rotating chamber assembly, at which time it received extensive degassing.

The vacuum oven degassing procedure obviates the need for any chemical cleaning of the vacuum container since any surface contaminants are evaporated and pumped away. This provides the distinct advantage of not creating leaks in hard to repair welds, since no etchants are used. Also, vacuum oven degassing is much more effective than simple surface cleaning, since the vacuum oven process depletes the dissolved gases in the metal for a depth of several millimeters, whereas surface cleaning has no effect on these dissolved gases. The degassing process is also much more effective than in situ, high temperature bakeout, since, in the bakeout process, one becomes limited by the diffusion rate of atmospheric gases through the metal. The fact that gases released during bakeout are not removed from the system, but rather are trapped in the ion pumps where they produce a finite background pressure due to diffusion and sputtering induced release, is also a disadvantage of the bakeout process.

MULTICHANNEL SCALER AND COMPUTER SYSTEM

Concurrent with the design of the new apparatus, a new high speed multichannel scaler (MCS) was being designed to improve the high velocity time-of-flight capabilities of all of our machines. This new scaler was first implemented on the new 35" machine along with a new on-line computer system for data acquisition and analysis. The MCS

itself is CAMAC compatible and thus is independent of the particular computer it is used with. This same MCS design is presently in use on at least five separate machines here at Lawrence Berkeley Laboratory. The details of the computer system are specific to the 35" crossed beams machine.

The MCS unit was designed both to allow for fast timing needed in single shot and photofragmentation time-of-flight studies and to allow for compatibility with our cross-correlation TOF procedure. For fast timing, counting times can be as small as 1 μs per channel, while the unit allows for a software programmable number of channels between 1 and 255. The 255 maximum channel number was chosen for compatibility with our 255 channel cross-correlation sequence.

The basic elements of the scaler consist of dual data scalers, on board random access memory (RAM), a trigger counter, and a sweep counter. After an appropriate initialization sequence from the computer, the module begins counting data in one of its data scalers upon receipt of a trigger signal. At the end of the first channel time, the first data scaler is gated off and the second one gated in. Data is then read from the first channel of the onboard RAM and is added to the data in the first scaler. The sum data is then written back into the first RAM address. The first counter is then cleared and the unit waits for the end of the second dwell time. When the second dwell time is over, the first scaler is gated back in and the second out. Data from the second scaler is then added into the

second RAM address. This alternating process continues until either all channel addresses are consumed or a new trigger signal arrives. Receipt of a new trigger signal causes the unit to reset to the initial channel and start the process over. Each trigger pulse received causes the preset trigger counter to decrement by one. All of these processes occur entirely on board and do not require any host processor intervention.

The trigger counter is used as the control to request data read-in by the computer. When the trigger counter has counted down to zero a request for service (LAM) signal is asserted, and the sweep counter is decremented by one. At this point, the host processor reads in the data, checks for overflows, and reinitializes the module for another sweep cycle. The processor is then free to perform its designated tasks until another sweep is complete. Upon completion of the designated number of sweeps (sweep counter set to zero) a stoprun bit is also asserted along with the LAM signal to inform the computer that the scaler has completed its prescribed data taking cycle.

The unit is provided with visual readouts of the trigger counter, sweep counter, and channel time as well as an input for an external time reference and an output for use in synchronizing the TOF wheel motor frequency. A more detailed description of the performance and the command structure of the module is included below.

MOLECULAR BEAM MULTICHANNEL SCALER-
DESCRIPTION 13X3381-D1

Vince Randolph, Engineer

The Molecular Beam Multichannel Scaler is designed to be a fast computer controlled data acquisition system with data rates up to 20 MHz. The addressing sequence in the accumulate mode is initialized by an input trigger pulse. The trigger pulse should be positive and between 300 to 900 ns in width. It should be TTL compatible. A trigger pulse can occur any time during the accumulate mode. This causes a restart at the initial address and increments the trigger counter. (All pulses into and out of the front panel Lemo connectors are TTL compatible.)

The trigger pulse initializes a preset dwell time starting at the initial address. The dwell time in this first address is 300 ns less than all the other addresses. The 300 ns is used to halt, set up, and restart the accumulate mode. The dwell time is precisely the same for each ensuing address. There is zero dead time between addresses, because the dual data scalers eliminate the problems of scaling and transferring the data. If the internal dwell time is set at 1 μs per address, the initial address will have a dwell time of 700 ns, and all successive addresses will be 1 μs. An external dwell time can be used by coupling to the "EXT DWELL CLK IN" on the front panel. The external dwell clock can vary from DC to 1 MHz as needed.

Input data can be fed to the unit at rates up to 20 MHz. Caution should be taken in calculating the dwell time and trigger count so that the data counters or RAM do not overflow.

The "motor sync out" is a 100 ns pulse that occurs at every dwell time pulse used to generate the address advances.

The three position front panel switch used to change the display may be changed at any time without affecting the contents of the Multichannel Scaler (MCS). The first position displays the number of counts allotted to each address at a particular dwell clock rate. The internal dwell CLK is 1 MHz. Therefore the display reading will be in number of micro sec of dwell time per address. The second position displays present number of trigger counts remaining before an "end sweep" is generated. The trigger counter decrements by one for every input trigger received while in the accumulate mode. The third position displays the number of sweeps remaining before the signal "stoprun" is generated when the sweep counter decrements to zero. At this time the unit is halted and no more trigger or data signals can be accepted to the MCS.

SUMMARY OF CAMAC COMMANDS:

F(0)A(0) - READS DATA WORD (R1-R16) BINARY

F(0)A(1) - READS INITIAL ADDRESS (R1-R8) BINARY

F(0)A(2) - READS OVERFLOWS AND STOPRUN (R1-R3) BINARY

R1 = COUNT OVERFLOW

R2 = RAM OVERFLOW

R3 = STOPRUN

F(0)A(3) - READS SWEEP COUNTER (R1-R16) BCD

F(8)A(0)S1 - TESTS LAM DIRECTLY

F(9)A(0)S1 - CLEARS LAM

CLEARS RAM FROM INITIAL ADDRESS TO ADDRESS 255,

CLEARS COUNTERS AND RAM OVERFLOWS,

RESETS TRIGGER COUNTER, INITIAL ADDRESS AND DWELL TIMER

SETS HLT MODE

F(18)A(0)S1 - LOADS DWELL TIMER WORD (W1-W8) BCD

F(18)A(1)S1 - LOADS INITIAL ADDRESS (W1-W8) BINARY

F(18)A(2)S1 - LOADS TRIGGER WORD COUNTER (W1-W16) BCD

F(18)A(3)S1 - LOADS SWEEP COUNTER (W1-W16) BCD

F(18)A(4)S1 - SETS INT. DWELL CLK.

F(18)A(5)S1 - SETS EXT. DWELL CLK.

F(24)A(0)S1 - DISABLES LAM

F(26)A(0)S1 - SET HLT MODE, DOES NO CLEARS OR RESETS,

BLOCKS INPUT TRIGGERS AND DATA.

F(26)A(1)S1 - ENABLES LAM

F(26)A(6)S1 - SETS ACCUM MODE, DOES NO CLEARS OR RESETS

ZS2 OR CS2 - DISABLES LAM

CLEARS LAM

CLEARS RAM FROM INITIAL ADDRESS TO ADDRESS 255,

CLEARS COUNTERS AND RAM OVERFLOWS,

RESETS TRIGGER COUNTER, INITIAL ADDRESS AND DWELL TIMER

SETS HLT MODE

SEQUENCE OF OPERATION

Using the list of CAMAC commands on the previous page, one can easily program the appropriate signals to the MCS to provide meaningful data. The following steps should be used:

1. Load initial address (W1-W8), BINARY, F(18)A(1)S1
2. Clear RAM, F(9)A(0)S1
3. Load dwell timer word (W1-W8), BCD, F(18)A(0)S1
4. Load trigger word (W1-W16), BCD, F(18)A(2)S1
5. Load sweep counter (W1-W16), BCD, F(18)A(3)S1
6. Set internal dwell CLK, F(18)A(4)S1
7. Set HLT MODE, F(26)A(0)S1 (optional)
8. Enable "LAM", F(26)A(1)S1
9. Set ACCUM MODE, F(26)A(6)S1
   (Immediately goes into the accumulate mode, then goes into a halt and sets "LAM" when end sweep is generated.)
10. Read overflows and stoprun (R1-R3), BINARY, F(0)A(2)

    R1 = Count overflow

    R2 = RAM overflow

    R3 = Stoprun

11. Read sweep counter (R1-R16), BCD, F(0)A(3) (optional)
12. Load initial address (W1-W8), BINARY, F(18)A(1)S1
    (same as step 1)
13. Read data word (R1-R16), BINARY, F(0)A(0)
    (number of read commands should equal 255-initial address)
14. Load initial address (W1-W8), BINARY, F(18)A(1)S1
    (same as step 1)
15. Clear RAM, F(9)A(0)
    (same as step 2)

16. Load sweep counter (W1-W16) BCD, F(18)A(3)S1 (as needed)

17. Repeat steps 9 through 16 as needed

The computer system is organized around an LSI-11 16 bit microcomputer (Digital Equipment Corporation) with full PDP-11 instruction set compatibility. The system contains a single CAMAC crate and interface as well as a dual floppy disc system. A video terminal, fast printer and two separate graphics plotters are also included. An interface to the Lawrence Berkeley Laboartory interactive computing system (RECC) is also provided and is primarily used for automatic transfer of data to the laboratory's mainframe computer system. A layout of the system is shown in Fig. 4.

The particular LSI-11 processor used is the KD11-F model which contains on board 4K words of dynamic RAM in addition to the processor chips. An EIS/FIS microm chip was installed on the processor to allow use of floating point and extended instructions. The system also contains an additional 24K words of add-in memory. The CAMAC crate controller and interface are the Kinetic Systems[2] model 3912 controller with a Q-bus to Unibus adapter card. Real time display of accumulating data is accomplished via the Nuclear Enterprises[3] Harwell 7011-2 Display Driver which is used to drive a Tektronix 604 display monitor. The floppy disc system is a Data Systems Design[4] model 210-L11 which is totally software and media compatible with DEC's RX01 floppy disc system. The video terminal and the printer

are standard DEC items. The terminal is a DEC VT52 video terminal with 24 line by 80 characters per line display and a 20 ma. current loop interface. The printer is DEC's LA180 DECPRINTER I, which is a 180 character per second 132 column dot matrix impact printer. It is interfaced through DEC's LAV11 interface card. The two graphics plotters are a Hewlett-Packard model 7221A which we operated at 600 baud and a Hewlett-Packard 7200A operating at 110 baud. The interface to the LBL RECC system is accomplished via a lab designed FUDLA II module which allows long distance transmission of standard serial data.

REFERENCES

1. Y. T. Lee, J. D. McDonald, P. R. LeBreton, and D. R. Herschbach, Rev. Sci. Instrum. 40, 1402 (1969).

2. Kinetic Systems Corporation, 11 Mayknoll Drive, Lockport, Illinois 60441.

3. Nuclear Enterprises, Incorporated, 935 Terminal Way, San Carlos, California 94070.

4. Data Systems Design, Incorporated, 3130 Coronado Drive, Santa Clara, California 95051.

FIGURE CAPTIONS

Fig. 1. Side view of top plate and rotating seal design. View is through a vertical plane passing through a beam source axis. A - top plate. B - Tec-ring seal. C - ball bearing. D - rotating ring. E - detector top plate.

Fig. 2. Schematic top view of machine layout. Beam sources and differential pumping wall are shown. Differential pumping regions I, II and III of the detector are indicated.

Fig. 3. Example detail of replaceable detector aperture. (a) front view. (b) side view. (c) back view.

Fig. .. Block diagram of computer system components. Directions of device communication are indicated by arrows.

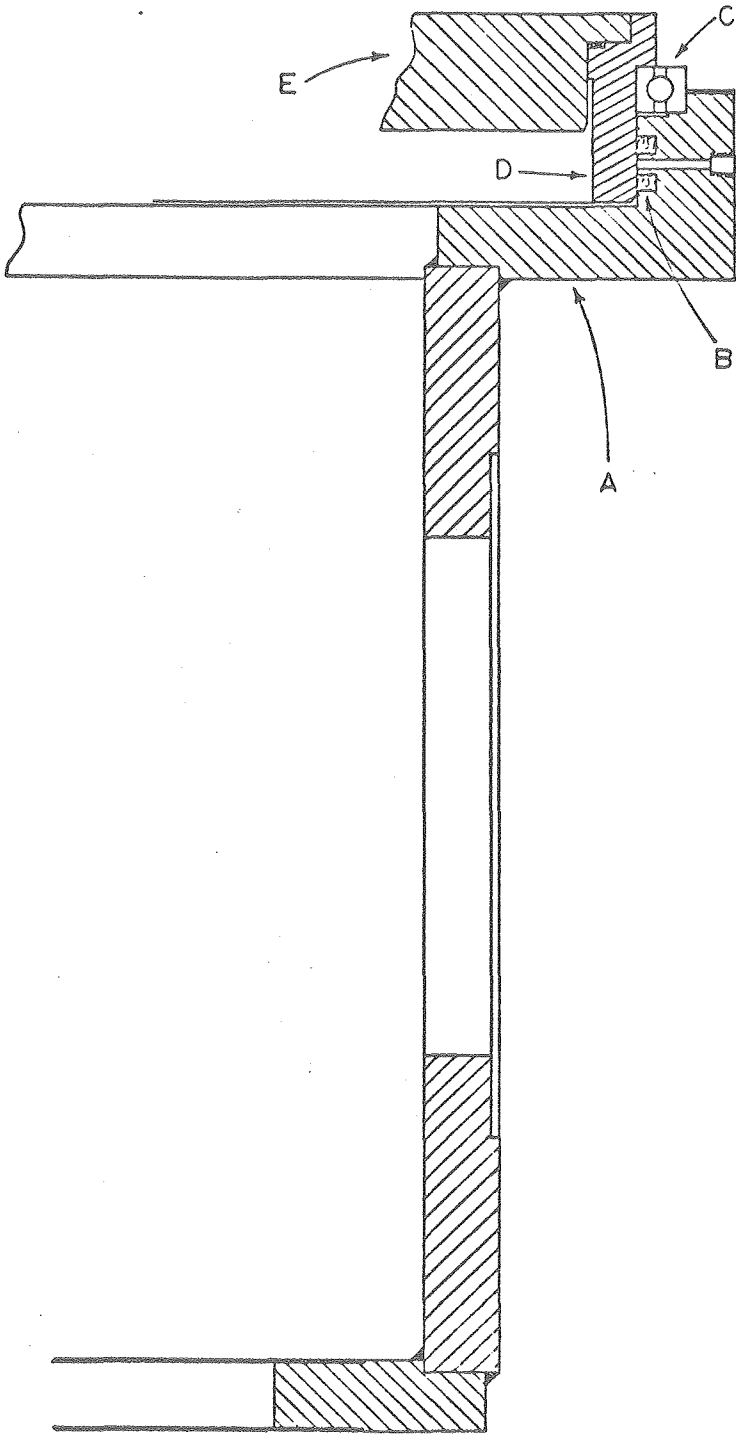

Fig. 1

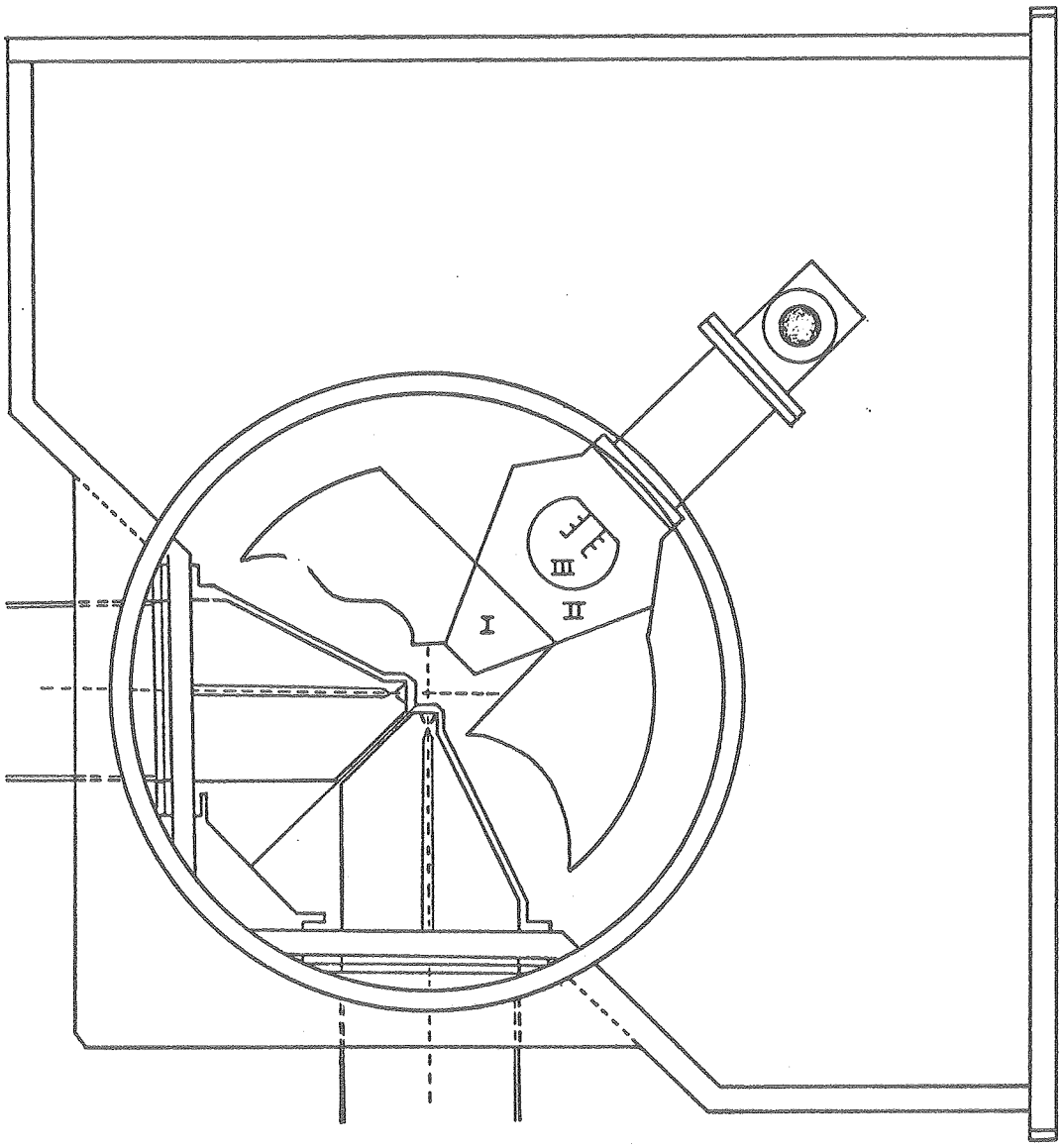

Fig. 2

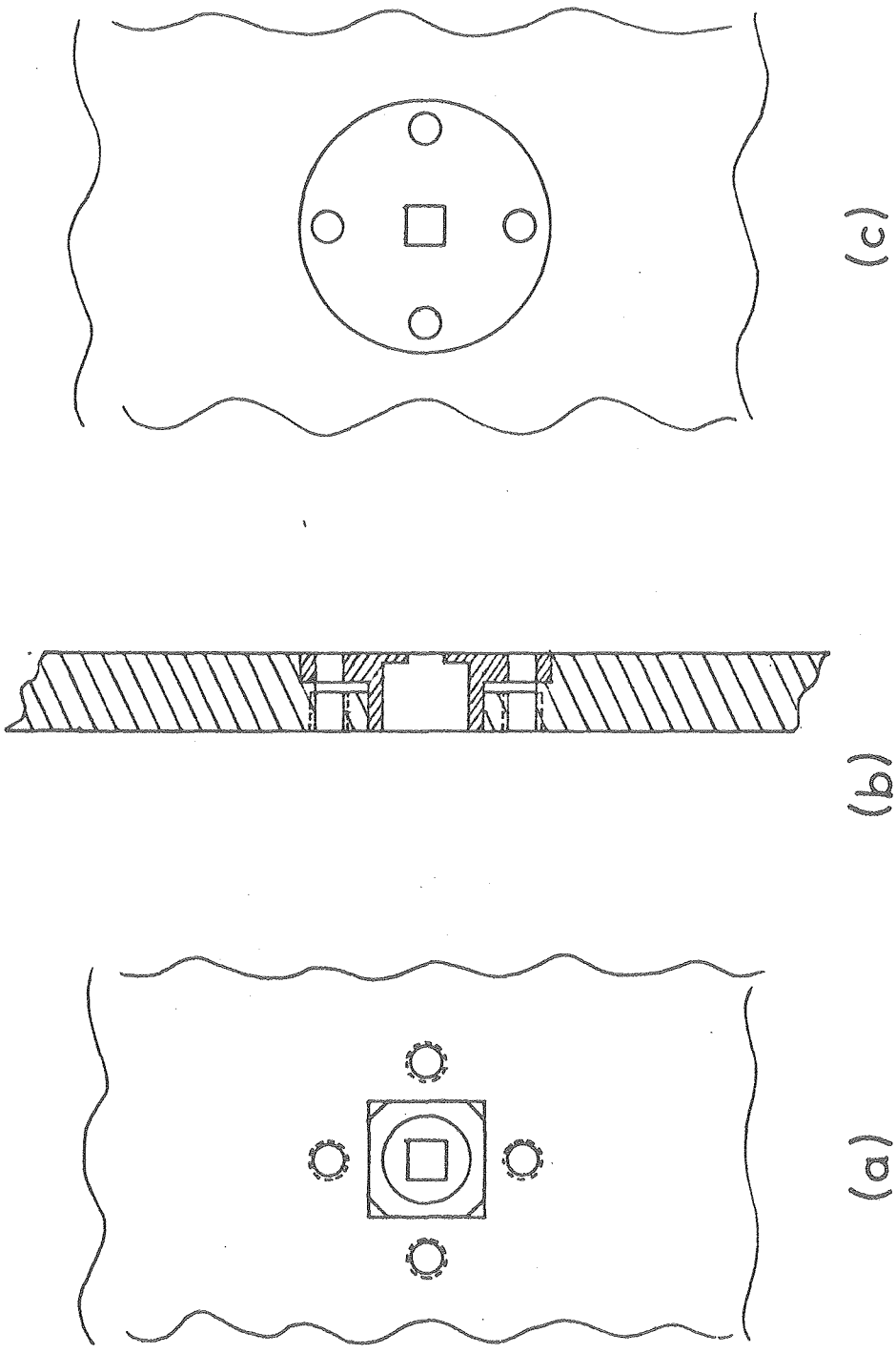

Fig. 3

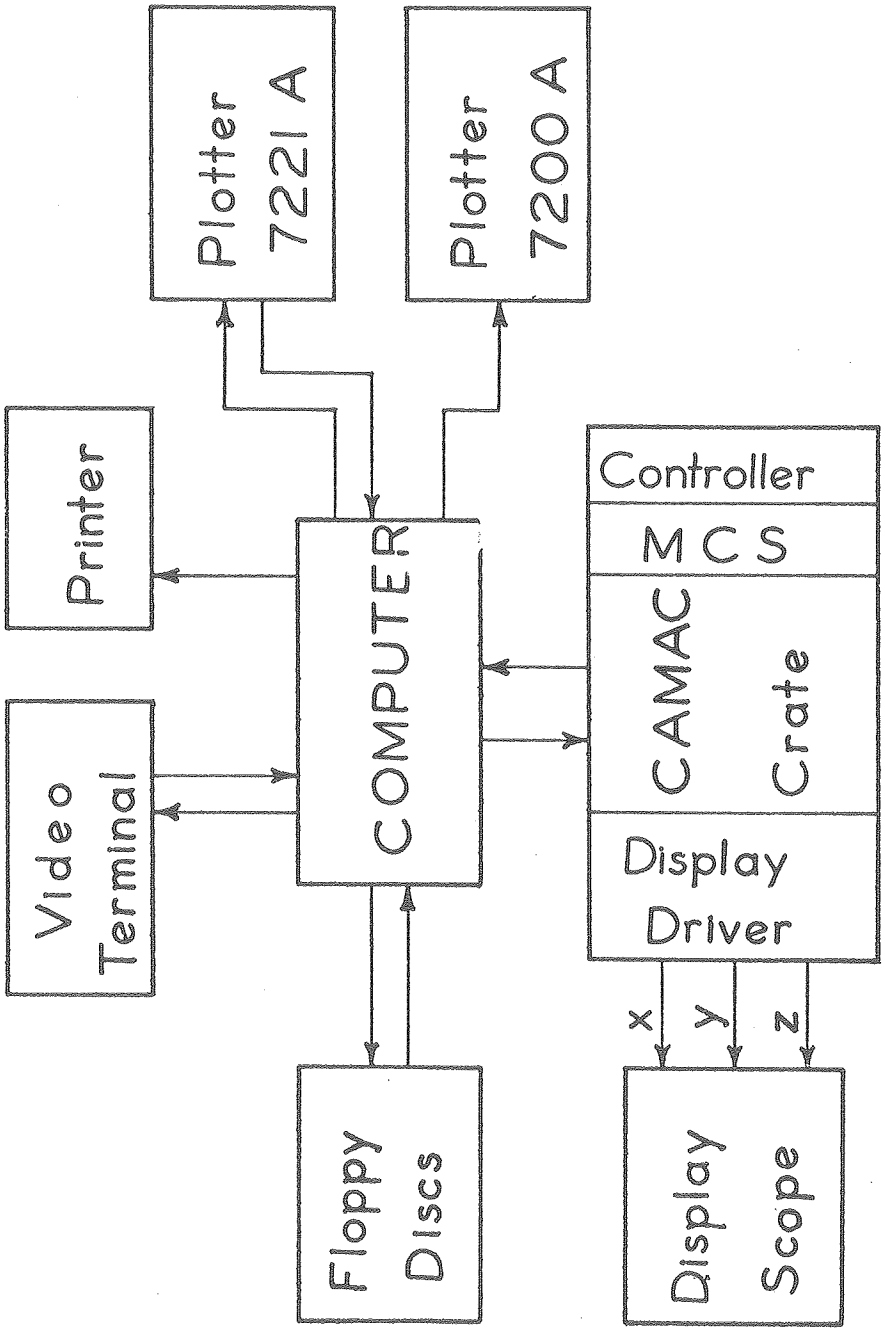
Plotter 7221 A
Plotter 7200 A
Printer
Video Terminal
COMPUTER
Controller
M C S
CAMAC Crate
Display Driver
x
y
z
Floppy Discs
Display Scope

Fig. 4

Appendix B. Computer Programs

MCSTF7

MCSTF7 is the seventh version of a MACRO-11 assembly language data acquisition program for time-of-flight with the multi-channel scaler and computer system described in Appendix A. The program supports data output to all of the system devices except the 7221A high speed plotter and the RECC interface. Data is written onto the floppy disks in a simple format that allows later access by Fortran programs. The program can display and print either the direct data from the MCS, for use in single-shot applications, or the cross-correlated data. Only the direct data is written to disc, however, to allow for flexibility and to avoid propagation of errors in the correlated data. In general, an analysis program will use a more sophisticated method of correlating the raw data than is feasible for real-time display purposes. Upon program start-up, the system is in a single-shot mode and the existence of the cross-correlation capabilities are transparent to the user. They must be specifically invoked from the console terminal in order to use them.

The program is oriented around a simple command structure that allows flexibility and simplicity. No action is taken by the program unless the operator commands it, and all commands are processed and executed in the order of their input. The only exceptions are the oscilloscope display of the data and the collection of the data from the MCS. The oscilloscope display runs continuously under hardware

interrupt control from the time the program is started. Commands can be used to request display of either correlated or uncorrelated data, but display is continuous. The read-in of data from the MCS is also under hardware interrupt control and cannot be disturbed by any command not directly addressing the MCS unit.

The commands and the actions they invoke are given below. All commands consist of two letters followed by a carriage return.

Command	Name and action invoked
ID	Initial dialogue The system requests information from the operator necessary to initialize the multi-channel scaler and system counters. This must always be the first command executed. It needs to be repeated only when the operator desires to change the parameters. Old parameters remain resident in memory otherwise.
ST	Start Clears present data buffers and display buffer. Loads the MCS with all parameters specified in the last ID command, clears MCS RAM, and sets MCS into accumulate mode.
PC	Print Console Prints out the data of the present display buffer on the console terminal.
PL	Print Line Printer Prints out on the line printer the data that had accumulated in the present data buffers at the time the last STOPRUN bit was detected. If correlated data was being displayed when STOPRUN was detected, both correlated and uncorrelated data are valid and may be output under the control of the CD and UD commands. If uncorrelated data was being displayed, the correlated data buffer was not updated and only the uncorrelated data will be valid.

PP — Point Plot
Outputs the data to the HP7200A graphics plotter under the same restrictions as the PL command. Each data point is plotted as a point.

LP — Line Plot
Same as PP except data points are connected by straight lines.

SE — Scan Extend
Used to extend the number of sweeps beyond that requested in the ID command so that additional data may be added to that already in memory. System requests the number of additional sweeps desired. The settings of the ID command are not disturbed. Present data buffers and display buffer are not cleared.

WD — Write to Disk
Write to disk the uncorrelated data that had accumulated in the present data buffers at the time the last STOPRUN bit was detected. System engages in dialogue to establish an informational header and identifying file name.

UD — Uncorrelated Data
Causes uncorrelated data to be displayed on oscilloscope and sets internal flags so that uncorrelated data will be printed or plotted with the next print or plot command. This is default setting.

CD — Correlated Data
Same as above but sets display and flags for correlated data.

OF — Offset
Used to define the offset in number of channels between zero time and the trigger pulse for use in the correlation procedure. Default value is zero but standard correct value is 191. Causes translation of display of correlated data on the oscilloscope.

A sample dialogue session and the listing of the program are given below. To a reader familiar with standard PDP-11 assembly language programming the comments provided should be adequate to allow an

understanding of the program. Where comments are sparse, the names assigned to the variables and addresses should be a very good indication of their function. Almost all of the instructions handling the CAMAC modules are hardware dependent. Anyone wishing a detailed understanding of these sections should consult the manufacturers instruction manuals for the crate controller and display driver and Appendix A for the MCS. The program was written for use with DEC's RT-11 version 2C operating system. Explanations of the system features and of the MACRO-11 assembly language conventions may be found in the relevant manuals for the version 2C or later releases of the RT-11 system.

SAMPLE DIALOGUE SESSION

```
000000
@173000G
$DX0
RT-11SJ     V02C-02B

.RUN MCSTF7
TOF DATA ACQUISITION PROGRAM
ID
DWELL TIME (1-99 MICROSECONDS)=3
TRIGGER COUNT=100
SWEEP COUNT=100
NUMBER OF CHANNELS (1-255)=255
DO YOU WANT INTERNAL DWELL CLOCK (TYPE Y OR N)?Y
ST
RUN IS COMPLETED
SE
NUMBER OF ADDITIONAL SWEEPS = 50
RUN IS COMPLETED
PL
WD
ENTER THE INFORMATIONAL HEADER.
HEADER MAY CONTAIN UP TO 512 CHARACTERS INCLUDING CR,LF.
END OF HEADER IS INDICATED BY AN UP-ARROW (↑) AND A RETURN
THIS IS AN EXAMPLE HEADER. ANY INFORMATION MAY GO HERE.↑
ENTER FILE NAME AFTER *, EXAMPLE
*DX1:NAME.EXT=
 THE DEFAULT IF NO EXTENSION IS GIVEN IS .DAT
THE = MUST FOLLOW FILE NAME
*DX1:EXAMPL.FIL=
FILE SUCCESSFULLY WRITTEN, YOU MAY CONTINUE.
ST
```

```
        .TITLE  MULTICHANNEL SCALER TIME OF FLIGHT
        .MCALL  ..V2..,.REGDEF,.PRINT,.TTYIN,.TTINR,.CSIGEN,.WRITW,.CLOSE
        ..V2..
        .REGDEF
        .GLOBL  JMUL,JDIV
MCSA0   =167200
MCSA1   =167202
MCSA2   =167204
MCSA3   =167206
MCSA4   =167210
MCSA5   =167212
MCSA6   =167214
MCSNVC  =530
DATALO  =166000
DATAHI  =166002
LAMLO   =166004
LAMHI   =166006
STATU1  =166010
STATU2  =166012
DIDRA0  =166100
DIDRA1  =166102
DIDNVC  =410
LPSTA   =177514
LPBUF   =177516
LPNVC   =200

START:  MOV     #UDBUF,R1               ;CLEAR DATA BUFFER
        MOV     #510.,R2                ;WORD COUNTER
1$:     CLR     (R1)+
        SOB     R2,1$
        MOV     #OTPTBF,R1
        MOV     #510.,R2
3$:     CLR     (R1)+
        SOB     R2,3$
        BIS     #1,@#RUNDNE
        BIC     #1,@#NWMDFG
        MOV     #MCSINT,@#MCSNVC
        MOV     #340,@#MCSNVC+2
        MOV     #DIDINT,@#DIDNVC        ;LOAD DISPLAY DRIVER
                                        ;INTERRUPT VECTOR
        MOV     #0,@#DIDNVC+2
        MOV     #DIBFBG,R1              ;CLEAR THE DISPLAY BUFFER
        MOV     #256.,R2
2$:     CLR     (R1)+
        SOB     R2,2$
        BIC     #70,@#STATU1            ;CLEAR NQE, NXE, I
        MOV     @#CONREG,@#DATALO       ;DATA FOR DISPLAY DRIVER
                                        ;CONTROL REGISTER
        MOVB    #17.,@#DIDRA0           ;F17A0 LOAD CONTROL REGISTER
        MOV     @#NUMPTS,@#PTCNTR       ;INITIALIZE LOOP COUNTER
        MOV     #DIBFBG,@#BEGADR        ;LOAD BEGINNING ADDRESS FOR BUFFER
        MOV     @#BEGADR,@#PTADR        ;SET BEGINNING ADDRESS
                                        ;TO FIND POINTS
        CLR     @#DATALO                ;LOAD A ZERO
        MOVB    #16.,@#DIDRA1           ;F16A1 SEND FIRST X=0 TO
                                        ;INITIALIZE DISPLAY
        MOV     @PTADR,@#DATALO         ;LOAD FIRST Y VALUE
        ADD     #2,@#PTADR              ;INCREMENT ADDRESS COUNTER
        MOVB    #16.,@#DIDRA0           ;F16A0 SEND FIRST Y VALUE
        BIS     #300,@#STATU1           ;SET INE, AND REIN
```

```
        .PRINT  #HELLO
WAIT:   .TTINR
        BCC     MODEIN                  ;CHECK FOR MODE INPUT
        TST     @#NWDTFG                ;CHECK FOR NEW DATA
        BGT     JMPCRN                  ;JUMP TO CRUNCH IF NEW DATA
        BIT     #1,@#OVFLSR
        BGT     CNTOVF
        BIT     #2,@#OVFLSR
        BGT     RAMOVF
        BIT     #4,@#OVFLSR
        BGT     ENDRUN
        BIT     #1,@#NWMDFG
        BGT     MDHDLR
        JMP     WAIT
JMPCRN: JMP     CRUNCH
MDHDLR: BIC     #1,@#NWMDFG
        BIT     #1,@#RUNDNE
        BGT     JMPCRN
        BIT     #1,@#CORFLG
        BEQ     JMPCRN
        JMP     WAIT
CNTOVF: .PRINT  #CNTMSG
        BIC     #1,@#OVFLSR
        JMP     WAIT
RAMOVF: .PRINT  #RAMMSG
        BIC     #2,@#OVFLSR
        JMP     WAIT
ENDRUN: MOV     #UDBUF,R1
        MOV     #OTPTBF,R2
        MOV     #510.,R5
1$:     MOV     (R1)+,(R2)+
        SOB     R5,1$
        MOV     #CDBUF,R1
        MOV     #COUTBF,R2
        MOV     #510.,R5
2$:     MOV     (R1)+,(R2)+
        SOB     R5,2$
        .PRINT  #BELLS
        .PRINT  #ENDMSG
        BIC     #4,@#OVFLSR
        BIS     #1,@#RUNDNE
        JMP     WAIT
MODEIN: MOV     #INBUF,R1
        MOVB    R0,(R1)+
        .TTYIN
        CMP     R0,#12
        BEQ     SYN
        MOVB    R0,(R1)+
        .TTYIN
        CMP     R0,#12
        BEQ     SYN
1$:     .TTYIN
        CMP     R0,#12
        BNE     1$
CHKMOD: CMP     @#INBUF,#"ID
        BNE     NOID
        JMP     INIDIA
NOID:   CMP     @#INBUF,#"ST
        BNE     NOST
        JMP     SCNST
NOST:   CMP     @#INBUF,#"PC
```

```
        BNE     NOPC
        JMP     PRTCNS
NOPC:   CMP     @#INBUF,#"PL
        BNE     NOPL
        JMP     PRTLP
NOPL:   CMP     @#INBUF,#"PP
        BNE     NOPP
        JMP     PLOT
NOPP:   CMP     @#INBUF,#"SE
        BNE     NOSE
        JMP     SCNEXT
NOSE:   CMP     @#INBUF,#"LP
        BNE     NOLP
        JMP     LPLOT
NOLP:   CMP     @#INBUF,#"WD
        BNE     NOWD
        JMP     WRTDSK
NOWD:   CMP     @#INBUF,#"UD
        BNE     NOUD
        BIC     #1,@#CORFLG
        BIS     #1,@#NWMDFG
        JMP     WAIT
NOUD:   CMP     @#INBUF,#"CD
        BNE     NOCD
        BIS     #1,@#CORFLG
        BIS     #1,@#NWMDFG
        JMP     WAIT
NOCD:   CMP     @#INBUF,#"OF
        BNE     SYN
        JMP     OFSTIN
SYN:    .PRINT  #SYNTAX
        JMP     WAIT
INIDIA: .PRINT  #DWLMSG
        MOV     #INBUF,R1
1$:     .TTYIN
        CMP     R0,#15
        BEQ     2$
        MOVB    R0,(R1)+
        BR      1$
2$:     .TTYIN                          ;BRING IN LF
        MOV     #DWLBCD,R5
        JSR     PC,BCDIN
        MOV     #DWLBIN,R5
        JSR     PC,BININ
TRGIN:  .PRINT  #TRGMSG
        MOV     #INBUF,R1
1$:     .TTYIN
        CMP     R0,#15
        BEQ     2$
        MOVB    R0,(R1)+
        BR      1$
2$:     .TTYIN                          ;BRING IN LF
        MOV     #TRGBCD,R5
        JSR     PC,BCDIN
        MOV     #TRGBIN,R5
        JSR     PC,BININ
SWPIN:  .PRINT  #SWPMSG
        MOV     #INBUF,R1
1$:     .TTYIN
        CMP     R0,#15
        BEQ     2$
```

```
        MOVB    R0,(R1)+
        BR      1$
2$:     .TTYIN
        MOV     #SWPBCD,R5
        JSR     PC,BCDIN
        MOV     #SWPBIN,R5
        JSR     PC,BININ
NCHIN:  .PRINT  #NCHMSG
        MOV     #INBUF,R1
1$:     .TTYIN
        CMP     R0,#15
        BEQ     2$
        MOVB    R0,(R1)+
        BR      1$
2$:     .TTYIN
        MOV     #NCHBIN,R5
        JSR     PC,BININ
        MOV     #255.,@#IADBIN
        SUB     @#NCHBIN,@#IADBIN
CLKIN:  .PRINT  #CLKMSG
        CLR     @#CLKFLG
        .TTYIN
        CMP     R0,#'Y
        BEQ     1$
        BIS     #1,@#CLKFLG
1$:     .TTYIN
        CMP     R0,#12
        BNE     1$
        JMP     WAIT
OFSTIN: .PRINT  #FSTMSG
        MOV     #INBUF,R1
1$:     .TTYIN
        CMP     R0,#15
        BEQ     2$
        MOVB    R0,(R1)+
        BR      1$
2$:     .TTYIN
        MOV     #CCOFST,R5
        JSR     PC,BININ
        BIS     #1,@#NWMDFG
        JMP     WAIT
SCNST:  CLR     @#SXTBCD                ;CLEAR SCAN EXTEND LOCATIONS
        CLR     @#SXTBIN
        BIC     #1,@#RUNDNE
        MOV     @#SWPBIN,@#NUMSWP       ;LOAD NUMBER SWEEPS COUNTER
        MOV     #UDBUF,R1               ;CLEAR DATA BUFFER
        MOV     #510.,R2
1$:     CLR     (R1)+
        SOB     R2,1$
        MOV     #DIBFBG,R1              ;DISPLAY BUFFER CLEAR LOOP
        MOV     #256.,R2
4$:     CLR     (R1)+
        SOB     R2,4$
        BIC     #70,@#STATU1            ;CLEAR NQE, NXE, I
        MOV     #0,@#DATALO
        MOVB    #18.,@#MCSA1            ;SET INITIAL ADDRESS=0
        MOVB    #9.,@#MCSA0             ;F9A0CLEAR
        MOV     #50,R5                  ;WAIT LOOP FOR MEMORY CLEAR
2$:     NOP
        SOB     R5,2$
        MOV     @#DWLBCD,@#DATALO
```

```
        MOVB    #18.,@#MCSA0            ;F18A0 LOAD DWELL TIME
        MOV     @#IADBIN,@#DATALO
        MOVB    #18.,@#MCSA1            ;F18A1, LOAD INITIAL ADDRESS
        MOV     @#TRGBCD,@#DATALO
        MOVB    #18.,@#MCSA2            ;F18A2 LOAD TRIGGER WORD
5$:     MOV     @#SWPBCD,@#DATALO
        BIS     #1,@#STATU1             ;SET DII BIT FOR LOOP BACK
                                        ;AFTER CLEARING
        MOVB    #18.,@#MCSA3            ;F18A3 LOAD SWEEP COUNTER
        BIC     #1,@#STATU1             ;CLEAR DII BIT FOR CMP OPERATION
        CMP     @#MCSA3,@#SWPBCD        ;F0A3 COMPARE SWEEP COUNTER
        BNE     5$                      ;CHECK FOR EQUALITY, RELOAD IF NOT
        BIS     #1,@#STATU1             ;RESET DII
        MOVB    #18.,@#MCSA4            ;F18A4 SET INTERNAL DWELL
        BIT     #1,@#CLKFLG             ;SEE IF WANT EXTERNAL DWELL
        BEQ     3$                      ;NO, THEN GO AROUND
        MOVB    #18.,@#MCSA5            ;F18A5,SET EXTERNAL DWELL
3$:     MOVB    #26.,@#MCSA1            ;F26A1, ENABLE LAM
        MOVB    #26.,@#MCSA6            ;F26A6, SET ACCUMULATE
        BIS     #301,@#STATU1           ;SET REIN,INE,DII
        JMP     WAIT
PRTCNS: MOV     @#NCHBIN,R1
        BIT     #1,@#CORFLG
        BEQ     1$
        MOV     #CDBUF,R4
        BR      2$
1$:     MOV     #UDBUF,R4
2$:     MOV     #22.,@#LNCNTR
AGIN:   MOV     #OUTSTR,R3
        MOV     #6,R2
2$:     MOV     (R4)+,HIORD
        MOV     (R4)+,LOWORD
        JSR     PC,DPIDCO
        DEC     R1
        BEQ     CHPSTR
        DEC     R2
        BEQ     SEND
        MOVB    #40,(R3)+
        MOVB    #40,(R3)+
        BR      2$
SEND:   MOVB    #0,(R3)+
        .PRINT  #OUTSTR
        DEC     @#LNCNTR
        BEQ     1$
        BR      AGIN
1$:     BIS     #10000,@#44
        .TTYIN
        BIC     #10000,@#44
        BR      AGIN
CHPSTR: MOVB    #0,(R3)+
        .PRINT  #OUTSTR
        JMP     WAIT
PRTLP:  BIT     #1,@#CORFLG
        BEQ     NOCMSG
        MOV     #CDPMSG,R0
        JSR     PC,PRINT
        MOV     @#CCOFST,R5
        MOV     #OUTSTR,R3
        JSR     PC,ASCDG4
        MOVB    #0,(R3)+
        MOV     #OUTSTR,R0
```

```
        JSR     PC,PRINT
        CLR     @#OUTSTR
        MOV     #OUTSTR,R0
        JSR     PC,PRINT
        MOV     #OUTSTR,R0
        JSR     PC,PRINT
        MOV     #OUTSTR,R0
        JSR     PC,PRINT
NOCMSG: MOV     #DWLMSG,R0          ;GET DWELL MESSAGE ADDRESS
        JSR     PC,PRINT            ;OUTPUT IT
        MOV     @#DWLBIN,R5         ;GET DWELL SETTING
        MOV     #OUTSTR,R3          ;SET UP STRING
        JSR     PC,ASCDG4           ;CONVERT TO ASCII
        MOVB    #0,(R3)+            ;TERMINATE STRING
        MOV     #OUTSTR,R0
        JSR     PC,PRINT            ;OUTPUT DWELL SETTING
        CLR     @#OUTSTR            ;ROUTINE FOR OUTPUTTING THREE
                                    ;LINE FEEDS
        MOV     #OUTSTR,R0
        JSR     PC,PRINT
        MOV     #OUTSTR,R0
        JSR     PC,PRINT
        MOV     #OUTSTR,R0
        JSR     PC,PRINT
        MOV     #TRGMSG,R0          ;GET TRIGGER MESSAGE ADDRESS
        JSR     PC,PRINT            ;OUTPUT IT
        MOV     @#TRGBIN,R5         ;GET TRIGGER SETTING
        MOV     #OUTSTR,R3
        JSR     PC,ASCDG4
        MOVB    #0,(R3)+
        MOV     #OUTSTR,R0
        JSR     PC,PRINT            ;OUTPUT TRIGGER SETTING
        CLR     @#OUTSTR            ;OUTPUT THREE MORE LINE FEEDS
        MOV     #OUTSTR,R0
        JSR     PC,PRINT
        MOV     #OUTSTR,R0
        JSR     PC,PRINT
        MOV     #OUTSTR,R0
        JSR     PC,PRINT
        MOV     #SWPMSG,R0          ;GET SWEEP MESSAGE
        JSR     PC,PRINT
        BIC     #1,@#STATUI         ;CLEAR DII BIT FOR
                                    ;DIRECT ADDRESSING
        MOV     @#MCSA3,R5          ;F0A3 GET UNCOMPLETED  SWEEPS
        BIS     #1,@#STATUI         ;RESET DIPI BIT
        JSR     PC,BCDBIN           ;CONVERT TO BINARY
        NEG     R5                  ;MAKE NEGATIVE
        ADD     @#NUMSWP,R5         ;ADD REQUESTED SWEEPS
        MOV     #OUTSTR,R3          ;SET UP STRING
        JSR     PC,ASCDG4           ;CONVERT TO ASCII
        MOVB    #0,(R3)+            ;TER/MINSATE STRING
        MOV     #OUTSTR,R0
        JSR     PC,PRINT            ;OUTPUT SWEEP COUNT
        CLR     @#OUTSTR            ;OUTPUT THREE MORE LINE FEEDS
        MOV     #OUTSTR,R0
        JSR     PC,PRINT
        MOV     #OUTSTR,R0
        JSR     PC,PRINT
        MOV     #OUTSTR,R0
        JSR     PC,PRINT
        MOV     #NCHMSG,R0          ;GET CHANNEL NUMBER MESSAGE
```

```
        JSR     PC,PRINT
        MOV     @#NCHBIN,R5
        MOV     #OUTSTR,R3
        JSR     PC,ASCDG4
        MOVB    #0,(R3)+
        MOV     #OUTSTR,R0
        JSR     PC,PRINT                ;OUTPUT NUMBER OF CHANNELS
        CLR     @#OUTSTR                ;OUTPUT THREE LINE FEEDS
        MOV     #OUTSTR,R0
        JSR     PC,PRINT
        MOV     #OUTSTR,R0
        JSR     PC,PRINT
        MOV     #OUTSTR,R0
        JSR     PC,PRINT
        MOV     @#NCHBIN,R1
        BIT     #1,@#CORFLG
        BEQ     UDPRNT
        MOV     #COUTBF,R4
        BR      OUTRLP
UDPRNT: MOV     #OTPTBF,R4
OUTRLP: MOV     #5,@#GPCNTR             ;LOOP FOR SPACING EVERY FIVE LINES
AGINLP: MOV     #OUTSTR,R3
        MOV     #10.,R2
2$:     MOV     (R4)+,HIORD
        MOV     (R4)+,LOWORD
        JSR     PC,DPIDCO
        DEC     R1
        BEQ     CHPSLP
        DEC     R2
        BEQ     SENDLP
        MOVB    #40,(R3)+
        MOVB    #40,(R3)+
        BR      2$
SENDLP: MOVB    #0,(R3)+
        MOV     #OUTSTR,R0
        JSR     PC,PRINT
        DEC     @#GPCNTR
        BEQ     GAPLIN          ;SEE IF READY TO SPACE ONE LINE
        BR      AGINLP
GAPLIN: TSTB    @#LPSTA         ;SEND EXTRA LINE FEED TO LINE PRINTER
        BPL     GAPLIN
        MOVB    #12,@#LPBUF
        BR      OUTRLP
CHPSLP: MOVB    #0,(R3)+
        MOV     #OUTSTR,R0
        JSR     PC,PRINT
        JMP     WAIT
CRUNCH: CLR     @#NWDTFG
        TST     @#CORFLG
        BEQ     UDSCL           ;GO SCALE UNCORRELLATED DATA
CRLLAT: MOV     #510.,R1
        MOV     #UDBUF,R2       ;TRANSFER ALL DATA TO WORK BUFFER
        MOV     #WRKBUF,R3
1$:     MOV     (R2)+,(R3)+
        SOB     R1,1$
        MOV     #UDBUF+4,R2     ;REPLACE FIRST POINT WHICH IS USUALLY BAD
        MOV     #WRKBUF,R3      ;BY THE SECOND POINT
        MOV     (R2)+,(R3)+
        MOV     (R2)+,(R3)+
        MOV     #UDBUF+1008.,R2 ;REPLACE LAST TWO POINTS BY THIRD TO LAST
        MOV     #WRKBUF+1012.,R3
```

```
        MOV     (R2)+,(R3)+
        MOV     (R2)+,(R3)+
        MOV     #UDBUF+1008.,R2
        MOV     (R2)+,(R3)+
        MOV     (R2)+,(R3)+
;BEGIN CORRELLATION ON WRKBUF
        CLR     @#CCCNTR        ;CLEAR RESULT INDEX LOOP COUNTER
        MOV     #CDBUF,R1
2$:     MOV     #WRKBUF,R2
        MOV     #SEQNBF+255.,R3
        ADD     @#CCOFST,R3
        SUB     @#CCCNTR,R3
        MOV     #255.,R0        ;SET SEQUENCE INDEX COUNTER
        CLR     R4
        CLR     R5              ;CLEAR TO STORE HIGH AND LOW ORDER RESULT
3$:     BITB    #1,(R3)+        ;CHECK WHETHER SHOULD ADD OR SUBTRACT
        BEQ     5$              ;GO THERE FOR SUBTRACTION
        ADD     2(R2),R5        ;DOUBLE PRECISION ADDITION INTO RESULT
        ADC     R4
        ADD     (R2),R4
        ADD     #4,R2           ;KICK UP WRKBUF POINTER
        SOB     R0,3$           ;SEE IF DONE WITH THIS POINT
        TST     R4
        BGE     4$              ;CHECK FOR NEGATIVE RESULT
        CLR     R4              ;CLEAR IT IF NEGATIVE
        CLR     R5
4$:     MOV     R4,(R1)+
        MOV     R5,(R1)+        ;LOAD POINT INTO CDBUF
        ADD     #1,@#CCCNTR     ;KICK UP RESULT INDEX COUNTER
        CMP     @#CCCNTR,#255.  ;SEE IF DONE WITH LAST POINT
        BEQ     CCDONE
        BR      2$              ;DO NEXT POINT IF NOT DONE
5$:     SUB     2(R2),R5        ;DOUBLE SUBTRACTION INTO RESULT
        SBC     R4
        SUB     (R2),R4
        ADD     #4,R2           ;KICK UP WRKBUF POINTER
        SOB     R0,3$           ;SEE IF DONE WITH THIS POINT
        TST     R4              ;CHECK FOR NEGATIVE RESULT
        BGE     6$              ;GO AROUND IF POSITIVE
        CLR     R4              ;CLEAR IT IF NEGATIVE
        CLR     R5              ;DISPLAY SCALING DOESN'T LIKE NEG NUMBERS
6$:     MOV     R4,(R1)+
        MOV     R5,(R1)+        ;LOAD POINT INTO CDBUF
        ADD     #1,@#CCCNTR     ;KICK UP RESULT INDEX COUNTER
        CMP     @#CCCNTR,#255.  ;SEE IF DONE WITH LAST POINT
        BNE     2$              ;DO NEXT POINT IF NOT
CCDONE: MOV     #CDBUF,@#SCBFBG ;SET UP TO SCALE CORRELLATED DATA
        BR      BT32SC
UDSCL:  MOV     #UDBUF,@#SCBFBG ;SCALE UNCORRELLATED DATA
BT32SC: CLR     @#MAGFLG
        CLR     @#BITNUM
        MOV     #255.,R2
        MOV     @#SCBFBG,R5
1$:     MOV     (R5)+,R1
2$:     DEC     R2
        BEQ     3$
        ADD     #2,R5
        CMP     (R5),R1
        BHI     1$
        ADD     #2,R5
        BR      2$
```

```
3$:     CMP     R1,#0
        BNE     MAGFND
        BIT     #1,@#MAGFLG
        BNE     MAGFND
        BIS     #1,@#MAGFLG
        MOV     @#SCBFBG,R5
        ADD     #2,R5
        MOV     #255.,R2
        BR      1$
MAGFND: BIT     #1,@#MAGFLG
        BGT     1$
        MOV     #16.,@#BITNUM
1$:     JSR     PC,NUMBIT
        ADD     R4,@#BITNUM
        SUB     #10.,@#BITNUM
        BLE     NOSHFT
        NEG     @#BITNUM
        MOV     #255.,R1
        MOV     @#SCBFBG,R5
        MOV     #DIBFBG,R4
2$:     MOV     (R5)+,R2
        MOV     (R5)+,R3
        ASHC    @#BITNUM,R2
        MOV     R3,(R4)+
        DEC     R1
        BEQ     JMPWAT
        BR      2$
NOSHFT: MOV     #255.,R1
        MOV     @#SCBFBG,R5
        MOV     #DIBFBG,R4
1$:     ADD     #2,R5
        MOV     (R5)+,(R4)+
        DEC     R1
        BGT     1$
JMPWAT: JMP     WAIT
LPLOT:  MOVB    #'L,@#PLPMSG+4          ;SET FOR LINE PLOT MESSAGE
        BR      LPLOT1
PLOT:   MOVB    #'P,@#PLPMSG+4          ;MAKE SURE IS POINT PLOT MESSAGE
LPLOT1: BIT     #1,@#CORFLG
        BEQ     1$
        MOV     #COUTBF,R5
        BR      2$
1$:     MOV     #OTPTBF,R5              ;GET OUTPUT BUFFER ADDRESS
2$:     CLR     @#ORD                   ;CLEAR X VALUE LOCATION
        CLR     @#ABS                   ;CLEAR Y VALUE LOCATION
        CLR     @#SIZFLG                ;CLEAR DATA SIZE FLAG
        MOV     @#NCHBIN,R1             ;INITIALIZE COUNTER
MAXFND: MOV     (R5)+,R2                ;PLACE HIGH ORDER DATA IN R2
        MOV     (R5)+,R3                ;PLACE LOW ORDER DATA IN R3
1$:     DEC     R1                      ;DECREMENT COUNTER
        BEQ     2$                      ;STORE VALUES IF DONE
        SUB     2(R5),R3                ;COMPARE PRESENT WITH NEXT VALUE
        SBC     R2
        SUB     (R5),R2
        BLT     MAXFND                  ;PUT IN NEW VALUE IF GREATER
        ADD     2(R5),R3                ;RESTORE OLD VALUE IF IT GREATER
        ADC     R2
        ADD     (R5),R2
        ADD     #4,R5                   ;INCREMENT ADDRESS
        BR      1$                      ;COMPARE WITH NEXT VALUE
2$:     MOV     R2,@#MAXHI              ;STORE HIGH ORDER OF LARGEST POINT
```

```
        MOV     R3,@#MAXLO              ;STORE LOW ORDER OF LARGEST POINT
        BIT     #1,@#CORFLG
        BEQ     3$
        MOV     #COUTBF,R5
        BR      4$
3$:     MOV     #OTPTBF,R5              ;INITIALIZE FOR SMALLEST POINT SEAR
4$:     MOV     @#NCHBIN,R1
MINFND: MOV     (R5)+,R2
        MOV     (R5)+,R3
1$:     DEC     R1
        BEQ     2$
        SUB     2(R5),R3
        SBC     R2
        SUB     (R5),R2
        BGE     MINFND
        ADD     2(R5),R3
        ADC     R2
        ADD     (R5),R2
        ADD     #4,R5
        BR      1$
2$:     MOV     R2,@#MINHI              ;STORE HIGH ORDER OF SMALLEST POINT
        MOV     R3,@#MINLO              ;STORE LOW ORDER
        MOV     @#MAXHI,@#SIZHI         ;SUBTRACT SMALLEST FROM LARGEST
                                        ;FOR SIZE
        MOV     @#MAXLO,@#SIZLO
        SUB     @#MINLO,@#SIZLO
        SBC     @#SIZHI
        SUB     @#MINHI,@#SIZHI
        CMP     #40,@#SIZHI             ;COMPARE SIZE WITH 2^21
        BGT     3$                      ;GO AROUND FOR SMALL SIZE DATA
        BIS     #1,@#SIZFLG             ;SET FLAG FOR LARGE SIZE DATA
        MOV     @#SIZLO,@#OPR1          ;DIVIDE SIZE BY 9990 TO GET DIVISOR
        MOV     @#SIZHI,@#OPR1+2        ;FOR SCALING OF LARGE DATA
        MOV     #9990.,@#OPR2
        MOV     #0,@#OPR2+2
        MOV     #LIST,R5                ;ADDRESS OF ADDRESS LIST FOR SYSLIB
        JSR     PC,JDIV                 ;CALL SYSLIB INTEGER*4 DIVISION
        MOV     @#RESULT,@#TEMPLO
        MOV     @#RESULT+2,@#TEMPHI     ;STORE SCALING DIVISOR
3$:     MOV     #PLPMSG,R0              ;ADDRESS OF PLOTTER INIT. MESSAGE
        JSR     PC,PRTPLT               ;SEND PLOTTER INIT. MESSAGE
        MOV     @#NCHBIN,@#PLTCNT       ;INIT. POINT COUNTER
        BIT     #1,@#CORFLG
        BEQ     4$
        MOV     #COUTBF,@#PLTADR
        BR      NEWPNT
4$:     MOV     #OTPTBF,@#PLTADR        ;INIT. ADDRESS OF POINTS
NEWPNT: MOV     @PLTADR,@#OPR1+2        ;LOAD HIGH ORDER OF DATA
        ADD     #2,@#PLTADR             ;INCREMENT ADDRESS
        MOV     @PLTADR,@#OPR1          ;LOAD LOW ORDER OF DATA
        ADD     #2,@#PLTADR             ;INCREMENT ADDRESS
        SUB     @#MINLO,@#OPR1          ;SUBTRACT BASELINE FROM POINT
        SBC     @#OPR1+2
        SUB     @#MINHI,@#OPR1+2
        BIT     #1,@#SIZFLG             ;CHECK DATA SIZE
        BEQ     SMLSCL                  ;GO AROUND IF SMALL DATA
LRGSCL: MOV     @#TEMPLO,@#OPR2         ;LOAD LARGE DATA SCALING DIVISOR
        MOV     @#TEMPHI,@#OPR2+2
        MOV     #LIST,R5
        JSR     PC,JDIV                 ;PERFORM SYSLIB DIVISION
        CMP     #-3,R0
```

```
        BNE     1$
        .PRINT  #ERR4
1$:     BR      PNTOUT                  ;OUTPUT THE POINT
SMLSCL: MOV     #999.,@#OPR2            ;MUL FIRST TO AVOID UNDERFLOW BUT
        MOV     #0,@#OPR2+2             ;NOT BY 9990 TO AVOID OVERFLOW
        MOV     #LIST,R5
        JSR     PC,JMUL                 ;PERFORM SYSLIB MULTIPLICATION
        CMP     #-2,R0
        BNE     1$
        .PRINT  #ERR1
1$:     MOV     @#RESULT,@#OPR1         ;RESET FOR DIVISION BY SIZE
        MOV     @#RESULT+2,@#OPR1+2
        MOV     @#SIZLO,@#OPR2
        MOV     @#SIZHI,@#OPR2+2
        MOV     #LIST,R5
        JSR     PC,JDIV                 ;PERFORM DIVISION
        CMP     #-3,R0
        BNE     2$
        .PRINT  #ERR2
2$:     MOV     @#RESULT,@#OPR1         ;SET FOR MUL BY 10
                                        ;TO GET 9990 SCALING
        MOV     @#RESULT+2,@#OPR1+2
        MOV     #10.,@#OPR2
        MOV     #0,@#OPR2+2
        MOV     #LIST,R5
        JSR     PC,JMUL                 ;PERFORM THE MULTIPLICATION
        CMP     #-2,R0
        BNE     PNTOUT
        .PRINT  #ERR3
PNTOUT: ADD     #39.,@#ORD              ;INCREMENT THE X VALUE
        MOV     @#RESULT,@#ABS          ;STORE THE Y VALUE
        MOV     #OUTSTR,R3              ;LOAD ADDRESS OF OUTPUT STRING
        MOV     @#ORD,R5                ;LOAD THE X VALUE
        JSR     PC,ASCDG4               ;CONVERT TO ASCII AND LOAD OUTSTR
        MOVB    #40,(R3)+               ;SEPARATE BY A SPACE
        MOV     @#ABS,R5                ;LOAD THE Y VALUE
        JSR     PC,ASCDG4               ;CONVERT TO ASCII AND LOAD
        MOVB    #0,(R3)+                ;TERMINATE OUTSTR WITH ZERO
        MOV     #OUTSTR,R0              ;LOAD ADDRESS FOR OUTPUT
        JSR     PC,PRTPLT               ;OUTPUT THE STRING TO THE PLOTTER
        DEC     @#PLTCNT                ;DECREMENT POINT COUNTER
        BNE     NEWPNT                  ;GET ANOTHER POINT IF NOT DONE
        MOV     #PLTMSG,R0              ;LOAD TERMINATION MESSAGE ADDRESS
        JSR     PC,PRTPLT               ;SEND TERMINATION MESSAGE
        JMP     WAIT                    ;RETURN TO MODE CHECK LOOP
SCNEXT: .PRINT  #SCXMSG
        MOV     #INBUF,R1
1$:     .TTYIN
        CMP     R0,#15
        BEQ     2$
        MOVB    R0,(R1)+
        BR      1$
2$:     .TTYIN
        MOV     #SXTBCD,R5
        JSR     PC,BCDIN
        MOV     #SXTBIN,R5
        JSR     PC,BININ
3$:     MOV     @#SXTBCD,@#DATALO
        BIS     #1,@#STATUI             ;SET DII BIT FOR LOOP BACK
                                        ;AFTER CLEARING
        MOVB    #18.,@#MCSA3            ;F18A3 LOAD SWEEP COUNTER
```

```
        BIC     #1,@#STATUI             ;CLEAR DII FOR CMP OPERATION
        CMP     @#MCSA3,@#SXTBCD        ;F0A3 COMPARE SWEEP COUNTER
        BNE     3$                      ;CHECK FOR EQUALITY, RELOAD IF NOT
        BIS     #1,@#STATUI             ;RESET DII BIT
        ADD     @#SXTBIN,@#NUMSWP       ;UPDATE NUMBER OF SWEEPS REQUESTED
        MOVB    #26.,@#MCSA6            ;SET ACCUM
        BIC     #1,@#RUNDNE
        JMP     WAIT
WRTDSK: MOV     R4,@#SVR4
        MOV     R5,@#SVR5
        MOV     #DSKBUF,R5
1$:     CLR     (R5)+
        CMP     R5,#DSKBUF+2048.
        BLT      1$
        MOV     #DSKBUF,R5
HEDLD:  .PRINT  #HEDMSG
1$:     .TTYIN
        CMP     R0,#'↑
        BEQ     2$
        MOV     R0,(R5)+
        CMP     R5,#DSKBUF+1024.
        BLT     1$
        .PRINT  #TOOLNG
2$:     .TTYIN
        CMP     R0,#12
        BNE     2$
DATLD:  MOV     #DSKBUF+1024.,R5
        MOV     #OTPTBF,R4
1$:     MOV     2(R4),(R5)+
        MOV     (R4),(R5)+
        ADD     #4,R4
        CMP     R4,#OTPTBF+1020.
        BLT     1$
        CLR     (R5)+
        CLR     (R5)+
        .PRINT  #NAMMSG
        .CSIGEN #DEVSPC,#DEFEXT,#0
        CLR     R4                      ;USE AS BLOCK COUNTER
        MOV     #DSKBUF,R5              ;USE AS BUFFER ADDRESS
2$:     .WRITW  #WAREA,#0,R5,#256.,R4
        BCS     WRITER
        CMP     R0,#256.
        BNE     3$
        ADD     #512.,R5
        INC     R4
        CMP     R4,#4
        BLT     2$
        .CLOSE  #0
        MOV     @#SVR4,R4
        MOV     @#SVR5,R5
        .PRINT  #WRTDNE
        JMP     WAIT
3$:     .PRINT  #BDWRNO
WRITER: TSTB    @#52
        BNE     1$
        .PRINT  #EOFER
        BR      4$
1$:     CMPB    @#52,#1
        BNE     2$
        .PRINT  #HDWERR
        BR      4$
```

```
2$:     CMPB    @#52,#2
        BNE     3$
        .PRINT  #CHNERR
        BR      4$
3$:     .PRINT  #UNDFER
4$:     .CLOSE  #0
        MOV     @#SVR4,R4
        MOV     @#SVR5,R5
        JMP     WAIT
MCSINT: MOV     R2,@#SAVR2
        MOV     R3,@#SAVR3
        BIC     #1,@#STATUI             ;CLEAR DII BIT
        MOV     @#MCSA2,@#OVFLSR        ;READ OVFL AND STOPRUN
        BIT     #3,@#OVFLSR             ;CHECK FOR OVFL
        BEQ     1$
        RTI
1$:     MOV     #UDBUF,R2
        MOV     @#NCHBIN,R3
2$:     ADD     @#MCSA0,2(R2)
        ADC     (R2)
        ADD     #4,R2
        SOB     R3,2$
        BIS     #1,@#NWDTFG
        BIS     #1,@#STATUI             ;SET DII BIT
        MOVB    #9.,@#MCSA0             ;F9A0 CLEAR RAM
        MOV     #50,R3                  ;WAIT LOOP FOR RAM CLEAR
3$:     NOP
        SOB     R3,3$
        BIT     #4,@#OVFLSR             ;? IS RUN FINISHED
        BNE     4$                      ;YES, THEN RETURN
        MOVB    #26.,@#MCSA6            ;NO, SET ACCUMULATE
4$:     MOV     @#SAVR2,R2
        MOV     @#SAVR3,R3
        BIS     #300,@#STATUI           ;SET INE,REIN
        RTI
DIDINT: DEC     @#PTCNTR                ;DECREMENT LOOP COUNTER
        BEQ     RESTRT                  ;RESTART IF DONE
        MOV     @PTADR,@#DATALO         ;SEND NEXT POINT IF NOT
        MOVB    #16.,@#DIDRA0           ;F16A0 SEND NEXT Y
        ADD     #2,@#PTADR              ;UPDATE POINT ADDRESS
        BIS     #300,@#STATUI           ;SET INE, AND REIN
        RTI
RESTRT: MOV     @#CONREG,@#DATALO       ;RELOAD CONTROL REGISTER
        MOVB    #17.,@#DIDRA0           ;F17A0 SEND NEW CONTROL REGISTER
        MOV     @#NUMPTS,@#PTCNTR       ;RESET LOOP COUNTER
        MOV     @#BEGADR,@#PTADR        ;RESET ADDRESS OF POINTS
        CLR     @#DATALO                ;READY TO LOAD FIRST X=0
        MOVB    #16.,@#DIDRA1           ;F16A1 LOAD FIRST X
        MOV     @PTADR,@#DATALO         ;READY FOR FIRST Y
        MOVB    #16.,@#DIDRA0           ;LOAD FIRST Y
        ADD     #2,@#PTADR              ;UPDATE POINT ADDRESS
        BIS     #300,@#STATUI           ;SET INE, AND REIN
        RTI
;SUBROUTINE SECTION
;
;
;SUBROUTINE PRINT EMULATES THE MONITOR .PRINT REQUEST BUT SENDS OUTPUT
;TO THE LA180 FAST PRINTER. IT IS ACCESSED BY PLACING THE BEGINNING ADDRESS
;OF THE BYTE BY BYTE ASCII STRING TO BE OUTPUT IN R0 FOLLOWED BY THE
;INSTRUCTION  JSR     PC,PRINT. CARRIAGE RETURN AND LINE FEED HANDLING ARE
;SAME AS THE MONITOR .PRINT REQUEST
```

```
PRINT:  CMPB    (R0),#200               ;? TERMINATOR FOR NO CRLF
        BEQ     2$                      ;YES, THEN ARE FINISHED
        CMPB    (R0),#0                 ;? TERMINATOR FOR CRLF
        BEQ     3$                      ;YES, THEN OUTPUT LF
1$:     TSTB    @#LPSTA                 ;READY FOR NEW CHARACTER?
        BPL     1$                      ;NO, THEN LOOP
        MOVB    (R0)+,@#LPBUF           ;SEND CHARACTER
        BR      PRINT                   ;GO FOR ANOTHER
2$:     RTS     PC                      ;QUIT WITH NO CRLF
3$:     TSTB    @#LPSTA
        BPL     3$
        MOVB    #12,@#LPBUF             ;SEND LF, GET AUTO CR
        RTS     PC                      ;RETURN TO CALLER
;
;
;SUBROUTINES BCDIN AND BININ CONVERT AN ASCII NUMERAL STRING TO BINARY CODED
;DECIMAL REPRESENTATION OR DIRECT BINARY REPRESENTATION RESPECTIVELY. THE
;ASCII STRING IS ASSUMED TO BE IN DECIMAL REPRESENTATION. THE SUBROUTINES
;ARE ACCESSED BY JSR     PC,BCDIN OR BININ. ON ENTRY R1 SHOULD CONTAIN
;THE BYTE ADDRESS+1 OF THE LAST NUMERAL ENTERED IN THE ASCII STRING. R5
;SHOULD CONTAIN THE ADDRESS OF THE LOCATION WHERE THE RESULT IS TO BE STORED
;ON EXIT, THE CONTENTS OF R1 AND R5 REMAIN UNCHANGED. THE CONTENTS OF R2 AND
;R3 ARE DESTROYED BY BOTH ROUTINES WHILE BININ ADDITIONALLY DESTROYS THE
;CONTENTS OF R4.

BCDIN:  MOV     #INBUF,R2
        CLR     (R5)
        CLR     R3
1$:     ASL     (R5)
        ASL     (R5)
        ASL     (R5)
        ASL     (R5)
        MOVB    (R2)+,R3
        SUB     #60,R3
        ADD     R3,(R5)
        CMP     R2,R1
        BNE     1$
        RTS     PC
BININ:  MOV     #INBUF,R2
        CLR     (R5)
        CLR     R3
1$:     MOV     (R5),R4
        ASL     R4
        ASL     (R5)
        ASL     (R5)
        ASL     (R5)
        ADD     R4,(R5)
        MOVB    (R2)+,R3
        SUB     #60,R3
        ADD     R3,(R5)
        CMP     R2,R1
        BNE     1$
        RTS     PC
;
;
;SUBROUTINE TO TAKE A 16-BIT BCD NUMBER IN R5 AND CONVERT IT TO THE
;CORRESPONDING BINARY NUMBER IN R5. THE NUMBER IS ASSUMED POSITIVE.
;NO REGISTERS OTHER THAN R5 ARE ALTERED.

BCDBIN: CLR     @#TEMP2                 ;CLEAR ADDER LOCATION
        MOV     R5,@#TEMP1              ;SAVE BCD WORD
```

```
        BIC     #177760,R5              ;CLEAR HIGH DIGITS
        ADD     R5,@#TEMP2              ;ADD IN
        MOV     @#TEMP1,R5              ;RESTORE BCD WORD
        ASH     #-4,R5                  ;SHIFT ONE BCD DIGIT
        BIC     #177760,R5              ;CLEAR HIGH DIGITS
        MUL     #10.,R5                 ;X10 FOR TENS PLACE
        ADD     R5,@#TEMP2              ;ADD IN
        MOV     @#TEMP1,R5              ;RESTORE WORD
        ASH     #-8.,R5                 ;SHIFT TWO BCD DIGITS
        BIC     #177760,R5              ;CLEAR HIGH DIGITS
        MUL     #100.,R5                ;X100 FOR HUNDREDS PLACE
        ADD     R5,@#TEMP2              ;ADD IN
        MOV     @#TEMP1,R5              ;RESTORE WORD
        ASH     #-12.,R5                ;SHIFT THREE BCD DIGITS
        BIC     #177760,R5              ;CLEAR HIGH DIGITS
        MUL     #1000.,R5               ;X1000 FOR THOUSANDS PLACE
        ADD     @#TEMP2,R5              ;ADD UP INTO R5
        RTS     PC
;
;
;DOUBLE PRECISION INTEGER ASCII DECIMAL OUTPUT PROGRAM-WILL PLACE INTO A
;SPECIFIED BYTE STRING 10 ASCII NUMERALS AND A SIGN IF NEGATIVE. LEADING
;ZEROES ARE SUPRESSED AND THE SIGN IS PLACED IMMEDIATELY BEFORE THE
;FIRST NON-ZERO DIGIT OF THE NUMBER.
;TO ENTER:
;       1. MOVE HIGH ORDER PART OF WORD TO BE OUTPUT TO HIORD
;       2. MOVE LOW ORDER PART OF WORD TO BE OUTPUT TO LOWORD
;       3. PLACE ADDRESS OF FIRST BYTE OF OUTPUT STRING IN R3
;       4. R5 MUST BE SAVED IF IT IS USEFUL
;       5. CALL PROGRAM BY JSR     PC,DPIDCO
;
DPIDCO: CLR     NEGFLG                  ;CLEAR NEGATIVE # FLAG
        CLR     LZSFLG                  ;CLEAR LEADING ZERO SUPPRESS FLAG
        MOV     #-1,CNTR                ;INITIALIZE SUBTRACT LOOP COUNTER
        TST     HIORD                   ;IS INTEGER NEGATIVE
        BMI     NEGSET                  ;YES, THEN CONVERT IT
POSOUT: MOV     #DIG9,R5                ;LOAD BEGINNING ADDRESS OF 10↑N LST
MORYET: INC     CNTR                    ;COUNT # SUBTRACTION LOOPS
        SUB     2(R5),LOWORD            ;THREE STEP DOUBLE PREC. SUBTRACT
        SBC     HIORD
        SUB     (R5),HIORD
        BPL     MORYET                  ;SUBTRACT AGAIN IF STILL POSITIVE
        ADD     2(R5),LOWORD            ;KILL LAST SUBTRACTION IF NEGATIVE
        ADC     HIORD
        ADD     (R5),HIORD
        ADD     #4,R5                   ;READY FOR 10↑N-1
        JSR     PC,ASCOUT               ;OUTPUT THE CHARACTER
        MOV     #-1,CNTR                ;RESET LOOP COUNTER
        CMP     R5,#<DIGI+4>            ;? LAST DIGIT YET
        BLT     MORYET                  ;NO, DO ANOTHER
        MOV     LOWORD,CNTR             ;YES, SEND IT OUT
        INC     R5                      ;TRACER FOR LAST DIGIT
        JSR     PC,ASCOUT
        RTS     PC                      ;RETURN TO CALLING PROGRAM
NEGSET: BIS     #1,NEGFLG               ;SET FLAG FOR MINUS SIGN OUTPUT
        SUB     #1,LOWORD               ;4 STEP CONVERSION TO POS. INTEGER
        SBC     HIORD
        COM     HIORD
        COM     LOWORD
        JMP     POSOUT                  ;DECODE TO ASCII
ASCOUT: CMP     CNTR,#0                 ;? GOT A ZERO
```

```
        BEQ     LZS                     ;YES, SEE IF NEEDS SUPPRESSED
        BIS     #1,LZSFLG               ;NO, PREVENT FURTHER SUPPRESSION
LZSDN:  ADD     #60,CNTR                ;ADD ASCII BIAS
        BIT     #2,NEGFLG               ;IS SIGN OR SPACE ALREADY PRINTED?
        BPL     CHROUT                  ;YES, JUST SEND CHARACTER
        BIT     #1,NEGFLG               ;NO, DO WE NEED A MINUS SIGN?
        BPL     MINOUT                  ;YES, DO IT
        MOVB    #40,(R3)+               ;NO, SEND A SPACE
        MOVB    CNTR,(R3)+              ;THEN SEND CHARACTER
        BIS     #2,NEGFLG               ;NO MORE SPACES
        RTS     PC                      ;BACK TO CALLER
MINOUT: MOVB    #55,(R3)+               ;SEND MINUS SIGN
        MOVB    CNTR,(R3)+              ;SEND CHARACTER
        BIC     #1,NEGFLG               ;MINUS SIGN DONE
        BIS     #2,NEGFLG               ;NO SPACES WANTED
        RTS     PC
LZS:    TST     LZSFLG                  ;LEADING ZEROES OVER WITH?
        BGT     LZSDN                   ;YES, DON'T SUPPRESS
        CMP     R5,#<DIGI+4>            ;LAST DIGIT YET?
        BGT     LZSDN                   ;YES, THEN PRINT EVEN IF ZERO
        MOVB    #40,(R3)+               ;NO, SEND A SPACE
        RTS     PC
CHROUT: MOVB    CNTR,(R3)+              ;SEND CHARACTER
        RTS     PC
;
;
;SUBROUTINE NUMBIT WILL CALCULATE THE NUMBER OF SIGNIFICANT BITS
;IN A POSITIVE 16 BIT INTEGER IN R1. THE NUMBER OF BITS IS RETURNED IN
;R4. R2 AND R3 ARE USED BY THE SUBROUTINE AND THUS THEIR PREVIOUS VALUES
;ARE DESTROYED. THEY MUST BE SAVED IF VALUABLE. PROGRAM IS CALLED BY
;JSR    PC      NUMBIT
;
NUMBIT: MOV     #400,R2
        MOV     #4,R3
        MOV     #8.,R4
OVER:   CMP     R1,R2
        BHIS    HIGHER
LOWER:  SUB     R3,R4           ;SETS NEW BIT COUNT
        NEG     R3
        ASH     R3,R2           ;SHIFT COMPARISON NUMBER RIGHT R3 BITS
        NEG     R3
        ASR     R3              ;DIVIDE R3 BY 2
        BNE     OVER
        BR      LAST
HIGHER: ADD     R3,R4
        ASH     R3,R2
        ASR     R3
        BNE     OVER
LAST:   CMP     R1,R2
        BHIS    1$
        BR      DONE
1$:     ADD     #1,R4
DONE:   RTS     PC
;
;
;SUBROUTINE PRTPLT IS A ROUTINE TO OUTPUT ASCII STRINGS TO A DEVICE
;WITH RECEIVER STATUS AND BUFFER ADDRESSES OF 177574 AND 177576 RESPECTIVELY
;THESE ADDRESSES ARE INTENDED TO BE ASSOCIATED WITH THE HEWLEIT PACKARD
;GRAPHICS PLOTTER. THE ROUTINE HANDLES CR AND LF IN THE SAME WAY AS THE
;MONITOR .PRINT REQUEST. TO ENTER, THE ADDRESS OF THE OUTPUT STRING SHOULD
;BE PLACED IN R0, THEN THE ROUTINE CALLED BY JSR     PC,PRIPLT.
```

```
;
PRTPLT: CMPB    (R0),#200
        BEQ     2$
        CMPB    (R0),#0
        BEQ     3$
1$:     TSTB    @#177574
        BPL     1$
        MOVB    (R0)+,@#177576
        BR      PRTPLT
2$:     RTS     PC
3$:     TSTB    @#177574
        BPL     3$
        MOVB    #15,@#177576
4$:     TSTB    @#177574
        BPL     4$
        MOVB    #12,@#177576
        RTS     PC
;
;
;SUBROUTINE ASCDG4 IS A ROUTINE TO CONVERT A BINARY NUMBER TO A FOUR DIGIT
;ASCII REPRESENTATION AND OUTPUT THE ASCII DIGITS TO A BYTE STRING FOR
;OUTPUT. THE INPUT NUMBER SHOULD BE POSITIVE AND SHOULD NOT EXCEED 9999 IN
;MAGNITUDE. TO ENTER, PLACE THE NUMBER TO BE CONVERTED IN R5, PLACE THE
;BEGINNING ADDRESS OF THE BYTE STRING IN R3, AND CALL BY JSR     PC,ASCDG4.
;
ASCDG4: CLR     R4                      ;CLEAR POSSIBLE HIGH ORDER PARTS
        DIV     #1000.,R4               ;EIS CHIP DIVISION
        ADD     #60,R4                  ;ADD ASCII BIAS
        MOVB    R4,(R3)+                ;LOAD INTO BYTE STRING
        CLR     R4                      ;DO AGAIN
        DIV     #100.,R4
        ADD     #60,R4
        MOVB    R4,(R3)+
        CLR     R4
        DIV     #10.,R4
        ADD     #60,R4
        MOVB    R4,(R3)+
        ADD     #60,R5                  ;BIAS THE LAST DIGIT
        MOVB    R5,(R3)+                ;LOAD LAST DIGIT
        RTS     PC
;
;ASCII STRINGS, VARIABLES, FLAGS, AND BUFFERS
;
CNTMSG: .ASCIZ  /COUNT OVERFLOW HAS OCCURRED/
RAMMSG: .ASCIZ  /RAM OVERFLOW HAS OCCURRED/
ENDMSG: .ASCIZ  /RUN IS COMPLETED/
BELLS:  .ASCII  <7><7><7><7><7><7><7><7><7><7><7><7><7><7><7><7><7><7><7><7>
        .BYTE   200
HELLO:  .ASCIZ  /TOF DATA ACQUISITION PROGRAM/
SYNTAX: .ASCIZ  /SYNTAX ERROR, INVALID MODE DESIGNATION/
DWLMSG: .ASCII  /DWELL TIME (1-99 MICROSECONDS)=/
        .BYTE   200
TRGMSG: .ASCII  /TRIGGER COUNT=/
        .BYTE   200
SWPMSG: .ASCII  /SWEEP COUNT=/
        .BYTE   200
NCHMSG: .ASCII  /NUMBER OF CHANNELS (1-255)=/
        .BYTE   200
CLKMSG: .ASCII  /DO YOU WANT INTERNAL DWELL CLOCK (TYPE Y OR N)?/
        .BYTE 200
SCXMSG: .ASCII  /NUMBER OF ADDITIONAL SWEEPS = /
```

```
        .BYTE   200
PLPMSG: .ASCIZ  / PLTP /
PLTMSG: .ASCIZ  / PLTT /
ERR1:   .ASCIZ  /ERROR 1/
ERR2:   .ASCIZ  /ERROR 2/
ERR3:   .ASCIZ  /ERROR 3/
ERR4:   .ASCIZ  /ERROR 4/
HEDMSG: .ASCII  /ENTER THE INFORMATIONAL HEADER./
        .BYTE   15,12
        .ASCII  /HEADER MAY CONTAIN UP TO 512 CHARACTERS INCLUDING CR,LF./
        .BYTE   15,12
        .ASCIZ  /END OF HEADER IS INDICATED BY AN UP-ARROW (↑) AND A RETURN
TOOLNG: .ASCIZ  /HEADER IS TOO LONG, CONTINUE, BUT HEADER WILL BE TRUNCATED
NAMMSG: .ASCII  /ENTER FILE NAME AFTER *, EXAMPLE/
        .BYTE   12,15
        .ASCII  /*DX1:NAME.EXT=/
        .BYTE   12,15
        .ASCII  /THE DEFAULT IF NO EXTENSION IS GIVEN IS .DAT/
        .BYTE   12,15
        .ASCIZ  /THE = MUST FOLLOW FILE NAME/
BDWRNO: .ASCII  /IMPROPER NUMBER OF WORDS WRITTEN/
        .BYTE   12,15
        .ASCIZ  /CHECK DISK TO INSURE 8 OPEN BLOCKS/
EOFER:  .ASCII  /ATTEMPT TO WRITE PAST END OF FILE/
        .BYTE   12,15
        .ASCIZ  /CHECK DISK TO INSURE 8 OPEN BLOCKS/
HDWERR: .ASCIZ  /HARDWARE ERROR ON WRITE ATTEMPT/
CHNERR: .ASCIZ  /CHANNEL NOT OPEN FOR WRITE ATTEMPT/
UNDFER: .ASCIZ  /UNDEFINED ERROR ON WRITE ATTEMPT/
WRTDNE: .ASCII  <7><7><7><7><7><7><7>
        .ASCIZ  /FILE SUCCESSFULLY WRITTEN, YOU MAY CONTINUE./
FSTMSG: .ASCII  /CROSS CORR ONLY, ENTER NUMBER OF CHANNELS/
        .BYTE   12,15
        .ASCII  /BY WHICH TRIGGER COMES LATE/
        .BYTE   12,15
        .ASCII  /CROSS CORR OFFSET=/
        .BYTE 200
CDPMSG: .ASCII  /CORRELATED DATA, TRIGGER OFFSET (CHANNELS LATE) =/
        .BYTE   200
        .EVEN
UDBUF:  .BLKW   510.
CDBUF:  .BLKW   510.
WRKBUF: .BLKW   510.
OTPTBF: .BLKW   510.
COUTBF: .BLKW   510.
SEQNBF: .BYTE   1,1,1,1,1,1,1,1,0,0,1,0,1,1,1,1,0,1,0,0
        .BYTE   1,0,1,0,0,0,0,1,1,0,1,1,1,0,1,1,0,1,1,1
        .BYTE   1,1,0,1,0,1,1,1,0,1,0,0,0,0,0,1,1,0,0,1
        .BYTE   0,1,0,1,0,1,0,0,0,1,1,0,1,0,1,1,0,0,0,1
        .BYTE   1,0,0,0,0,0,1,0,0,1,0,1,1,0,1,1,0,1,0,1
        .BYTE   0,0,1,1,0,1,0,0,1,1,1,1,1,1,0,1,1,1,0,0
        .BYTE   1,1,0,0,1,1,1,1,0,1,1,0,0,1,0,0,0,0,1,0
        .BYTE   0,0,0,0,0,1,1,1,0,0,1,0,0,1,0,0,1,1,0,0
        .BYTE   0,1,0,0,1,1,1,0,1,0,1,0,1,1,0,1,0,0,0,1
        .BYTE   0,0,0,1,0,1,0,0,1,0,0,0,1,1,1,1,1,0,0,0
        .BYTE   0,0,0,0,1,0,1,1,1,0,0,0,1,1,1,0,1,1,1,1
        .BYTE   0,0,0,1,0,1,1,0,0,1,1,0,1,1,0,0,0,0,1,1
        .BYTE   1,1,0,0,1,1,1,0,0,0,0,1,0,1,0
        .BYTE   1,1,1,1,1,1,1,1,0,0,1,0,1,1,1,1,0,1,0,0
        .BYTE   1,0,1,0,0,0,0,1,1,0,1,1,1,0,1,1,0,1,1,1
        .BYTE   1,1,0,1,0,1,1,1,0,1,0,0,0,0,0,1,1,0,0,1
```

```
        .BYTE   0,1,0,1,0,1,0,0,0,1,1,0,1,0,1,1,0,0,0,1
        .BYTE   1,0,0,0,0,0,1,0,0,1,0,1,1,0,1,1,0,1,0,1
        .BYTE   0,0,1,1,0,1,0,0,1,1,1,1,1,1,0,1,1,1,0,0
        .BYTE   1,1,0,0,1,1,1,1,0,1,1,0,0,1,0,0,0,0,1,0
        .BYTE   0,0,0,0,0,1,1,1,0,0,1,0,0,1,0,0,1,1,0,0
        .BYTE   0,1,0,0,1,1,1,0,1,0,1,0,1,1,0,1,0,0,0,1
        .BYTE   0,0,0,1,0,1,0,0,1,0,0,0,1,1,1,1,1,0,0,0
        .BYTE   0,0,0,0,1,0,1,1,1,0,0,0,1,1,1,0,1,1,1,1
        .BYTE   0,0,0,1,0,1,1,0,0,1,1,0,1,1,0,0,0,0,1,1
        .BYTE   1,1,0,0,1,1,1,0,0,0,0,1,0,1,0
        .BYTE   1,1,1,1,1,1,1,1,0,0,1,0,1,1,1,1,0,1,0,0
        .BYTE   1,0,1,0,0,0,0,1,1,0,1,1,1,0,1,1,0,1,1,1
        .BYTE   1,1,0,1,0,1,1,1,0,1,0,0,0,0,0,1,1,0,0,1
        .BYTE   0,1,0,1,0,1,0,0,0,1,1,0,1,0,1,1,0,0,0,1
        .BYTE   1,0,0,0,0,0,1,0,0,1,0,1,1,0,1,1,0,1,0,1
        .BYTE   0,0,1,1,0,1,0,0,1,1,1,1,1,1,0,1,1,1,0,0
        .BYTE   1,1,0,0,0,1,1,1,1,0,1,1,0,0,1,0,0,0,0,1,0
        .BYTE   0,0,0,0,0,0,1,1,1,0,0,1,0,0,1,0,0,1,1,0,0
        .BYTE   0,1,0,0,1,1,1,0,1,0,1,0,1,1,0,1,0,0,0,1
        .BYTE   0,0,0,1,0,1,0,0,1,0,0,0,1,1,1,1,1,0,0,0
        .BYTE   0,0,0,0,1,0,1,1,1,0,0,0,1,1,1,0,1,1,1,1
        .BYTE   0,0,0,1,0,1,1,0,0,1,1,0,1,1,0,0,0,0,1,1
        .BYTE   1,1,0,0,1,1,1,0,0,0,0,1,0,1,0
        .EVEN
DIBFBG: .BLKW   256.
OUTSTR: .BLKB   140.
INBUF:  .BLKB   82.
CORFLG: .WORD   0
CCCNTR: .WORD
CCOFST: .WORD   0
RUNDNE: .WORD
NWMDFG: .WORD
LNCNTR: .WORD
GPCNTR: .WORD
NWDTFG: .WORD   0
OVFLSR: .WORD   0
TEMP:   .WORD
DWLBCD: .WORD
DWLBIN: .WORD
TRGBCD: .WORD
TRGBIN: .WORD
SWPBCD: .WORD
SWPBIN: .WORD
NUMSWP: .WORD
NCHBIN: .WORD
IADBIN: .WORD
HIORD:  .WORD
LOWORD: .WORD
NEGFLG: .WORD
LZSFLG: .WORD
CLKFLG: .WORD
SAVR2:  .WORD
SAVR3:  .WORD
CNTR:   .WORD
CONREG: .WORD   20
NUMPTS: .WORD   256.
PTCNTR: .WORD
BEGADR: .WORD
PTADR:  .WORD
SCBFBG: .WORD
MAGFLG: .WORD
```

```
BITNUM: .WORD
SIZFLG: .WORD
MAXHI:  .WORD
MAXLO:  .WORD
MINHI:  .WORD
MINLO:  .WORD
SIZHI:  .WORD
SIZLO:  .WORD
TEMPHI: .WORD
TEMPLO: .WORD
PLTCNT: .WORD
PLTADR: .WORD
ORD:    .WORD
ABS:    .WORD
SXTBCD: .WORD
SXTBIN: .WORD
TEMP1:  .WORD
TEMP2:  .WORD
LIST:   .WORD   3
        .WORD   OPR1
        .WORD   OPR2
        .WORD   RESULT
OPR1:   .BLKW   2
OPR2:   .BLKW   2
RESULT: .BLKW   2
DIG9:   .WORD   35632,145000
DIG8:   .WORD   2765,160400
DIG7:   .WORD   230,113200
DIG6:   .WORD   17,41100
DIG5:   .WORD   1,103240
DIG4:   .WORD   0,23420
DIG3:   .WORD   0,1750
DIG2:   .WORD   0,144
DIG1:   .WORD   0,12
SVR4:   .WORD
SVR5:   .WORD
DSKBUF: .BLKW   1024.
DEFEXT: .WORD   0
        .RAD50  "DAT"
        .WORD   0
        .WORD   0
WAREA:  .BLKW   5
DEVSPC: .WORD
        .END    START
*
```

CMNRG4

CMNRG4 is the fourth version of a Fortran program used to convert single beam photofragmentation time-of-flight data into center-of-mass (C.M.) flux as a function of C.M. energy. The transformation equations have been discussed in Chapter I and are quite straightforward. Upon starting the program, the user is asked by the program for all necessary input data to define the solution. Choices of output options are also requested. Once all parameters are input, the user is asked for the disk file name of the data which is to be converted. This disk file should be in exactly the same format as a file generated by the WD command of the program MCSTF7.

Output may be directed to either the line printer or the HP7200A graphic plotter or both. The line printer output reiterates the input parameters and then lists, for each of the 255 channels, the original data, the background subtracted data, the C.M. flux, the C.M. energy, and the C.M. angle corresponding to that point.

The plotter output gives a graph of C.M. flux as a function of the C.M. energy. The maximum energy plotted (in kcal/mole) and the interval of hash marks on the energy scale axis (in kcal/mole) are determined by the input dialogue. The program chooses scaling so as to display both positive and negative flux values. Also, a vertical line is drawn by the plotter at the energy corresponding to the minimum energy of all of the measured points. Since, for some Newton diagrams, it is possible for this minimum energy to occur before the last channel of data, and

thus have the energy increasing in the final channels, this vertical line is not always at the left extreme of the graph. Also, the vertical line will never occur at zero center-of-mass energy since such particles do not scatter out of the beam and cannot be seen in a photofragmentation experiment.

Most of the input parameters to the program are self-explanatory but a few are not totally defined by the interactive requests. The variable DWELL is the dwell or counting time of each MCS channel measured in microseconds. The OFFSET is the number of channels by which the data arrives late due to the instrument factors. These effects include the flight time of the ions through the ionizer lenses and quadrupole regions as well as the time by which a trigger signal might precede (or negative effect it follows) the laser pulse. The lab angle is the angle of the detector relative to the molecular beam. The reduced mass should be input in atomic mass units. The velocity ratio is the ratio of the relative velocity of the two photofragments to the center-of-mass velocity of the detected photofragment. This number is unitless and is always greater than one.

The program is written in Fortran IV with system dependent features of DEC's RT-11 version 2C operating system and their Fortran-IV version 1C. Output to the HP7200A graphic plotter was achieved through a device handler we had written and named GR. This handler is assigned the Fortran logical unit number 9. A listing of the program follows.

```
C FORTRAN PROGRAM TO CALCULATE FLUX IN CENTER OF MASS ENERGY SPACE
C FROM SINGLE NEWTON DIAGRAM TRANSFORMATION FOR PHOTOFRAGMENT DYNAMICS
C
C       PROGRAM TO CALCULATE C.M. ENERGY SPACE FLUX
C
C
        INTEGER*2 COMMEN(512),IX(255),IY(255)
        INTEGER*2 AV,FRSTCH,IARCHN,IARCH1,BAKCHN
        INTEGER*2 OFFSET,NMMRKS,PLTFLG,PRTFLG,CONTFL
        INTEGER*4 INDATA(256)
        REAL*4 TIM,DWELL,LABVEL,PATH,LBANGL,AJFLT
        REAL*4 CMVELY,CMVELX,BEMVEL,CMANGL(255)
        REAL*4 CMENRG(255),REDMAS,VELRAT,BKGRND
        REAL*4 FLCMEN(255),BKSDAT(255),CHDAT(255)
        REAL*4 X(255),Y(255),TMPSCL,MINEN
        REAL*4 MAXEN2,ARCHAN,MAXFLX,MINFLX,MAXEN
        REAL*4 LSTABS,NEWABS,ORDNAT,ABSCSA,ENTRVL,DENOM
C
10      CALL PRINT (' FLUX IN C.M. ENERGY SPACE')
C BRING IN INPUT DATA
C
        CALL PRINT (' DO YOU WANT LINE PRINTER OUTPUT?')
        CALL PRINT (' TYPE 1 FOR YES, 0 FOR NO.')
        READ (5,110) PRTFLG
        CALL PRINT (' WHAT TYPE OF PLOTTING DO YOU WANT?')
        CALL PRINT (' TYPE 0 FOR NO PLOT, 1 FOR LINE PLOT,
     1 2 FOR POINT PLOT')
        READ (5,110) PLTFLG
        CALL PRINT (' TYPE IN DWELL IN F3.0 FORMAT')
        READ (5,100)DWELL
100     FORMAT (F3.0)
        CALL PRINT (' TYPE IN OFFSET IN I3 FORMAT')
        READ (5,110)OFFSET
110     FORMAT (I3)
        CALL PRINT (' TYPE IN FLIGHT PATH IN CM. USING F6.2 FORMAT')
        READ (5,115)PATH
115     FORMAT (F6.2)
        CALL PRINT (' TYPE IN LAB ANGLE IN DEGREES WITH F6.2 FORMAT')
        READ (5,115)LBANGL
        LBANGL=LBANGL/57.29578
        CALL PRINT (' TYPE IN BEAM VELOCITY IN CM./SEC. INF7.0')
        READ (5,120)BEMVEL
120     FORMAT (F7.0)
        CALL PRINT (' TYPE IN REDUCED MASS IN F6.2')
        READ (5,115)REDMAS
        CALL PRINT (' TYPE IN VELOCITY RATIO IN F6.2 FORMAT')
        READ (5,115)VELRAT
        CALL PRINT('TYPE IN MAX. ENERGY OF GRAPH IN F6.2')
        READ (5,115) MAXEN
        CALL PRINT('TYPOE IN SPACING OF AXIS MARKS IN F6.2')
        READ (5,115) ENTRVL
        CALL PRINT (' TYPE IN NO. OF INITIAL CHANNELS TO AVERAGE FOR')
        CALL PRINT (' BACKGROUND DETERMINATION IN I3 FORMAT.')
        READ (5,110) BAKCHN
        DEFINE FILE 2(2,512,U,AV)
        WRITE (5,170)
170     FORMAT (' ENTER DATA FILE SPECIFICATION',/2X)
        CALL ASSIGN (2,NAME,-1,'NEW')

        READ (2'1)(COMMEN(I),I=1,512)
        READ (2'2)(INDATA(J),J=1,256)
```

```
      CALL CLOSE (2)
      DO 200 I=1,255
      CHDAT(I)=AJFLT(INDATA(I))
200   CONTINUE
C
C
C     PROGRAM SUBSECTION TO SUBTRACT BACKGROUND
C
C
C     CALCULATE BACKGROUND VALUE FOR SUBTRACTION
C     WILL BE AVERAGE OF FIRST BAKCHN CHANNELS
      BKGRND=0.
      DO 2520 I=1,BAKCHN
      BKGRND=BKGRND+CHDAT(I)
2520  CONTINUE
      BKGRND=BKGRND/FLOAT(BAKCHN)
C     SUBTRACT THE BACKGROUND FROM THE DATA
      DO 2600 I=1,255
      BKSDAT(I)=CHDAT(I)-BKGRND
2600  CONTINUE
C
C
C     PROGRAM SUBSECTION TO FILL THE FLUX, ENERGY, AND ANGLE ARRAYS
C
C
      DO 3990 I=1,255
C     FILL ARRAYS WITH ZEROES IF NONSENSE OCCURS
      IF (I.LE.OFFSET) GO TO 3900
C     IF DATA VALID --PROCEED
      TIM=(FLOAT(I-OFFSET)-.5)*DWELL
C     CALCULATES TIME IN MICROSECONDS
      LABVEL=PATH/TIM
C     CALCULATES LAB VELOCITY IN CM/MICROSECONDS
      CMVELX=LABVEL*SIN(LBANGL)
C     CALCULATES X COMPONENT OF C.M. VELOCITY
      CMVELY=LABVEL*COS(LBANGL)-BEMVEL*1E-6
C     CALCULATES Y COMPONENT OF C.M. VELOCITY
      CMANGL(I)=ATAN2(CMVELX,CMVELY)
      CMANGL(I)=CMANGL(I)*57.29578
C     CALCULATES C.M. ANGLE
C     -----------------
C     CALCULATE C.M. ENERGY IN KCAL/MOLE
      CMENRG(I)=(11.95)*REDMAS*(VELRAT**2)*(CMVELX**2+CMVELY**2)
C     CALCULATE C.M. FLUX IN COUNTS*CM*MICROSECONDS**2
      FLCMEN(I)=(TIM**3)*SQRT(CMVELX**2+CMVELY**2)*BKSDAT(I)
      GO TO 3990
3900  CMANGL(I)=0.
      CMENRG(I)=0.
      FLCMEN(I)=0.
3990  CONTINUE
      IF (PRTFLG .NE. 1) GO TO 5300
      WRITE (6,5000)
5000  FORMAT (1H1)
      WRITE (6,5020)(COMMEN(I),I=1,255)
5020  FORMAT (1H$,255A1)
      WRITE (6,5030)(COMMEN(I),I=256,510)
5030  FORMAT (1H+,255A1)
      WRITE (6,5110)DWELL
      WRITE (6,5112) OFFSET
      WRITE (6,5114) PATH
      DLBNGL=LBANGL*57.29578
```

```
      WRITE (6,5120)DLBNGL
      WRITE (6,5130)BEMVEL
      WRITE (6,5132) REDMAS
      WRITE (6,5134) VELRAT
      WRITE (6,5136) MAXEN
      WRITE (6,5138) ENTRVL
      WRITE (6,5139) BAKCHN
      WRITE (6,5140)
5110  FORMAT (1H0,30X,28H THE TIME OF FLIGHT DATA IS ,F3.0,
     1  26H MICROSECONDS PER CHANNEL.)
5112  FORMAT (1H ,30X,34H THE NUMBER OF CHANNELS OFFSET IS ,
     1  I3,10H CHANNELS.)
5114  FORMAT (1H ,30X,28H THE PRODUCT FLIGHT PATH IS ,
     1  F6.2,13H CENTIMETERS.)
5120  FORMAT (1H ,30X,14H LAB ANGLE IS ,F7.2,
     1  2X,26HDEGREES FROM PRIMARY BEAM.)
5130  FORMAT (1H ,30X,44H BEAM VELOCITY OBTAINED FROM TIME OF FLIGHT=,
     1  F7.0,9H  CM/SEC.)
5132  FORMAT (1H ,30X,35H THE REDUCED MASS OF THE SYSTEM IS ,
     1  F6.2,7H A.M.U.)
5134  FORMAT (1H ,30X,62H THE RELATIVE VELOCITY TO DETECTED
     1 PARTICLE VELOCITY RATIO IS ,F6.2,1H.)
5136  FORMAT (1H ,30X,37H THE MAXIMUM ENERGY TO BE PLOTTED IS ,
     1  F6.2,11H KCAL/MOLE.)
5138  FORMAT (1H ,30X,39H THE ENERGY INTERVALS ON THE GRAPH ARE ,
     1  F6.2,11H KCAL/MOLE.)
5139  FORMAT (1H ,30X,11H THE FIRST ,I3,
     1  51H CHANNELS WERE AVERAGED FOR BACKGROUND SUBTRACTION.)
5140  FORMAT (1H0)
      WRITE (6,5150)
      WRITE (6,5160)
      WRITE (6,5170)
5150  FORMAT (10H    CHANNEL,13X,4HDATA,11X,13H       DATA    ,
     1  14X,4HFLUX,16X,6HENERGY,7X,9HC.M.ANGLE)

5160  FORMAT (9H    NUMBER,25X,21HBACKGROUND SUBTRACTED,6X,
     1  12HDISTRIBUTION,9X,11H(KCAL/MOLE),7X,9H(DEGREES))
5170  FORMAT (1H0)
      DO 5300 I=1,255
      WRITE (6,5200)I,CHDAT(I),BKSDAT(I),FLCMEN(I),CMENRG(I),CMANGL(I)
5200  FORMAT (1H ,I7,10X,F10.0,10X,F10.0,10X,F14.0,8X,F11.3,10X,F6.2)
5300  CONTINUE
C
C     PROGRAM SUBSECTION TO GENERATE SCALED ARRAYS FOR GRAPHING
C     AND TO OUTPUT THEM TO PLOTTER
C
C     CALCULATE ARRIVAL CHANNEL FOR LOWEST POSSIBLE C.M. ENERGY
      DENOM=BEMVEL*COS(LBANGL)*DWELL
C     AVOID FLOATING OVERFLOW
      IF (DENOM .GT. 1.E-10) GO TO 4050
      ARCHAN=1.E30
      GO TO 4055
4050  ARCHAN=1.E6*PATH/DENOM
C     CALCULATE LOWEST POSSIBLE C.M. ENERGY FOR THIS LAB ANGLE
4055  MINEN=(11.95E-12)*REDMAS*((VELRAT*BEMVEL*SIN(LBANGL))**2)
C     GET SECOND MAXIMUM IN ENERGY SCALE
C     WILL BE CHANNEL 255 IF SECOND MAXIMUM EXISTS
      MAXEN2=CMENRG(255)
C     FIND INDEX OF FIRST CHANNEL WITHIN GRAPH ENERGY LIMIT MAXEN
      FRSTCH=0
      DO 4100 I=1,255
```

```
      IF (FRSTCH .GT. 0) GO TO 4100
      IF (CMENRG(I) .GT. MAXEN) GO TO 4100
      IF (CMENRG(I) .EQ. 0.) GO TO 4100
      FRSTCH=I
4100  CONTINUE
C     GO TO 4200 FOR X SCALING OF SINGLE VALUED PROBLEM
C     STAY HERE FOR DOUBLE VALUED PROBLEM
      IF (ARCHAN .GE. 254.5) GO TO 4200
C     GET CHANNEL NO. OF FIRST POINT BEYOND MINIMUM POSSIBLE ENERGY
      IARCHN=INT(ARCHAN + 1.0)
C     CALCULATE X SCALING FOR CHANNELS BEFORE ENERGY MINIMUM
      TMPSCL=9999./(MAXEN+MAXEN2-2*MINEN)
      IARCH1=IARCHN-1
      DO 4120 I=FRSTCH,IARCH1
      X(I)=TMPSCL*(CMENRG(I)+MAXEN2-2*MINEN)
4120  CONTINUE
C     CALCULATE X SCALING FOR CHANNELS AFTER ENERGY MINIMUM
      DO 4140 I=IARCHN,255
      X(I)=TMPSCL*(MAXEN2-CMENRG(I))
4140  CONTINUE
C     GO AROUND SINGLE VALUED X SCALING TO DO ALL Y
      GO TO 4300
C     DO X SCALING FOR SINGLE VALUED PROBLEM
4200  TMPSCL=9999./(MAXEN-MAXEN2)
      DO 4210 I=FRSTCH,255
      X(I)=TMPSCL*(CMENRG(I)-MAXEN2)
4210  CONTINUE
C     DO ALL Y SCALING
C     FIND MAXIMUM AND MINIMUM IN FLUX ARRAY
4300  MAXFLX=FLCMEN(FRSTCH)
      MINFLX=FLCMEN(FRSTCH)
      DO 4307 I=FRSTCH,255
      IF (MAXFLX .GE. FLCMEN(I)) GO TO 4303
      MAXFLX=FLCMEN(I)
4303  IF (MINFLX .LE. FLCMEN(I)) GO TO 4307
      MINFLX=FLCMEN(I)
4307  CONTINUE
C     IF MINFLX GREATER THAN ZERO, MUST SET TO ZERO
      IF (MINFLX .LE. 0.) GO TO 4308
      MINFLX=0.
4308  TMPSCL=9999./(MAXFLX-MINFLX)
      DO 4310 I=FRSTCH,255
      Y(I)=TMPSCL*(FLCMEN(I)-MINFLX)
4310  CONTINUE
C     GET ARRAYS INTO INTEGERS
      DO 4410 I=FRSTCH,255
      IX(I)=INT(X(I))
      IY(I)=INT(Y(I))
4410  CONTINUE
C     PLOT OUT DATA IN POINT PLOT OR LINE PLOT OR NO PLOT
      CALL ASSIGN(9,'GR:',3)
      IF (PLTFLG-1) 6590,4430,4440
4430  WRITE (9,4950)
      GO TO 4450
4440  WRITE (9,4940)
4450  CONTINUE
4940  FORMAT (' PLTP')
4950  FORMAT (' PLTL')
      DO 4420 I=FRSTCH,255
      WRITE (9,4960) IX(I),IY(I)
4960  FORMAT (1H ,I4,1H ,I4)
```

```
4420    CONTINUE
        WRITE (9,4970)
4970    FORMAT (' PLTT')
C       PROGRAM SUBSECTION TO DRAW VERTICAL AND HORIZONTAL AXES ON GRAPH
C       SHORT VERTICAL HASH MARKS WILL BE DRAWN ON FAST VELOCITY SIDE
C       OF GRAPH AT ENERGY INTERVALS OF ENTRVL KCAL/MOLE, WHICH
C       MUST BE INPUT BY OPERATOR. VERTICAL AXIS WILL BE DRAWN AT THE
C       MINIMUM ENERGY GRAPHED (MINEN FOR DOUBLE VALUED PROBLEM,
C       CMENRG(255) FOR SINGLE VALUED PROBLEM)
C
C       PLOT VERTICAL LINE AT MINIMUM ENERGY ON GRAPH
C       IF SINGLE VALUED PROBLEM, GO TO 6002, STAY FOR DOUBLE
        IF (ARCHAN .GE. 254.5) GO TO 6002
        ABSCSA=9999.*(MAXEN2-MINEN)/(MAXEN+MAXEN2-2*MINEN)
        GO TO 6004
6002    ABSCSA=0.
6004    ORDNAT=0.
        WRITE (9,6010)
        DO 6006 I=1,6
        WRITE (9,6030) ABSCSA,ORDNAT
        ORDNAT=ORDNAT+1999.
6006    CONTINUE
        WRITE (9,6210)
C       PLOT HORIZONTAL LINE ALONG 0 FLUX AXIS, INCLUDING
C       HASH MARKS, AGAIN DIFFERENT FORSINGLE AND DOUBLE VALUE PROB.
C       IF SINGLE VALUED PROBLEM, GO TO 6300, STAY HERE FOR DOUBLE
        IF (ARCHAN .GE. 254.5) GO TO 6300
C       CALCULATE AND OUTPUT HORIZONTAL LINE FOR DOUBLE VALUED PROBLEM
C       INITIALIZE ABSCISSA
        LSTABS=0.
C       FIND NUMBER OF HASH MARKS NEEDED
        NMMRKS=INT((MAXEN+.001)/ENTRVL)-INT(MINEN/ENTRVL)
C       SET THE ORDINATE CORRESPONDING TO THE ZERO FLUX LINE
        ORDNAT=-9999.*MINFLX/(MAXFLX-MINFLX)
C       GET SCALING FACTOR FOR POSITIONING OF HASH MARKS
        TMPSCL=9999./(MAXEN+MAXEN2-2*MINEN)
C       INITIALIZE PLOTTER TO PLOT LINES
        WRITE (9,6010)
6010    FORMAT (' PLTL ')
C       LOWER PEN AT LEFT EDGE
        WRITE(9,6030) LSTABS,ORDNAT
C       DO LOOP TO PLOT LINES AND MARKS UP TO AND INCLUDING
C       BUT NOT PAST THE LAST MARK
        DO 6150 I=1,NMMRKS
C       GET ABSCISSA CORRESPONDING TO NEXTHASH MARK
        NEWABS=TMPSCL*(FLOAT(I)*ENTRVL+MAXEN2-2*MINEN)
C       SEE IF VECTOR SHORT ENOUGH TO PLOT IN ONE OUTPUT (6100)
6020    IF ((NEWABS-LSTABS) .LT. 1500.) GO TO 6100
C       NO, VECTOR TOO LONG, DO IN SEGMENTS FROM LSTABS TO LSTABS+1500.
        LSTABS=LSTABS+1500.
C       PLOT IT
        WRITE (9,6030) LSTABS,ORDNAT
6030    FORMAT (1H ,F5.0,1H ,F5.0)
C       GO SEE IF CAN FINISH IN ONE STEP
        GO TO 6020
C       HERE WE FINISH LINE SEGMENT AND PLOT HASH MARK
6100    LSTABS=NEWABS
        WRITE (9,6030) LSTABS,ORDNAT
        ORDNAT=ORDNAT+150.
        WRITE (9,6030) LSTABS,ORDNAT
        ORDNAT=ORDNAT-150.
```

```
      WRITE (9,6030) LSTABS,ORDNAT
6150  CONTINUE
C     HASH MARKS ARE DONE, PLOT TO END OF SCALE
      NEWABS=9999.
C     CHECK FOR TOO LARGE VECTORS AGAIN
6170  IF ((NEWABS-LSTABS) .LT. 1500.) GO TO 6200
      LSTABS=LSTABS+1500.
      WRITE (9,6030) LSTABS,ORDNAT
      GO TO 6170
6200  LSTABS=NEWABS
      WRITE (9,6030) LSTABS,ORDNAT
      WRITE (9,6210)
6210  FORMAT (' PLTT ')
      GO TO 6590
C     PLOTTING OFHORIZONTAL LINE FOR SINGLE VALUED PROBLEM
C     SAME AS FOR COUBLE VALUED EXCEPT FORTMPSCL,NMMRKS, AND
C     NEWABS CALCULATION
C     INITIALIZE ABSCISSA
6300  LSTABS=0.
C     FIND NUMBER OF HASH MARKS NEEDED
      NMMRKS=INT((MAXEN+.001)/ENTRVL)-INT(MAXEN2/ENTRVL)
C     SET THE ORDINATE CORRESPONDING TO THE ZERO FLUX LINE
      ORDNAT=-9999.*MINFLX/(MAXFLX-MINFLX)
C     GET SCALING FACTOR FOR POSITIONING OF HASH MARKS
      TMPSCL=9999./(MAXEN-MAXEN2)
C     INITIALIZE PLOTTER TO PLOT LINES
      WRITE (9,6010)
C     LOWER PEN AT LEFT EDGE
      WRITE(9,6030) LSTABS,ORDNAT
C     DO LOOP TO PLOT LINES AND MARKS UP TO AND INCLUDING
C     BUT NOT PAST THE LAST MARK
      DO 6450 I=1,NMMRKS
C     GET ABSCISSA CORRESPONDING TO NEXT HASH MARK
      NEWABS=TMPSCL*(FLOAT(I+INT(MAXEN2/ENTRVL))*ENTRVL-MAXEN2)
C     SEE IF VECTOR SHORT ENOUGH TO PLOT IN ONE OUTPUT
6320  IF ((NEWABS-LSTABS) .LT. 1500.) GO TO 6400
C     NO, VECTOR TOO LONG, DO IN SEGMENTS
      LSTABS=LSTABS+1500.
C     PLOT IT
      WRITE (9,6030) LSTABS,ORDNAT
C     GO SEE IF CAN FINISH IN ONE STEP
      GO TO 6320
C     FINISH LINE SEGMENT AND PLOT HASH MARK
6400  LSTABS=NEWABS
      WRITE (9,6030) LSTABS,ORDNAT
      ORDNAT=ORDNAT+150.
      WRITE (9,6030) LSTABS,ORDNAT
      ORDNAT=ORDNAT-150.
      WRITE (9,6030) LSTABS,ORDNAT
6450  CONTINUE
C     HASH MARKS ARE DONE, PLOT TO END OF SCALE
      NEWABS=9999.
C     CHECK FOR TOO LARGE VECTORS AGAIN
6470  IF ((NEWABS-LSTABS) .LT. 1500.) GO TO 6500
      LSTABS=LSTABS+1500.
      WRITE (9,6030) LSTABS,ORDNAT
      GO TO 6470
6500  LSTABS=NEWABS
      WRITE (9,6030) LSTABS, ORDNAT
      WRITE (9,6210)
6590  CALL CLOSE (9)
```

```
6600    CONTINUE
        CALL PRINT(' DO YOU WANT TO CONTINUE?')
        CALL PRINT(' TYPE 1 FOR YES, 0 FOR NO.')
        READ (5,110) CONTFL
        IF ( CONTFL .NE. 0 ) GO TO 10
        STOP
        END
*
```

Flux Tail Removal Program

This program is a subsection of a general data manipulation program which we use to smooth data, combine data, subtract background, plot data, and other general utility functions. Each function is called by a number input at the console terminal. After execution of the function, the program returns to the function choice routine at statement 15.

The physical assumptions and the algorithm used in the program have been discussed in Chapter I. The specific equation is obvious from the program. The program is entered with the data to be stripped in ARRAY2 and exits with the stripped data having replaced the original data. The data upon entry must have already had the average background level subtracted from it in order to obtain proper results.

All input parameters are prompted by the program. The starting channel is the channel from which the program begins calculating and subtracting flux tail contributions. It should be the first channel in which actual signal has entered the detector. The variable NEGFLG is used to choose to maintain or to set to zero all negative numbers resulting from the calculation after the spectrum is calculated. Removal of negative numbers is a useful feature in plotting several sets of data on top of each other due to the way other sections of the program choose the plotting scale factors.

The program is in standard Fortran and will run on any system supporting CALL PRINT commands to the console. The CALL PRINT statement can easily be converted to a standard Hollerith formatted WRITE statement if desired.

```
C
C       PROGRAM SECTION TO REMOVE EXPONENTIAL FLUX TAILS
C       FROM DATA IN WHICH APPARENT PRODUCT IS PRODUCED
C       BY FRAGMENTATION OR DETECTION OF "PULSED BACKGROUND"
C       FUNCTION 24
C
2300    DO 2310 I=1,255
2310    ARRAY3(I)=ARRAY2(I)
        CALL PRINT(' ENTER STARTING CHANNEL IN I3 FORMAT')
        READ (5,2315) NST
        CALL PRINT (' ENTER INVERSE TIME CONSTANT IN F 12.0 FORMAT')
        READ (5,2320) AC
        CALL PRINT(' ENTER RELATIVE CONTRIBUTION FACTOR IN F 12.0')
        READ (5,2320) AK
        CALL PRINT(' ENTER 1 FOR NO NEGATIVES, 0 THEY STAY')
        READ (5,2315) NEGFLG
2315    FORMAT (I3)
2320    FORMAT (F12.0)
        NST=NST-1
        SUM=0.
        EXPNAC=EXP(-AC)
        DO 2350 I=1,255-NST
        VEL=1./(FLOAT(NST+I)-.5)
        ARRAY2(NST+I)=(ARRAY3(NST+I)-SUM)/(1.+AK*VEL)
        SUM=(SUM+AK*VEL*ARRAY2(NST+I))*EXPNAC
2350    CONTINUE
        IF (NEGFLG .NE. 1) GO TO 15
        DO 2360 I=1,255
2360    ARRAY2(I)=DIM(ARRAY2(I),0.)
        GO TO 15
*
```

U.S.GPO:1980-698-169/F-99